# A study of thermomigration in lead, aluminium and cadmium

## Thesis

# A study of thermomigration in lead, aluminium and cadmium

A Thesis submitted for the Degree

of

Doctor of Philosophy

of the Open University

in the discipline of Materials Science

by

R. Johns, B.Sc.

Oxford Research Unit,
Open University,
January 1975.

Date of Submission: 20.2.75

Date of award : 1.7.75

## ABSTRACT

Atomic transport produced by temperature gradients was measured by observation of the length changes induced in high purity rods of lead, aluminium and cadmium. Measurements were made on both single crystal and poly-crystal specimens and covered temperature ranges to as low as 0.5 times the melting point temperature.

Heats of transport were found to show no variation with temperature except at the very lowest annealing temperatures where an effect, governed by the presence of grain boundaries, was observed. Values for the reduced heat of transport ($Q^* - \Delta H_f$) were obtained such that for lead, aluminium and cadmium ($Q^* - \Delta H_f$) was equal to $(10.7 \pm 0.2)10^{-2}$ eV; $(8.32 \pm 0.07)10^{-2}$ eV; $(3.68 \pm 0.05)10^{-2}$ eV respectively, and it was shown that the heat of transport was, within experimental uncertainty, equal to the mean of the energy carried by the atoms making a diffusion jump.

CONTENTS


| | | | |
|---|---|---|---|
| Chapter 1 | | Thermomigration in pure metals | 3 |
| | 1.1 | Introduction | 3 |
| | 1.2 | Atomic movement in hot metals | 3 |
| | 1.3 | Presence of a driving force | 4 |
| | 1.4 | Non-equilibrium thermodynamics | 7 |
| | 1.4.1 | Thermal diffusion | 8 |
| | 1.4.2 | Phenomenological equations | 8 |
| | 1.5 | Heat of transport Q* | 10 |
| | 1.6 | Analysis of a driving force and its effects on atomic motion | 15 |
| | 1.7 | Measurement of Q* | 17 |
| | 1.7.1 | Anisotropy | 17 |
| | 1.8 | Conclusion | 19 |
| Chapter 2 | | Experimental considerations arising from the review of previous techniques | 20 |
| | 2.1 | Introduction | 20 |
| | 2.2 | Marker-motion technique | 20 |
| | 2.2.1 | Limitations of the marker-motion technique | 22 |
| | 2.3 | Radio-active tracer technique | 22 |
| | 2.3.1 | Limitations of the radio-active tracer technique | 23 |
| | 2.4 | Experimental considerations | 24 |
| | 2.4.1 | Choice of materials for this study | 25 |

| | | | |
|---|---|---|---|
| | 2.4.2 | Specimen shape and dimensions | 26 |
| | 2.4.3 | Temperature considerations | 27 |
| | 2.4.4 | Possibility of creep | 28 |
| | 2.4.5 | Measuring dimension changes | 28 |
| | 2.5 | Outline of experimental design | 29 |
| | 2.5.1 | Obtaining thermal gradients | 29 |
| | 2.5.2 | Measuring change in specimen length | 30 |
| | 2.5.3 | D values | 30 |
| | 2.6 | Conclusion | 31 |
| Chapter 3 | | The design and construction of the experiment | 32 |
| | 3.1 | Requirements | 32 |
| | 3.1.1 | Basic structure | 32 |
| | 3.1.2 | Creep | 33 |
| | 3.2 | Complete structure | 34 |
| | 3.2.1 | Furnace construction | 34 |
| | 3.2.1.1 | Furnace heat shield | 37 |
| | 3.2.2 | Specimen clamping | 37 |
| | 3.2.3 | Thermal gradient | 40 |
| | 3.2.3.1 | Choice of coolant | 40 |
| | 3.2.3.2 | Problems with coolant | 44 |
| | 3.2.4 | The transducer | 45 |
| | 3.2.4.1 | Probe geometry | 45 |
| | 3.2.4.2 | Monitoring transducer output | 46 |
| | 3.2.4.3 | Manual control of transducer probe position | 46 |
| | 3.2.5 | Securing the complete structure | 51 |
| | 3.2.6 | Necessary precautions | 52 |
| | 3.2.6.1 | Centralising specimens | 52 |
| | 3.2.6.2 | Mounting transducer and surface condition | 53 |

| | | | |
|---|---|---|---|
| | 3.2.7 | Vacuum system | 53 |
| | 3.3 | Control and measurement | 53 |
| | 3.3.1 | Furnace control | 53 |
| | 3.3.2 | Measurement of temperature | 55 |
| | 3.4 | Conclusion | 56 |
| Chapter | 4 | Specimen preparation and early observations | 57 |
| | 4.1 | Introduction | 57 |
| | 4.2 | Specimen preparation | 57 |
| | 4.2.1 | Machining of single and polycrystal specimens | 58 |
| | 4.2.2 | Annealing of polycrystal specimens | 59 |
| | 4.3 | Preparatory procedures | 60 |
| | 4.3.1 | Original studies in lead | 62 |
| | 4.3.2 | The need for dummy specimens | 64 |
| | 4.3.3 | Further measurements on lead | 64 |
| | 4.4 | The problems encountered | 66 |
| | 4.4.1 | Grain movement and temperature stability | 66 |
| | 4.4.2 | Pitting | 67 |
| | 4.5 | Conclusion | 68 |
| Chapter | 5 | Results obtained from studies of thermomigration in lead, aluminium and cadmium | 70 |
| | 5.1 | Introduction | 70 |
| | 5.2 | Thermomigration in lead | 70 |
| | 5.2.1 | Lead polycrystal I | 70 |
| | 5.2.1.1 | Results | 71 |
| | 5.2.2 | Further lead studies | 83 |
| | 5.2.3 | Conclusion for thermomigration in lead | 88 |

| | | |
|---|---|---|
| 5.3 | Thermomigration in aluminium | 92 |
| 5.3.1 | Further preparation of specimens | 92 |
| 5.3.2 | Results from aluminium | 93 |
| 5.3.3 | Conclusion for thermomigration in aluminium | 102 |
| 5.4 | Thermomigration in cadmium | 105 |
| 5.4.1 | Further preparation | 105 |
| 5.4.2 | Results obtained | 106 |
| 5.4.3 | Conclusion for thermomigration in cadmium | 110 |
| 5.5 | Grain boundary diffusion observation in lead | 112 |
| 5.5.1 | Introduction | 112 |
| 5.5.2 | Preparation of the polycrystal specimens | 114 |
| 5.5.3 | Results | 115 |
| 5.5.3.1 | Single crystal specimen | 115 |
| 5.5.3.2 | Large grained polycrystal specimen | 115 |
| 5.5.3.3 | Small grained specimen | 120 |
| 5.5.3.4 | Calculation of the grain boundary activation energy | 122 |
| 5.5.3.5 | Calculation of the grain boundary heat of transport | 126 |
| 5.6 | Conclusion | 127 |
| Chapter 6 | Interpretation of the results and some ideas for further study using this technique | 128 |
| 6.1 | Determination of Q* | 128 |
| 6.1.1 | Measurement of Q* | 129 |
| 6.2 | Thermomigration in lead, aluminium and cadmium | 129 |
| 6.2.1 | Driving force and biased atomic motion | 132 |
| 6.3 | Summary | 133 |

| | | | |
|---|---|---|---|
| | 6.4 | Relationship between $Q^*$ and $\Delta H_m$ | 137 |
| | 6.4.1 | Conclusion | 140 |
| | 6.5 | Further studies | 141 |
| | 6.5.1 | Other metals | 141 |
| | 6.5.2 | Transducer | 141 |
| | 6.5.3 | Electrotransport | 142 |
| Appendix 1 | | Anisotropy | 143 |
| Appendix 2 | | Biased atomic motion | 145 |
| Appendix 3 | | Grain boundary diffusion | 148 |
| Appendix 4 | | The deformability of a material under stress | 151 |
| References | | | 153 |
| Acknowledgements | | | 156 |

## INTRODUCTION

A flow of heat through a hot solid may promote a flow of material through the solid. The objective of this study was experimentally to relate flows of material through lead, aluminium and cadmium to an imposed temperature gradient.

To allow the study of this material flow, known as thermomigration, a new experimental technique was evolved. This technique used measurements of specimen deformation as an indicator of material flow. These measurements were continuous, non-destructive, and had a potential sensitivity of $\pm$.0005 eV in the evaluation of the heat of transport for a pure metal under the conditions considered.

The work represents an extension of the study of how atomic motion in solids may be biased by the imposition of a field of force. Such studies have been known now for about a century. The earliest recorded investigations of these phenomena were performed by Gerardin (52) in 1861, studying the effects of electrotransport in molten alloys, and Ludwig (5) and Soret (6) in the late 1850's, studying the effects of thermotransport in liquids.

It was not until 1950, however, that studies of thermotransport were performed on metals and alloys by Darken and Oriani (53), but since then interest in this research has avalanched and many experimentalists have studied this biased atomic motion in many metals and alloys.

Over the past twenty years, two techniques have been perfected to observe the drift velocity of the atomic mass flow in metals created by the imposition of thermal gradients: the marker-motion technique and the radio-active tracer technique.

Both these techniques allow the successful observation and calculation of the atomic drift velocity which can then be used to derive the value of the term called the heat of transport, but both have various experimental limitations. The experimental technique developed for use in this work was based on the criteria of minimising the limitations inherent in both these previous techniques.

# CHAPTER 1

## Thermomigration in pure metals

# CHAPTER 1

## Thermomigration in pure metals

### 1.1 Introduction

The observation of diffusion processes leads to a clearer picture of the changes that occur in solids at high temperatures and also the exact nature of atomic movement within the body of the solids.

Diffusion theory has developed along two main approaches: (i) the continuum process, a general thermodynamic approach which describes the mass flow in macroscopic terms and which is described by Fick's laws of diffusion, and (ii) the atomistic approach, where the atomic nature of the diffusing substance is explicitly considered.

In the second approach the macroscopic flows of the first approach are seen as a statistical consequence of individual atomic motion and relationships are determined between macroscopic quantities, such as diffusion fluxes, and atomic quantities, such as atomic jump frequencies.

### 1.2 Atomic movement in hot metals

Atoms in a hot solid diffuse by a mechanism which corresponds closely to a motion by random jumps. The jumps are distributed randomly in time and direction, but for minor deviations which may occur due to a correlation between the jump directions of successive jumps (2), (3).

Despite the randomness of the individual motions, the concentration distribution which results after diffusion from some given initial distribution is predictable, if only on a statistical

basis. Consider the simplest of idealised cases, movement in a 1-dimensional lattice of a series of atoms released sequentially from the origin and each allowed to perform a set number, N, jumps between adjacent points on a lattice on which possible atomic positions are described by co-ordinate positions x which may take only the values 0, $\pm$ a, $\pm$ 2a, $\pm$ 3a....

It is clear that the atomic distribution which must result if each atom at each jump has a probability 1/2 of moving in the + x direction and a probability 1/2 of moving in the - x direction will be symmetric about the origin. If large numbers of atoms and numbers of jumps are considered this distribution will effectively be a continuum and must be describable in terms of the known phenomenological laws of diffusion, as described by Fick, and on the initial distribution concentrated at the origin.

Concentration distributions which evolve to this general pattern are the norm in studies of diffusion in hot solids. Of importance in this work is the fact that in certain circumstances non-random atomic movement is possible with net material flow taking place in response to a driving force.

## 1.3 Presence of a driving force

Consider the pattern of atomic movement to be expected, again in a 1-dimensional co-ordinate system, when the individual atomic jumps are not quite random. Let the deviation from randomness be that although any given jump may still be in either the + x or - x direction, it is determined by a probability p of motion in the +x direction and q of motion in the -x direction.

For this case it can readily be shown, Reif (1), that the probability $p_N(m)$ of an atom, originally at the origin, reaching the m th lattice position after N jumps is:

$$p_N(m) = \frac{N\,!}{((N+m)/2)\,!\;((N-m)/2)\,!}\; p^{(N+m)/2}(1-p)^{(N-m)/2} \qquad 1.1$$

This is a distribution which is not symmetric about the origin. It is a distribution which spreads in the way associated with normal diffusion, but whose maximum advances with the number of jumps, N.

For large numbers of jumps this distribution may be described closely by:

$$p_N(m) = (2\pi Npq)^{-1/2} \exp - \left(\frac{(m - N((p-q))^2}{8Npq}\right) \qquad 1.2$$

In this form the distribution curve is Gaussian. It may be related to the concentration distribution that would be expected if a fixed amount of material were released at the origin of the co-ordinates and were allowed to diffuse following Fick's phenomenological laws of diffusion. For normal diffusion this would take the form

$$C(x,t) = \frac{1}{2\sqrt{\pi Dt}} \exp\left(-\frac{x^2}{4Dt}\right) \qquad 1.3$$

Identity can be found between the two distributions by taking:

$$x = ma \qquad 1.4$$

where x is the actual displacement variable.

$$\sigma = (2Dt)^{1/2} \qquad 1.5$$

where D and t are the diffusion coefficient and time respectively and

$$\mu = vt \qquad 1.6$$

where $V = (p - q)\frac{Na}{t}$ is the drift velocity. Hence

$$p(x)\,dx = \frac{1}{2\sqrt{\pi Dt}}\exp -\left(\frac{(x - vt)^2}{4Dt}\right) dx \qquad 1.7$$

In this form the concentration distribution may be taken as one drifting with a velocity v while spreading by diffusive flow in response to concentration gradients.

The equivalence of these two descriptions shows that if atomic motion is non-random, in the particular sense of a difference in jump probabilities with direction, a flow of material will result under diffusion, the drift velocity of the flow being related to the differences in the probability of jumping in the two possible directions. We shall describe flow of this type as due to a bias in the atomic motion.

This work is concerned with the degree of bias that can be brought into atomic motion by a flow of heat through a material. At the atomic level this bias may be seen as due mainly to unbalanced scattering interactions between the carriers of heat in the solid - charge carriers, or phonons - and atoms which are on the point of making a diffusion jump. In formal terms however, this material flow may more usefully be described in terms of a material flow locked to the flow of heat through the solid.

A description of the material flow in these terms uses the language of non-equilibrium thermodynamics. In this terminology we link the material flow to the heat flow by a coefficient known as a heat of transport, details of the atomic interactions and motions being ignored.

## 1.4 Non-equilibrium thermodynamics

So far this chapter has dealt with diffusion from the atomistic approach but an alternative thermodynamic approach is possible, and this can be usefully combined with kinetic models. This process treats the diffusion substance as a continuous medium so the atomistic nature of a structure is ignored.

Mazur and deGroot (4) presented this theory of non-equilibrium thermodynamics and began by considering the thermodynamic parameters involved, such as temperature, pressure and local concentrations.

Fluctuations of these parameters from their local equilibrium values in an adiabatically isolated system are termed state variables. Fluxes, $J_i$, are then defined which are the time derivatives of these state variables.

Certain 'thermodynamic forces' $X_i$ conjugate to these fluxes are then chosen. These forces are linear combinations of the state variables and it is possible to obtain an expression for the rate of entropy production per unit volume. This expression is

$$\delta T = \sum_i J_i . X_i \qquad 1.8$$

where T is the absolute temperature.

This calculation of the rate of entropy production is essential since an irreversible process is characterised by such a production.

The forces $X_i$ arise from the tendency of a system which has fluctuated away from equilibrium to return to a steady state condition. It is, in fact, usual to apply such a thermodynamic theory to systems in the steady state. This means that the parameters have time-independent values at every point in the system, despite the occurrence of dissipative processes.

By considering the idea of macroscopic reversibility it was possible for Onsager to express the fluxes as

$$J_i = \sum_{k=1} L_{ik} X_k \qquad 1.9$$

where $L_{ik}$ is the phenomenological coefficient and depends on the thermodynamic parameters but is not influenced by the magnitude of the forces $X_k$.

### 1.4.1 Thermomigration

One driving force which will cause a flow of material in the solid state is related to the imposition of a temperature gradient. It has been known for some time now that in liquids when a temperature gradient is maintained across a multi-component liquid a separation takes place (5) (6). The effect has also been recognised in the solid state (7) (8).

Material flow in these conditions is described as due to thermomigration.

### 1.4.2 Phenomenological equations

When a pure metal is subjected to a thermal gradient, there will be, as mentioned, fluxes of heat, atoms and vacancies through the metal.

From Onsager's expression, the phenomenological equations may be written for these three fluxes as:

$$J_q = L_{qv} (X_v - X_a) + L_{qq} X_q \qquad 1.9.1$$

$$J_a = - J_v \qquad 1.9.2$$

$$J_v = L_{vv} (X_v - X_a) + L_{vq} X_q \qquad 1.9.3$$

The subscripts q, a, and v, refer to heat, atoms and vacancies respectively.

In this system we are considering the flow of two constituents, atoms and vacancies, through a temperature gradient. The thermodynamic forces are given by:

$$X_q = - 1/T^2 \nabla T \qquad 1.10.1$$

$$X_v = - 1/T \nabla U_v \qquad 1.10.2$$

$$X_a = - 1/T \nabla U_a \qquad 1.10.3$$

where $U_v$ and $U_a$ are the chemical potentials of the vacancies and atoms of the system.

Substituting these values for the thermodynamic forces into the flux equations gives:

$$J_q = - \frac{L_{qv}}{T} \nabla(U_v - U_a) - \frac{L_{qq}}{T} \nabla T \qquad 1.9.4$$

$$J_a = - J_v \qquad 1.9.5$$

$$J_v = - \frac{L_{vv}}{T} \nabla(U_v - U_a) - \frac{L_{vq}}{T^2} \nabla T \qquad 1.9.6$$

Application of the Gibbs-Duhem relation and Onsager's reciprocity theorem to the expression for the vacancy flux results in the expression that

$$J_v = \frac{kL_{vv}}{N_v} \left(\nabla N_v - \frac{N_v}{kT^2} Q^* \nabla T\right) \qquad 1.11$$

where $N_v$ is the vacancy concentration, $Q_v^*$ is the heat of transport of the vacancy and $\nabla T \equiv$ grad T.

For an isothermal system $Q_v^*$ can be defined as the ratio $J_q/J_v$ and may be thought of as the heat transported by the moving vacancy. The atomic heat of transport $Q_a^*$ can similarly be defined where

$$Q_a^* = - Q_v^* \equiv Q^* \qquad 1.12$$

An experimental measurement, therefore, of $Q_a^*$ asserts a proportionality between a flow of heat and a flow of material, $Q_a^*$ being the constant of the proportionality.

If in equation 1.11 $D_v = \frac{kL_{vv}}{N_v}$ then

$$J_v = - D_v \left(\nabla N_v + \frac{N_v Q_v^*}{kT^2} \nabla T\right) \qquad 1.11.1$$

If the concentration of vacancies at any point in the system is considered to be the concentration at equilibrium at the temperature of that point and if the gradient of vacancies is due only to the gradient of temperature then

$$\nabla N_v = \frac{N_v \Delta H_f}{kT^2} \nabla T \qquad 1.12$$

where $\Delta H_f$ is the enthalpy of formation for vacancies. Then the vacancy flux becomes

$$J_v = - \frac{N_v D_v}{kT^2} (\Delta H_f + Q_v^*) \nabla T \qquad 1.11.2$$

or

$$J_a = - \frac{N D_s}{fkT^2} (Q_a^* - \Delta H_f) \nabla T \qquad 1.13$$

where $D_s$ is the tracer self-diffusion coefficient.

## 1.5 Heat of Transport

Formally the heat of transport may be defined as the ratio of two fluxes: it is the ratio of the flow of heat through a material to the flow of material created by this flow of heat. Hence for a species 'a' the heat of transport is

$$Q_a^* = J_q / J_a$$

Alternatively, when flow is by a vacancy mechanism with an atomic flow accompanied by an equal and opposite vacancy flow it may be written as

$$Q_a^* = -Q_v^* = J_q / J_a = -J_q / J_v$$

So $Q_v^*$ is due solely to the interference of two non-equilibrium processes, namely heat flow and vacancy migration. Thus if $Q_v^* > o$, a heat flux parallel to a vacancy flux will be generated, whereas if $Q_v^* < o$, $J_v$ and $J_q$ are in opposite direction and hence the region gaining vacancies must receive heat to keep it isothermal.

Nichols (9) stated that Q* can be thought of as the amount by which the energy of the atom in transit exceeds the average enthalpy of the surrounding atoms. Thus for any non-activated transport mechanism such as gaseous diffusion, Q* is zero. For a process such as vapourisation Q* simply becomes the enthalpy change for that process. For atomic migration within condensed phases no such simplicity exists and the appropriate Q* values must be determined experimentally.

Denbigh (10) used a simple model to explain the nature of Q*. He considered a system subdivided into two systems A and B, which are kept at constant pressure and constant temperatures T + dT, T - dT, respectively, by contacting heat reservoirs. He quoted that the heat of transport Q* of the i th component is then the heat that must be supplied from system B to system A to maintain pressure and temperature constant, when a mole of that component passed from A to B.

Leclaire (11) and Brinkman (12) tried a different approach and applied a kinetic treatment to thermal diffusion. Using Boltzman statistics in the case of the vacancy mechanism, they concluded that the heat of transport was the difference between an energy of migration and an energy of formation of the vacancies. That is

$$Q^* = \Delta H_m \qquad 1.15$$

From equations 1.11.2 and 1.13 (combination)

$$J_v = + \frac{ND_s}{fkT^2} (Q^*_a - \Delta H_f) \nabla T \qquad 1.16$$

So from Leclair and Brinkman, if $Q^* < 0$ then $\Delta H_m < \Delta H_f$ and J will have the same sign as the temperature gradient. This implies that the atoms will diffuse away from the low temperature region and accumulate at the hot region.

If $Q^* = 0$ then no thermal diffusion occurs.

If $Q^* > 0$ then the atoms will diffuse from the hot region to the cooler region.

Allnatt and Rice (13) arrived at a similar conclusion to Leclaire and Brinkman, but Brammer (14), who carried out experiments on thermal migration in $\alpha$- iron and copper, thought this final expression for $Q^*$ inadequate.

Brammer, having failed to observe any motion in $\alpha$- iron and copper, concluded that there were three possible causes if Leclaire and Brinkman's observations were correct: (i) that the vacancy mechnaism did not operate in the two metals, or (ii) $\Delta H_m$ and $\Delta H_f$ are nearly equal, or (iii) that the heat of transport was not simply $\Delta H_m - \Delta H_f$.

This third possibility suggested by Brammer led to a more detailed study of the jumping process which had been suggested at an earlier stage by Wirtz (15). This suggests that when an atom jumps from one site at a temperature T to a new site at temperature T - dT it may require three additional energies. An energy $H_m^1$ localised at its original position, an energy of vibration $H_b$ in the barrier atoms which ring the saddle point configuration at temperature $T - \frac{1}{2}dT$, and an energy $H_n$ at the original vacancy site to open it up from its relaxed state for occupancy.

This led to an expression for the heat of transport such that

$$Q^* = H_m^1 - H_f^1 \qquad 1.17$$

where

$$H_m^1 = \Delta H_m - H_b - H_n \qquad 1.18$$

and

$$H_f^1 = \Delta H_f + H_n \qquad 1.19$$

These modifications give a $Q^*$ less than $\Delta H_m - \Delta H_f$ by $H_b + 2\,H_n$, which could account for the unexpectedly large mass flow towards the hot end of a specimen.

Oriani (16), (17), applied a theory by Rice to self-diffusion via a vacancy mechanism and found an expression for the heat of transport such that

$$Q^* = H_c + H_v \qquad 1.20$$

where $H_c$ is the amount of excess vibrational energy that becomes converted into chemical energy when an atom changes sites, and $H_v$ represents the amount of vibrational energy transferred per atomic jump.

He considered the case where an atom at a position A exchanges with a vacancy at B. What happens at A is that a vacancy is created at the expense of some of the excess vibrational energy. This says, therefore, that thermal energy has been used to 'move' the atom, and this conversion of thermal energy implies a positive $H_c$. Oriani states that $H_c$ is not quite equal to $\Delta H_f$ because the vacancy to be created at A is at a position adjacent to the already existing vacancy at B.

Huntington (18), (19), developed a model for the heat of transport for pure metals which diffuse by means of the vacancy mechanism. He considered four effects which combine to form $Q_a^*$. These are the 'intrinsic' effect, which is essentially based on the Wirtz-Brinkman model; the phonon effect; the Thomson effect, and the charge carrier effect.

This theory gives calculated values of $Q_a^*$ which are in measurable agreement with experimentally obtained values in copper, aluminium, platinum and gold.

It is a fact that the most widely applied theory for the heat of transport corresponding to diffusion by the vacancy mechanism is the Wirtz-Brinkman model. This predicts that the intrinsic heat of transport is given by

$$Q^* = \beta \Delta H_m \qquad 1.21$$

where $\beta \Delta H_m$ is the fraction of the vacancy migration energy which is transported by the atom from the initial to final state.

This model was later verified by Shewmon (20) in his examination of thermal migration in pure metals where he found that

$$\beta \simeq 0.9$$

In another approach Haga (21) attempted to calculate the heat of transport by evaluating the net flow of energy accompanying a given flux of atoms, that is, an isothermal approach, so performed by applying the Wert (22) formulation of the rate-process description of an activated jump.

This theory calculates the jump probability of an atom in the lattice by assuming the equilibrium canonical distribution of atomic positions and momenta and then evaluating the number of atoms

passing in a given direction through saddle point configurations in unit time. Haga (21) adapted this calculation by also evaluating the energy carried by these atoms as they passed through the saddle point and hence obtained the heat of transport by dividing the energy flux by the atom flux. This method led to the result that Q* was equal to the heat of activation.

Lidiard (23) shows the limitations of any transition state approach, such as the Haga theory, namely that it is based only on the average probability of the saddle point and its immediately surrounding sites and says nothing about the correlations between the atomic motions necessary to produce this state. This limitation is a fundamental error in the description of the heat of transport since the flow of energy into the region around the defect before the transition state is achieved and the flow of energy out again afterwards are both important parts of the measured quantity Q*. Thus even if the mean energy flux at the saddle point is correctly given by the heat of activation the heat of transport necessarily contains other terms which may only be evaluated outside the transition state approach.

From these varying theories of Q* the Wirtz-Brinkman evaluation is considered the most valid and previous experimental studies performed by Shewmon and Huntington tend to substantiate this relationship where

$$Q^* = \beta \Delta H_m \qquad 1.21$$

## 1.6 Analysis of a driving force and its effects on atomic motion

When a thermal gradient is imposed upon a body, equilibrium is impossible since there is a non-zero heat flux. Furthermore,

the kinetic effect of the heat flux is to generate an atomic flux. Denbigh (10) obtained from irreversible thermodynamics that

$$F_T = - \frac{Q^*}{T} \nabla T \qquad 1.22$$

is the value of the driving force which is due to the imposition of a thermal gradient.

Since this heat flux creates an atomic flux, the atoms will migrate through the body with a certain velocity.

This drift velocity of the atoms can be related to the applied 'driving force' by the Nernst-Einstein equation such that

$$v_a = \frac{D \ F_T}{fkT} \qquad 1.23$$

By substitution from equation 1.22 we obtain an expression for the drift velocity in terms of the diffusion coefficient and the heat of transport such that

$$v_a = - \frac{D}{fkT^2} \ (Q^* - \Delta H_f) \nabla T \qquad 1.24$$

If then D, f and k are known, measurements of $v_a$, T and $\nabla T$ define $(Q^* - \Delta H_f)$.

This atomic motion in an idealised material under the influence of a thermal gradient can be described as biased, defining the bias as

$$b = \frac{F_T a}{2kT} \qquad 1.25$$

where a is the lattice width spacing. We now have a relationship between the driving force and the resulting biased motion of the atoms. The theory for this relationship is shown in Appendix 2.

## 1.7 Measurement of Q*

To define values of Q* measurements must be obtained for the atom drift velocity $v_a$. Two experimental techniques have been used extensively to measure the drift velocity in pure metals: the marker-motion technique and the radio-active tracer technique, and these are discussed fully in Chapter 2.

The marker-motion technique is used solely to observe the drift velocity whereas the tracer technique has the advantage of allowing a simultaneous measurement of the diffusion coefficient D.

Marker-motion requires the use of surface scratches or indentations on the specimen which is subjected to a thermal gradient, and values for the drift velocity are obtained by measuring distance changes between successive markers which occur due to the mass flow.

There is a problem, however, when such measurements are made on rod-shaped specimens since the mass flow may not be totally uniaxial, some mass flow being partially lateral.

### 1.7.1 Anisotropy

If lateral flow does occur then measurement of the distance change between successive markers scratched along the length of the specimen does not simply give $v_a$. Huntington and Ho (37) in their studies of thermomigration stated that

$$v_a = - \frac{v_m}{\alpha} \qquad 1.26$$

where $v_m$ is the drift velocity between successive markers and $\alpha$ is a lattice accommodation factor defined as the ratio of the longitudinal strain rate to the dilatation rate and can be expressed as

$$\alpha = \dot{e}_{xx}/(\dot{e}_{xx} + 2\dot{e}_{rr})$$

where $\dot{e}_{xx}$ is the longitudinal 'strain' rate and $(\dot{e}_{xx} + 2\dot{e}_{rr})$ is the volume dilatation rate.

Having defined this factor $\alpha$ Huntington equates the local volume change to the net influx of matter and obtains an expression for the atom drift velocity $v_a$ such that

$$v_a(x) = -\int_{x_a}^{x} (\dot{e}_{xx}(x^1) + 2\dot{e}_{rr}(x^1))\, dx^1$$

where $\dot{e}_{xx} = dv_m/dx$, and $x_a$ refers to the position of the reference marker where all strains are zero: that is, the atom flux at $x_a$ is zero. Therefore, the above expression can be rewritten

$$v_a(x) = -\left[v_m + 2\int_{x_a}^{x} \dot{e}_{rr}(x^1)\, dx^1\right] \qquad 1.29$$

and since

$$\int_{x_a}^{x} \dot{e}_{rr}(x^1)\, dx^1 = v_m(x) \qquad 1.30$$

and

$$\alpha = \dot{e}_{xx}/(\dot{e}_{xx} + 2\dot{e}_{rr}) \qquad 1.27$$

$$v_a(x) = -v_m(x)/\alpha \qquad 1.26$$

if $\alpha$ is a constant.

Equation 1.24 now becomes

$$v_m = \frac{\alpha D_s}{fkT^2} (Q_a^* - \Delta H_f)\, \nabla T \qquad 1.31$$

From this equation we can directly relate the heat of transport to the measured velocity of the surface markers.

## 1.8 Conclusion

This study describes a technique designed to measure the drift velocity of the biased atomic motion in lead, aluminium and cadmium, and hence values of the heats of transport defined from equation 1.31. This method does not use surface markers and measurements of the drift velocity are obtained by using a capacitative transducer.

It is hoped that by using this technique reliable, and reproducible, values for the heats of transport are obtained over as wide a temperature range as possible.

Chapter 2 describes the considerations which defined the experimental technique and gives a brief summary of previous techniques and the results obtained.

is this a conclusion to Ch. 1?

# CHAPTER 2

## Experimental considerations arising from the review of previous techniques

# CHAPTER 2

# Experimental considerations arising from the review of previous techniques

## 2.1 Introduction

To define values for the heat of transport of a material, such as a pure metal, it is necessary to obtain measurements of the drift velocity $v_m$ of the mass flow created by the imposition of a thermal gradient. Since it is impossible to observe individual atom movement within the material, measurements of the drift velocity must be obtained by relating the changes in the specimen dimensions to time. If this measurement is possible, values for $Q^*$ can be evaluated if only T and $\nabla T$ are known. In previous studies of self-diffusion in pure metals, two techniques have been perfected which allow the determination of the atom drift velocity: the marker-motion technique and the radio-active tracer technique.

## 2.2 Marker-motion technique

Equation 1.16 defines the flux of vacancies which occurs when a metal is subjected to a thermal gradient such that

$$J_v = \frac{DN}{fkT^2} (Q^* - \Delta H_f) \nabla T \qquad 1.16$$

As this flux is temperature and position dependent there is a non-zero divergence of flow. Inert markers attached to opposite ends of the gradient region will therefore move relative to one another due to a net flow of vacancies into or out of the region between them.

This movement of inert markers allows determination of the drift velocity from

$$v_m = \frac{D}{\alpha f k T^2} (Q^* - \Delta H_f) \nabla T \qquad 1.31$$

Therefore, a measurement of the change in distance between successive markers with time determines $v_m$. If D, f, and $\alpha$ are known and T and $\nabla T$ are measured, it is possible to estimate the quantity $(Q^* - \Delta H_f)$.

Studies using this technique have been performed on many metal specimens of varying geometry, from long, thin wires to short, squat specimens, and values for the heat of transport have been obtained. Recent studies by Shewmon and Jaffe (24) with copper and gold, Swalin and Yin (25) with zinc and Ho (26) with cobalt and platinum, have produced measurements of marker-motion and the resulting $Q^*$ values. The values for $Q^*$ obtained agree fairly well with the Wirtz-Brinkman theory, that is,

$$Q^* = \beta \Delta H_m$$

where $\beta = 0.8$ to 0.9, indicating that $Q^* < \Delta H_m$

In 1964, however, Ho, Hehenkemp and Huntington (27) completed a study of thermal diffusion in platinum from which there are two significant observations: that the sign of $Q^*$ was opposite to that predicted by the Wirtz-Brinkman theory and that the heat of transport appeared to be temperature dependent.

Later in 1970 Matlock and Stark (28) studying thermal diffusion of vacancies in aluminium observed that results obtained from polycrystals and single crystals gave values of $Q^*$ which varied not only in magnitude, but also in sign. Therefore, from these two studies appear three anomalies with known $Q^*$ theory.

### 2.2.1 Limitations of the marker-motion technique

This technique is time-consuming since it can take days to measure the drift velocity associated with one specific thermal gradient, and therefore, since values are required over a large temperature range each complete study on one specimen can take weeks. This time depends, however, on the metal under observation as different metals will obviously have various drift velocities associated with the mass flow created by the imposition of thermal gradients.

There is also doubt as to the validity of measuring the effect of volume diffusion using surface markers as these could act as sources and sinks of vacancies in such a way that the observed net drift velocity is appreciably less than that which does occur. This can be overcome by the use of internal markers as pioneered by Doan (29), where he used fine wires located internally in metal specimens.

Many of the studies have used thin wire specimens where lateral mass flow has been observed, that is, $\alpha \neq 1$. This, as Penney (30) predicts, is due to the large length to radius ratio which is inherent in the use of wires self-heated by the passage of an electric current.

Other studies with short, squat specimens, however, have shown that stable temperatures can be obtained and the mass flow is seen to be totally uniaxial since the length to radius ratio is small, that is, $\alpha$ is unity. Penney's theory is shown in Appendix 1.

## 2.3 Radio-active tracer technique

Tracer experiments have evolved from techniques developed for evaluation of diffusion coefficients. The method has been used

to obtain values for the heat of transport as shown by Mock (31) in his study of thermal diffusion in gold, where he found

$$(Q^* - \Delta H_f) = 0.18 \text{ eV}$$

This technique employs two radio-active tracers: one has a very low diffusion coefficient and the other is of the material under study. A small concentration of the non-diffusing internal tracer is coated onto one surface of mating flats of the specimen material, whilst a thin layer of the tracer material is coated onto the other. These optical flats are then welded together under vacuum conditions and the specimen is then placed in a thermal gradient for the diffusion anneal.

During this anneal the inert tracer moves little as the Einstein equation states low diffusion rates give low drift rates, whereas the other tracer diffuses more rapidly.

Once the anneal is complete the specimen is sectioned on a precision lathe and the penetration profile determined. The drift velocity is determined by measuring the shift of the specimen tracer with respect to the inert internal marker. Using this technique Mock (31) used $H_f{}^{187}O_2$ as the inert marker and $Au^{195}$ as the tracer.

### 2.3.1 Limitations of the radio-active tracer technique

Unlike the marker-motion technique, this method measures the net flux of atoms through the bulk of the lattice and therefore any surface effects are avoided. This technique is time-consuming, however, and necessitates the destruction of the specimen after each temperature anneal.

A nice feature of this technique is in the fact that the diffusion temperature can be determined to a high degree of accuracy by using the knowledge of the penetration profile, which is a skew Gaussian distribution. This determination is critical in studies of thermomigration and is one of the limitations of the marker-motion experiments.

It may be seen that the tracer technique has advantages over the marker-motion technique although the method is again time-consuming and requires a new specimen for each diffusion anneal.

## 2.4 Experimental considerations

The objective of this study is to obtain reliable and reproducible Q* values over a wide temperature range for various pure metals. Careful study of previous work highlighted a number of experimental limitations in accepted methods of measurement. Design criteria for the present work which emerged from this study were:

(1) to obtain values of the heat of transport, measurements of the drift velocity, temperature and temperature gradients, are required which are accurate and reproducible. To do this we required a sensitive method to measure the drift velocity $v_m$ and a temperature control which would allow stability over a wide range of temperature;

(2) to develop a technique which will not be time-consuming, and a sensitive measuring device which supplies continuous information concerning the change of specimen dimensions with time provides such a feature; and

(3) to develop a technique which avoids the use of surface markers and the destruction of each specimen, as well as ensuring that the mass flow is uniaxial by having a small

length to radius ratio. This assumes of course that the Penney theory is valid.

2.4.1 Choice of materials for this study

In a study of this type where the objective is to design, construct and test the reliability and precision of a method to determine $Q^*$ values of various pure metals, it is essential that the early studies repeat measurements made by established techniques. The results obtained from such a study show the reliability and reproducibility of the technique, and once this objective is achieved measurements on hitherto unexamined metals add much weight to the overall study.

In choosing the specimen metals for this work, materials with low melting points were preferred combined with a working temperature range which is a large fraction of the melting point temperature.

Because of this feature lead was thought of as a good material to begin the study as its melting point temperature was 600K, and it was hoped that a 100K temperature range could be obtained. Another justification for using lead is that Lodding and Thernqvist (32) predicted a value for $(Q^* - \Delta H_f)$ from an experimental study performed on electrotransport in lead, such that

$$(Q^* - \Delta H_f) = + 0.09 \pm 0.18 \text{ eV}$$

and to date this result has not been substantiated experimentally.

Aluminium was the second metal chosen to study as its melting point temperature is 934K and it is possible to study mass flow over a $200^{\circ}$ temperature range. This metal had previously been examined by Matlock and Stark (28) and Swalin and Yin (25).

By using both polycrystal and single crystal specimens in the study a comparison with these previous results could be made.

Cadmium was the third specimen material to be studied because of its low melting point temperature, 594K and the fact that unlike lead and aluminium it has a hexagonal close packed structure. To date mass flow in cadmium has not been studied although Wajda, Shirn and Huntington (33) have determined the diffusion coefficients of this material using the radio-active tracer technique. Since cadmium has a H.C.P. structure there are two principal directions along which mass flow can occur: parallel to the C axis and perpendicular to the C axis. In this study single crystal specimens of cadmium are used with their axes parallel to the C axis.

The three metals to be studied in this work were therefore lead and aluminium, with face centred cubic (F.C.C.) structure and cadmium with a hexagonal close packed structure and with melting point temperatures ranging from 594K for cadmium to 934K for aluminium.

### 2.4.2 Specimen shape and dimensions

For the present work it was decided that cylindrical specimens should be used, heat flow being from a large diameter head supported in a furnace, into a thin stem connected to a heat sink. Thermomigration was to be detected by length changes in the stem.

Details of the specimens are shown in Fig. 5. The large diameter head provides a surface from which a flow of heat, initially radial, turns to an axial flow into the stem. A heat sink, at a distance L from the shoulder, provides a second radial path for the flow of heat from the specimen. It was expected that the flow of heat in the stem would promote axial thermomigration and an

overall change in length of the specimen. Most of the flow was expected close to the shoulder, the rate decreasing to a negligible amount by comparison at the distance L from the shoulder, where the temperature was relatively cool.

It is also essential to vary the specimen dimensions during these experiments, not only because of the possible presence of high temperature creep, but also to ensure that reasonably high temperature gradients can be achieved for all three metals since their melting point temperatures vary considerably, from 594K for cadmium to 934K for aluminium.

### 2.4.3 Temperature considerations

It is important, when observing the effects of thermomigration, to ensure that the range of temperature is as wide as possible. If the heat of transport is temperature dependent, as suggested by Ho, Hehenkemp and Huntington (27), then it is necessary to measure the mass flow effect over a large temperature range so that there is an adequate study of this possible dependency. A previous study on thermomigration in lithium by Lodding and Thernqvist (34) had indicated that Q* was independent of temperature.

The dimensional changes which occur under the influence of mass flow are very small, fractions of microns a day. To measure these changes, the metal specimens must be subjected to a stable temperature gradient, since any fluctuation in this gradient would create thermal expansion. If the fluctuations are large, then the amount of thermal expansion associated with these changes in temperature would completely mask the drift rates expected from thermomigration.

It is obvious, therefore, that the temperatures involved must be very stable and the measurements of these temperatures must be accurate. Control of these temperatures is of prime concern in studies of thermomigration as are the methods involved in monitoring the temperatures.

### 2.4.4 Possibility of creep

Hot metals under stress deform progressively by a process called creep. Rod-like specimens of the type used in these thermomigration experiments are necessarily subject to two stresses, the first due to the weight of the specimen and the second to surface tension. Deformation due to these stresses may be detected as a drift rate and therefore could modify the apparent rate associated with the thermomigration process.

These two stresses are dependent on specimen geometry used and on the temperature of the experiment. It is therefore necessary to vary the specimen geometry throughout these studies and to operate at temperatures not too close to the melting point of the specimens. Adequate provision must be made when designing an experiment to study thermomigration so that any dimensional changes created by the creep process can be distinguished from the changes due to thermal migration. If the creep effect is small compared to that due to thermomigration, it can then be ignored or corrected for.

### 2.4.5 Measuring dimension changes

To measure the dimensional changes of a specimen due to the occurring mass flow a sensitive and accurate method is required.

When designing an apparatus which would allow such precise measurements there were other factors which required consideration: (a) that the technique avoided the use of surface markers; (b) that the technique avoided the destruction of the specimen, and (c) that measurement of the changes occurred continuously.

Such requirements were satisfied by employing a capacitative transducer probe whose design and use are discussed in Chapter 3.

## 2.5 Outline of experimental design

To determine the heats of transport of the three metals to be studied, experimental measurements of the drift velocity $v_m$ were required, as well as reliable measurements of the applied temperatures and temperature gradients.

### 2.5.1 Obtaining thermal gradients

The shape and dimension of the specimens are discussed in section 2.4.2 The wide diameter section was designed to seat in a heat source, the remaining stem section hanging freely from this source. At some distance down the length of this rod a heat sink was incorporated to remove the heat from the specimen, thus creating a thermal gradient down the length of the stem. The distance of the heat sink from the source was to be varied for different specimens, allowing a variation in the thermal gradient, and the dimensions were to be such that the ratio of the length to the radius was small. This, assuming Penney's theory of elastic plastic deformation is valid, ensures that the lattice accommodation factor $\alpha$ is approximately unity. Some check on the consistency, but not the value, of this factor was envisaged through the use of specimens of varying geometry.

This therefore modifies the equation for the drift velocity such that

$$v_m = \frac{D_s}{fkT^2} (Q^* - \Delta H_f) \nabla T \qquad 1.31$$

2.5.2 Measuring change in specimen length

The changes in the specimen length created by the biased atomic motion were to be measured by means of a capacitative transducer which would allow continuous observation of the length changes with time. The drift rates expected from these metals were as low as $10^{-9}$m/hour but could easily be detected by this technique which is a factor of ten more sensitive than the measuring process used in the marker-motion experiments. By integrating the output signal from the transducer a considerable reduction in the observed noise level was achieved, noise with periods up to ~15 minutes effectively being removed.

2.5.3 D values

With experimental values for $v_m$, T and $\nabla T$ and $f_2$ known from values computed by Compaan and Haven (2), (3), a value for $D_s (Q^* - \Delta H_f)$ may be computed. Unfortunately however no internal measurement of the diffusion coefficient was possible from the experiments so values for this parameter for the three metals were obtained from previous studies by Hudson and Hoffman (35) in lead, Lundy and Murdock (36) in aluminium and Wajda, Shirn and Huntington (33) in cadmium.

While the diffusion coefficient itself may not be derived from length change studies, the temperature variation of the product $D_s (Q^* - \Delta H_f)$ can. The calculation was first performed by Huntington and Ho (37) who combined the Arrhenius equation where

$$D = D_o \exp - (E_d/kT) \qquad 1.1$$

and the equation which relates the drift velocity to the heat of transport:

$$v_m = \frac{D_s}{fkT^2} (Q^* - \Delta H_f) \nabla T \qquad 1.31$$

By substituting D into equation 1.31 Huntington obtained the expression

$$v_m kT^2/\nabla T = D_o (\exp - (E_d/kT)) (Q^* - \Delta H_f) \qquad 2.1$$

and finally

$$\ln (v_m kT^2/\nabla T) = \ln (D_o (Q^* - \Delta H_f)) - E_d/kT \qquad 2.2$$

If therefore $(Q^* - \Delta H_f)$ is independent of temperature, a plot of $\ln (vkT^2/\nabla T)$ versus $1/T$ yields a slope which has the value $E_d/k$. Any systematic variation from accepted activation energies is a pointer suggesting variation of $(Q^* - \Delta H_f)$ with temperature.

Given values of $E_d$ being compatible with other work, only a knowledge of $D_o$, the frequency factor, is required for evaluation of $(Q^* - \Delta H_f)$.

## 2.6 Conclusion

This chapter has outlined the experimental procedure of this study after a discussion of the limitations of previous studies of thermomigration in pure metals. The possible problems which may arise during these experiments have been discussed such as temperature instability problems and creep, as well as the limitations in defining values for the diffusion coefficients.

Chapter 3 describes how the experimental equipment is designed and constructed to enable a measurement of the atomic drift velocity to be made.

# CHAPTER 3

## The design and construction of the experiment

# CHAPTER 3

## The design and construction of the experiment

### 3.1 Requirements

To study thermal transport in pure metals, specimens must be subjected to a thermal gradient. The mass flow produced to move in a direction parallel to the temperature gradient will have a certain drift velocity which is given by

$$V_m = \frac{D}{fkT^2} (Q^* - \Delta H_f) \nabla T$$

This flow of atoms through a metal specimen will produce changes in the specimen dimensions and by measuring these changes under known conditions of temperature and thermal gradients a value for $(Q^* - \Delta H_f)$ can be derived.

#### 3.1.1 Basic structure

The shape and dimensions of each specimen are shown in Fig. 5. Fig. 2 shows a specimen clamped at the top, with its thin stem hanging freely subjected to a thermal gradient $\nabla T$. This gradient is produced by clamping the specimen inside a heat source, where the heat flow is radial, and incorporating a heat sink at a distance L from the shoulder of the specimen, where again the heat flow is radial. The heat flow produced in the length L of the thin stem is linear and under these conditions the specimen dimensions will vary due to the mass flow produced. The magnitude and direction of this mass flow is governed by the value of the heat of transport $Q^*$ because if the value is positive the specimen will become longer and thinner since the atomic flux is in the same direction as the heat flux.

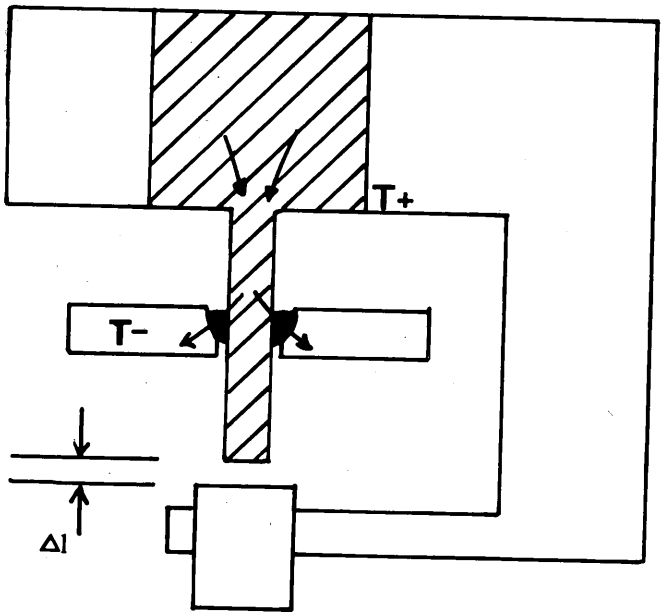


FIG. 2 Diagram showing the direction of the heat flow through the specimen and the relative position of the transducer

Conversely, if the value of Q* is negative the specimen will get shorter and fatter as the atomic flux is now in the opposite direction to the heat flux.

To measure these changes in length a capacitative transducer is seated against the bottom face of the specimen, as shown in Fig. 2. It is positioned in close proximity to the specimen and any changes in the specimen-transducer probe separation will vary the capacitance set up between the probe and the specimen, and these changes are calibrated directly to distance measurements.

3.1.2 Creep

In the discussion of the basic requirements, a method for measuring the drift velocity of the biased atomic motion was described. It depended on the measurement of length changes in a hot specimen hung from a furnace.

However a specimen hanging freely from a heat source is subject to high temperature creep which could modify the observed drift rate so that what is recorded is a combination of the drifts due to thermomigration and high temperature creep. Because of this possibility the equipment was designed so that if the drift rate under creep proved to be large it could be used in the inverted position, thus combining creep and thermomigration in the opposite relative sense. In this way any occurrence of creep might be corrected for when measurements of the drift velocity were made.

## 3.2 Complete structure

### 3.2.1 Furnace construction

The furnace was designed to support the specimen so that it hangs freely and to act as a heat source able to maintain the upper end of the specimen at the required temperature.

A schematic diagram of the furnace and its dimensions are shown in Fig. 4.a. The core of the furnace is copper whilst the remaining assembly is stainless steel.

The heating element was a coil of nichrome wire 1mm in diameter rated at 7 amps at 573K. Since this wire was unsheathed it had to be separated from the other metallic elements of the structure. To insulate the wire from the copper core a layer of Refrosil tape and adhesive was secured to the copper. The tape was a silicon fibre woven into tape of $1\frac{1}{4}$" width and the adhesive Autostik was a heat resistant substance manufactured by Rolls Royce guaranteed by the manufacturers to withstand temperatures of up to 1373K.

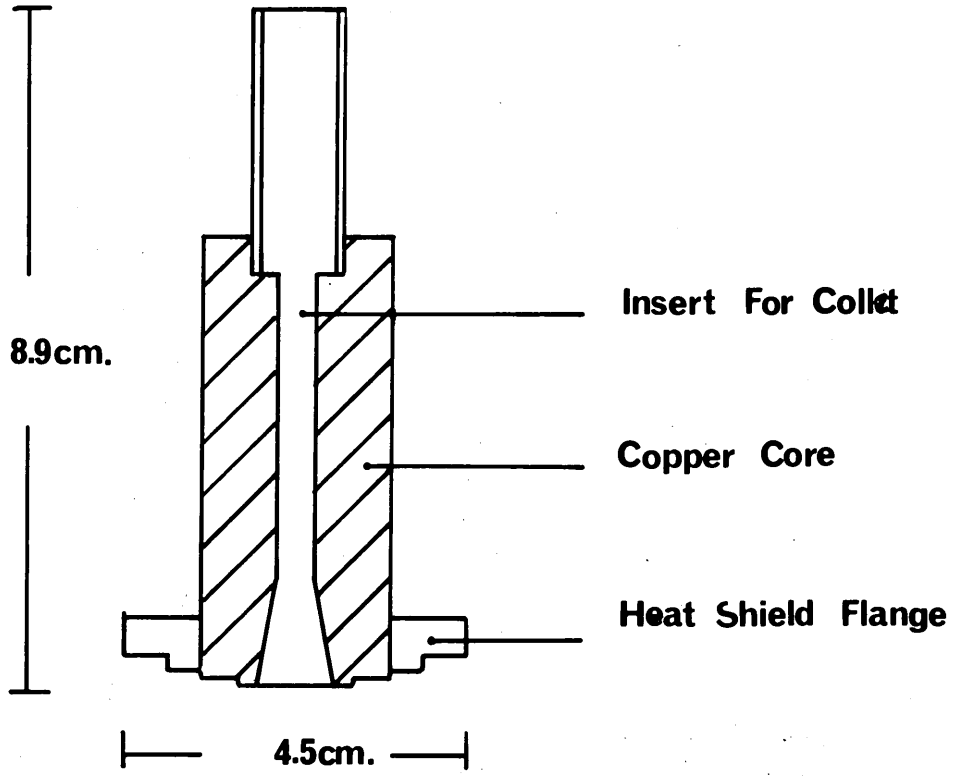


FIG. 4.a. Sectioned diagram of the furnace core

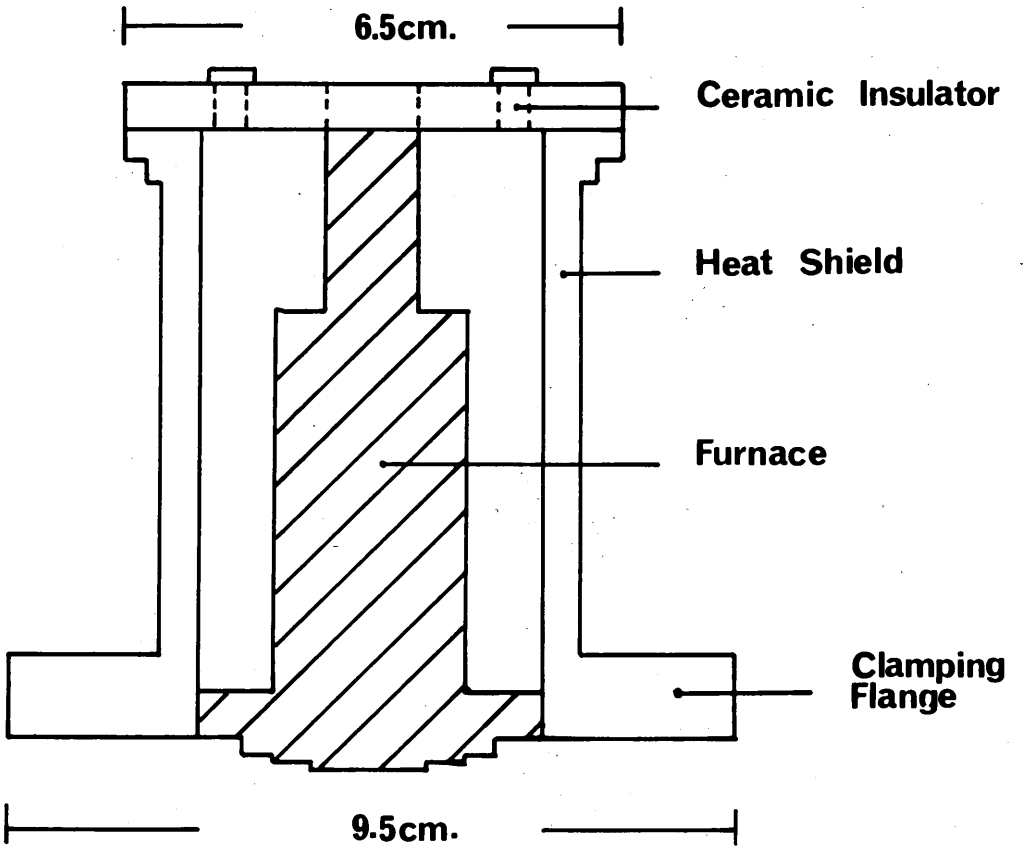


FIG. 4.b. Sectioned diagram showing the position of the heat shield with respect to the furnace core

The only problem with this method was that the nichrome wire had to be wound before the Autostik set hard otherwise the insulation became too brittle and disintegrated whilst winding was in progress. Two small clamps positioned at the top and bottom of the heating element secured the wire and prevented the coils from any slipping which might occur during the initial expansion of the material.

In the first designs it was decided to wind the nichrome wire so that the coils were separated from each other, since there was no insulating layer on the wire. This proved extremely difficult to produce and the resulting coil had a small resistance of 8-10 ohms.

The method finally employed in the construction was to wind the coils so that each separate turn was in contact with the others. Initially the resistance of such a coil was small, i.e. ~1 ohm. By supplying the coil with power while ensuring that the resulting current did not exceed 6 amps the nichrome wire was heated. Once the metal became sufficiently hot a reaction with the oxygen in the surrounding atmosphere occurred forming an oxide layer on the surface of the nichrome wire. As the oxide layer increased, the resistance increased and it was possible to periodically increase the voltage. This oxide coating formed an insulation between successive turns of the wire and resulted in an eventual coil resistance of 10-15 ohms.

A further layer of Refrosil tape was wound over the furnace winding to ensure that there was no thermal contact between the windings and the heat shields.

3.2.1.1 Furnace heat shield

The use of heat shields in the system was to minimise heat losses from the furnace and in so doing reduce the power needed to sustain a given temperature.

The design and location of these shields with respect to the furnace can be seen in Fig. 4.b. The material used for the shield was stainless steel, the flange being spot-welded to the case of the shield to provide a satisfactory means of clamping to the water-cooled specimen table.

The stainless steel casing was spot-welded in position over the furnace as shown in Fig. 4.b. The output leads from the windings were passed through ceramic plugs in the lid section of the casing to prevent contact between the wire and this casing. These output leads were connected to a power supply in conjunction with the temperature controller via internal connectors. Provision was made for further heat shields should the heat losses from the first have been excessive.

3.2.2 Specimen clamping

Fig. 5 shows the individual components which constitute the clamp assembly designed for securing each specimen inside the body of the furnace.

These components were machined from molybdenum, their dimensions being as indicated. The collet and its positioning inside the furnace core are shown in Fig. 6.

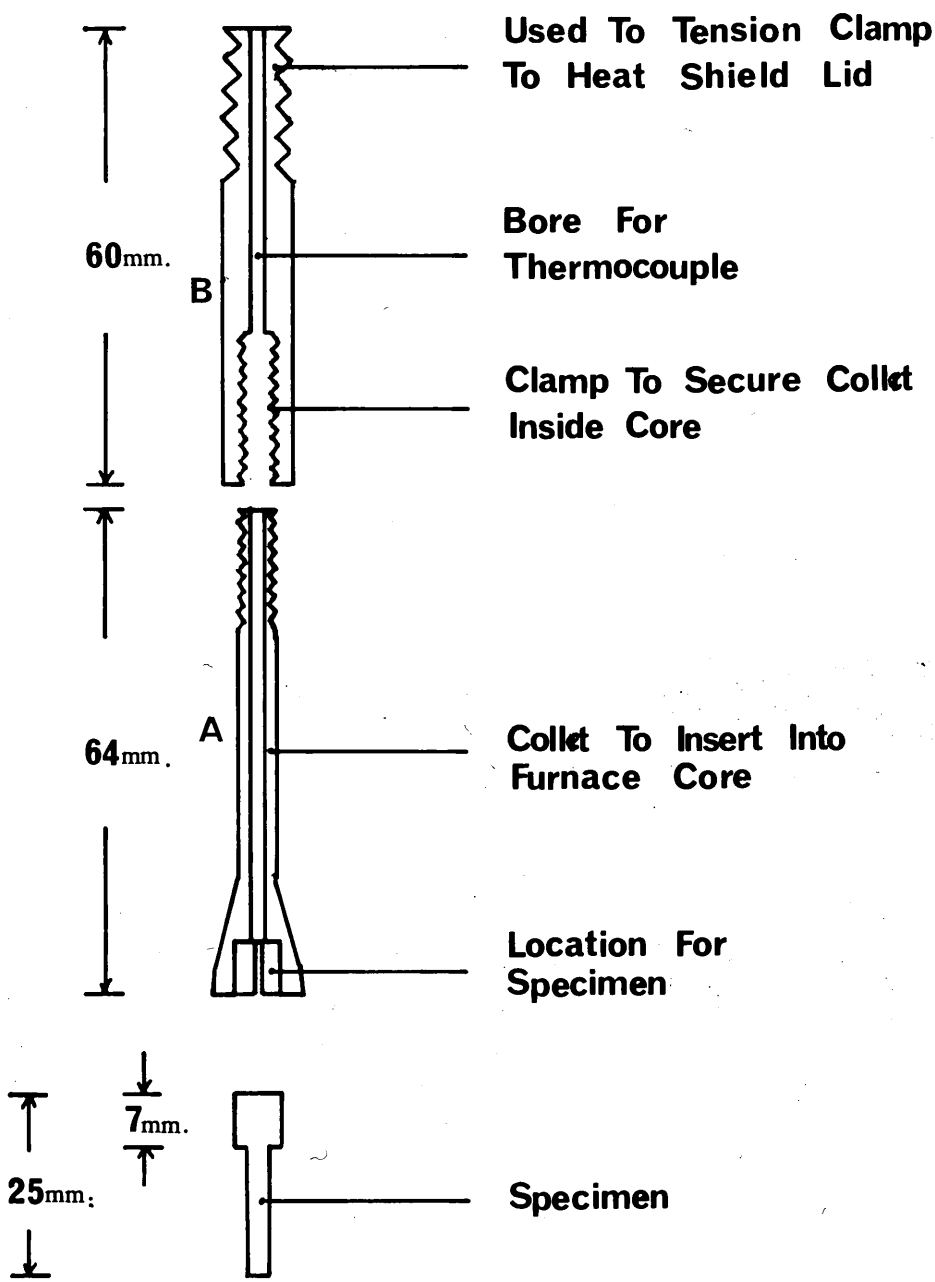


FIG. 5 Schematic diagram of collet and its clamping unit used to secure specimen inside the furnace

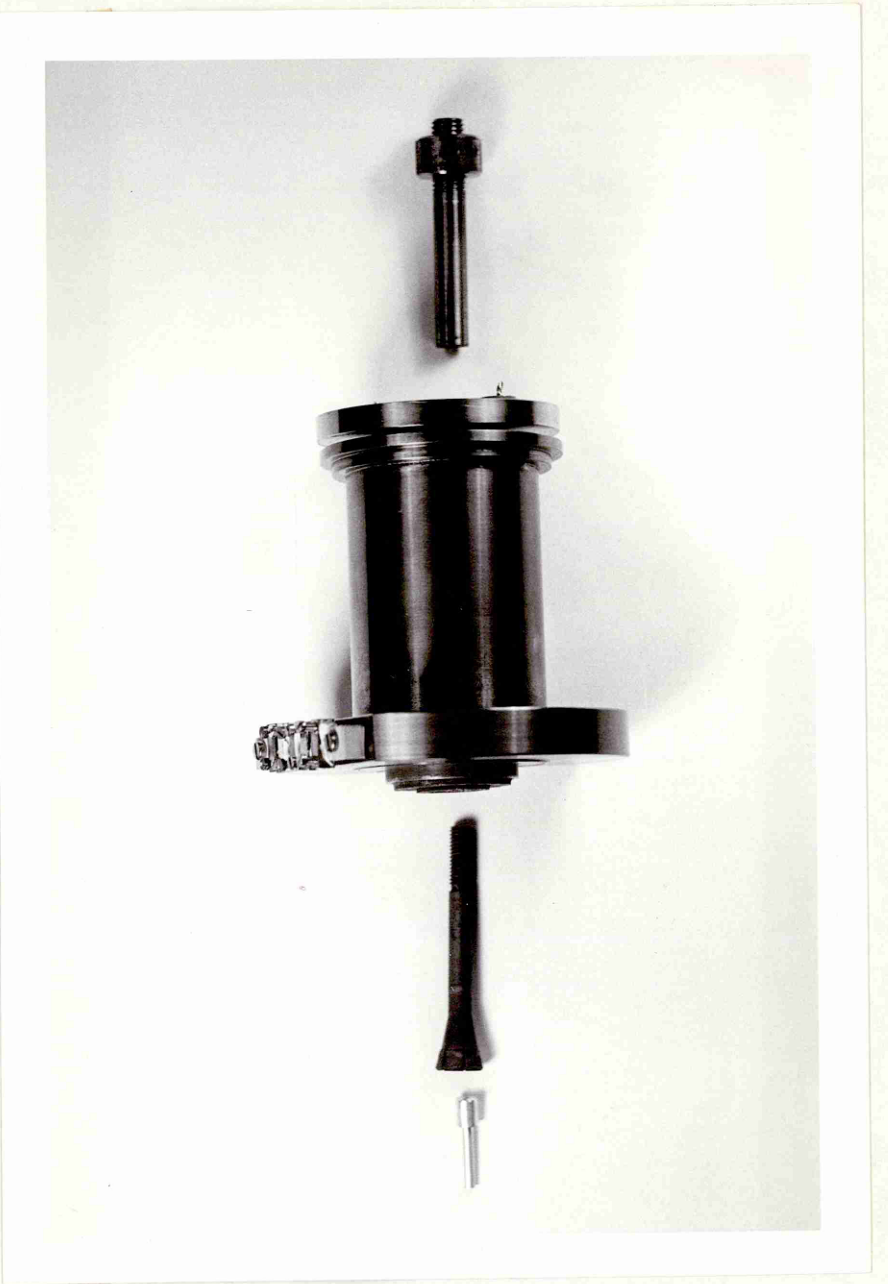

FIG. 6 Furnace assembly with specimen and collet

Section A of the collet is seated inside the conical insert in the furnace core, while section B is projected through the top of the core. The machined thread at the upper end of A allowed B to be screwed into place. As B was tightened the conical base of A was pulled against the walls of the furnace core. Since this section of the collet had slots machined into it, the effect of the tightening was to close these slots, the specimen inside section A then being clamped firmly.

Both sections A and B had a 2mm hole drilled down the centre to allow the insertion of a thermocouple to the specimen head. This thermocouple, plus the two output leads from the furnace winding, were secured to external couplings on the outside of the heat shield.

### 3.2.3 Thermal gradient

To produce mass flow in a crystalline material a flux of heat is required and therefore there must exist a heat source and a heat sink. Section 3.2.1 discussed the production of the heat source, namely the furnace, but the production of the necessary heat sink for these studies was more difficult to achieve, since any further clamping of the specimen would inhibit the mass flow. This necessitated the design of a cooling system which would remove heat from the system without solid contact with the specimen.

#### 3.2.3.1 Choice of coolant

Liquid coolants provided an ideal solution, possibilities being oil or a low melting point metal. Oil did not prove suitable because its temperature could not be held low enough either to prevent leakage past the specimen or to prevent evaporation sufficient to cause specimen deterioration. Oil would also have penetrated into the molecular sieve present in the

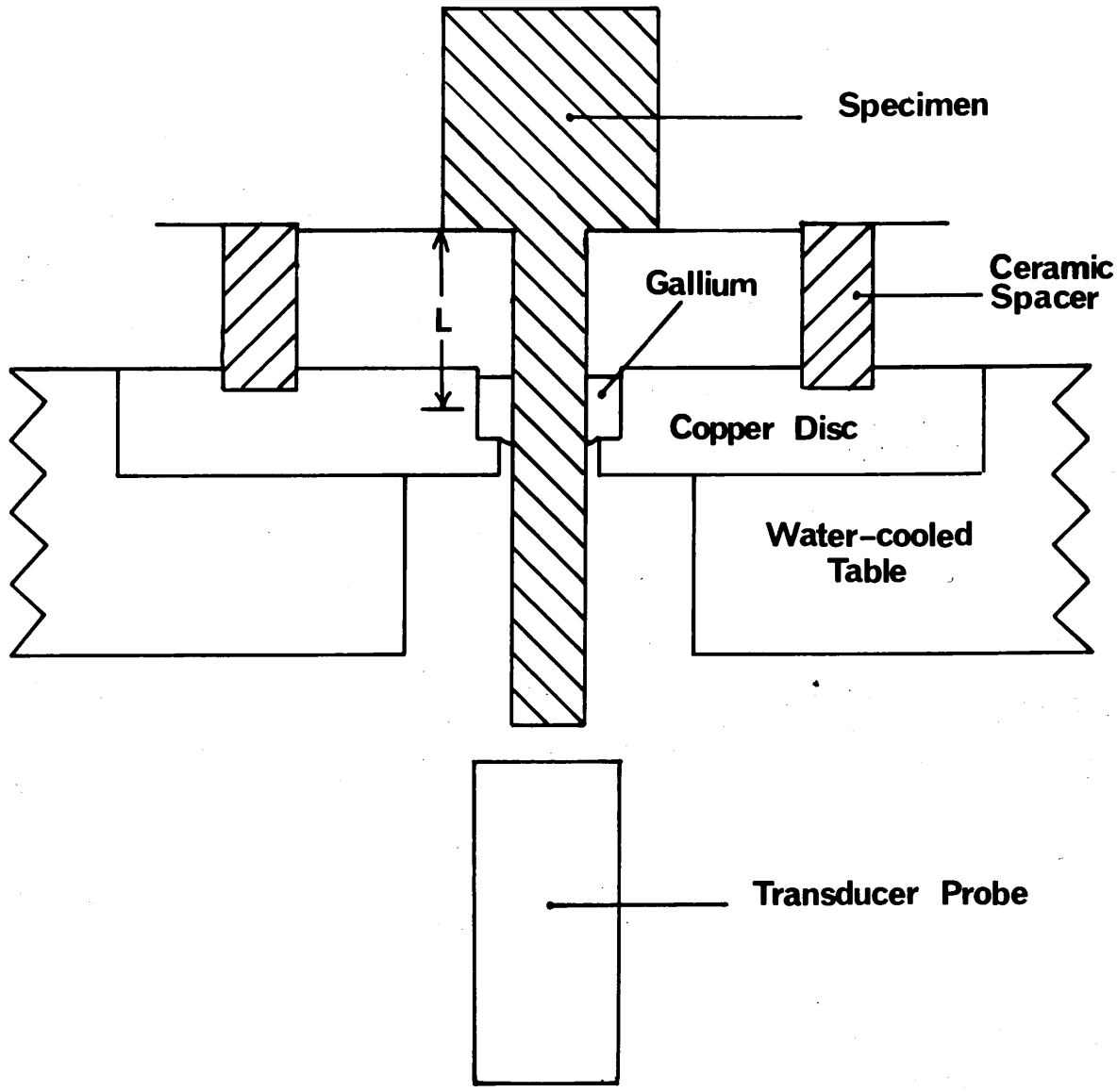


FIG. 3 Sectioned diagram showing the position of the gallium pool with respect to the specimen, copper disc, ceramic spacer and the water-cooled table

sorption pumps causing a reduction of the efficiency of this material during the pumping procedure.

Mercury was also unsuitable since although it is a liquid at room temperature it readily forms amalgams with most metals. Another alternative was gallium which is solid at room temperature but has a melting point of only 303K. Examination of phase diagrams in Hanson (38) showed that gallium reacts with many other metals at temperatures approaching 323K. If, however, the gallium could be used at temperatures below this level it seemed a possible coolant. Gallium is also more favourable than mercury because its saturation vapour pressure is extremely low and no specimen contamination need be expected from reaction between the vapour and hot parts of the specimens.

Experiments were performed by placing test metals in dishes of liquid gallium at various temperatures. With lead the gallium reacted quite vigorously at temperatures greater than 323K whereas with cadmium, reactions occurred at a much lower temperature. Such reactions caused the formation of voids and deep pitting and had this occurred during actual experiments on the effects of mass transport in metals it might have had a considerable effect on the changes monitored by the transducer. Gallium appeared a satisfactory coolant provided the interface temperature between the gallium and the specimen could be kept below 323K.

It was decided therefore to extract heat from the specimens through an annular pool of gallium surrounding the specimen stem.

The experimental arrangement used was based on a triangular stainless steel table, shown in Fig. 7. Inside this table was machined a concentric network of cooling channels which were coupled to a water system capable of supplying water at various temperatures

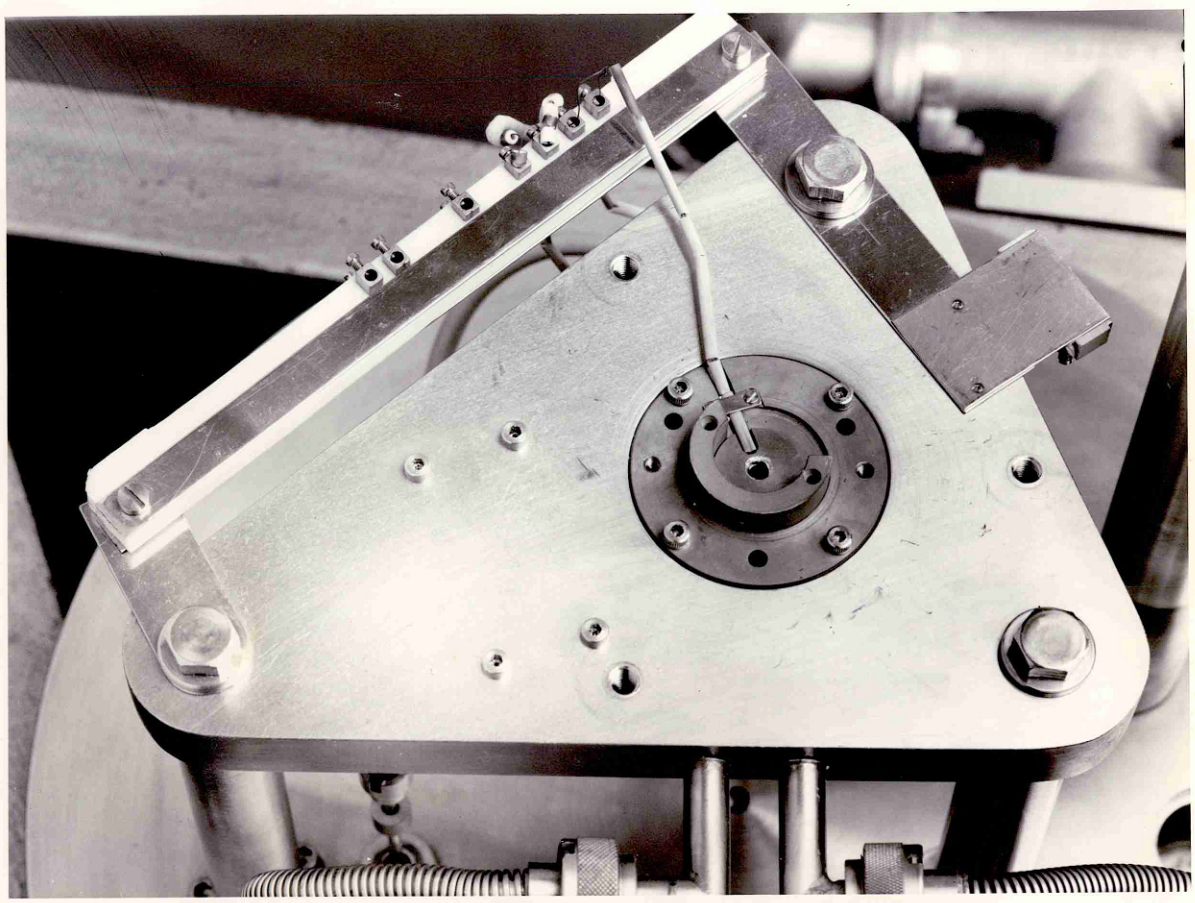

FIG. 7 Triangular water-cooled table with copper disc and ceramic spacer located in position

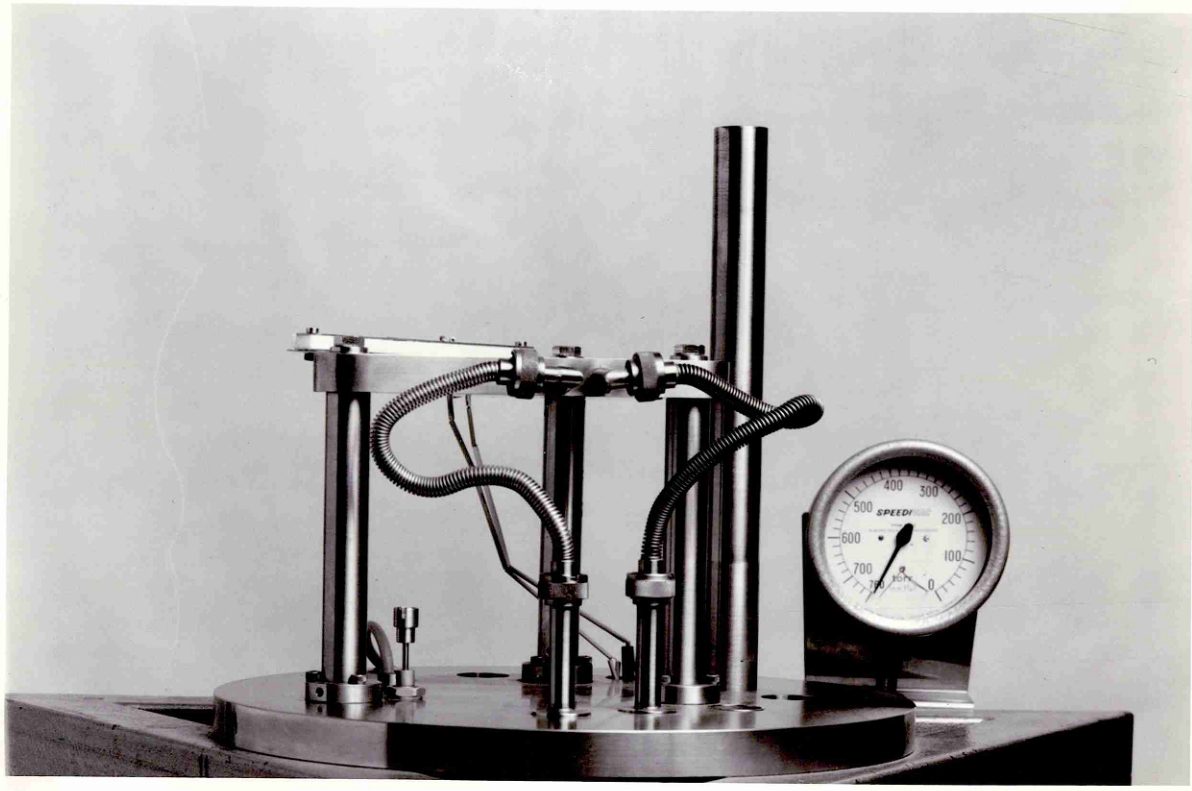


FIG. 8 Water-cooled table positioned above circular base plate

between 283K and 373K. Thermal contact between the water-cooled table, the copper disc and the gallium produced the necessary cooling.

This water-cooled table was supported by three stainless steel legs above a circular base plate, shown in Fig. 8, to allow sufficient space for the positioning of the transducer probe and its supports below the specimen.

To set up an experiment the specimen was passed through the hole in the copper disc, shown in Fig. 3, into a position where its end faced the transducer probe. Once the specimen rod had been positioned and clamped, liquid gallium was injected into the well formed between the disc and the specimen.

3.2.3.2 Problems with coolant

Since gallium is solid at temperatures below 303K, care had to be taken when inserting the gallium around the specimens. Insertion was performed by means of a hypodermic syringe and metal needle which were pre-heated to a temperature above 303K. The regions which would contact the gallium had to be maintained at a similar temperature otherwise the gallium would have solidified making further insertion impossible. This was done by passing hot water through the circuit normally used for cooling.

Insertion of the gallium inside the well surrounding the specimens created an extra problem, as small globules of the gallium sometimes penetrated down onto the probe face. Wide bore needles were therefore used for gallium injection and the injection rate was steady to inhibit break-up into globules.

The cooling system then had a dual purpose: at the times when the furnace was inactive it acted as a heat source supplying a temperature greater than 303K, but when the furnace was active it acted as a heat sink, removing the heat from the specimen and producing the necessary thermal gradient. While the experiments were in operation the gallium-specimen interface temperature was vigorously maintained in the range 303K to 323K and as close to the lower temperature as possible.

### 3.2.4 The Transducer

A major experimental problem is the small size of the displacement which takes place during thermomigration. A very sensitive, though not necessarily accurate, technique is required and to measure the variation in specimen lengths, which can be small fractions of a micron per day, a capacitative transducer was purchased from Wayne Kerr & Co. This instrument used capacitative probes driven by a 16 kHz oscillator, measurements being displayed continuously on a calibrated meter and brought out as an analogue voltage for external monitoring purposes. Two identical channels were provided, although they could not be used simultaneously. In this work, one of these channels was used for calibration purposes.

The instrument had a working range of 20 $\mu$m and a sensitivity better than $\pm$ 0.05 $\mu$m.

#### 3.2.4.1 Probe geometry

The probe for use with the instrument consisted of an inner electrode, guard ring and an outer metal sleeve. This probe was of circular cross-section with a plane end surface and was designed primarily for measurement of flat surfaces.

Because of the limited working range of the instrument - the separation of the probe from the specimen surface being only 20 $\mu$m maximum - it could not be used with rough surfaces, nor could it be used at an angle to the detector surface since the probe diameter was 6mm, and at an angle of $4^{o}$ would have made contact with the specimen before its central part came within the working range. The minimum usable separation between specimen and probe was 4 per cent F.S.D. or 0.8 $\mu$m.

3.2.4.2 Monitoring transducer output

Since during these experiments temperature fluctuations could cause a specimen expansion comparable with the change expected during hours of thermomigration, the transducer output was monitored through an integrating voltmeter. It was hoped in this way to eliminate noise from this source for all except the very lowest of temperature oscillation frequencies and integration times of some hours were envisaged. In the event, however, temperature stability was good enough to make fifteen-minute integrating periods quite adequate.

This integrating millivoltmeter was used in conjunction with a printing counter which totalised in synchronism with the integrator. This totalised integral was printed out at selected intervals of time.

A further visual means of observing the drift velocity was obtained by direct monitoring of the transducer output by a chart recorder. The complete monitoring system is shown schematically in Fig. 9.

3.2.4.3 Manual control of the transducer probe position

Positioning of the transducer probe close to the specimen

face was a very delicate manoeuvre. It was essential that the two faces remain accurately parallel and, therefore, because the specimen was fixed, any movement of the probe must be parallel to the vertical axis. Since specimen sizes did vary, provision was made for the transducer probe to be moved manually to give a probe-specimen distance within the F.S.D. of the probe, that is, 20 microns.

It is not a simple matter to control mechanical movements to such tolerances and it proved necessary to develop an unusual mount for the transducer probe. The device is based on an elastically deforming parallel movement device of the type described by Jones (39).

Jones states that the most effective anti-distortion mounting for translation is the parallel spring movement, which was originally pioneered by E. M. Eden at N.P.L. and which is shown in Fig. 10.

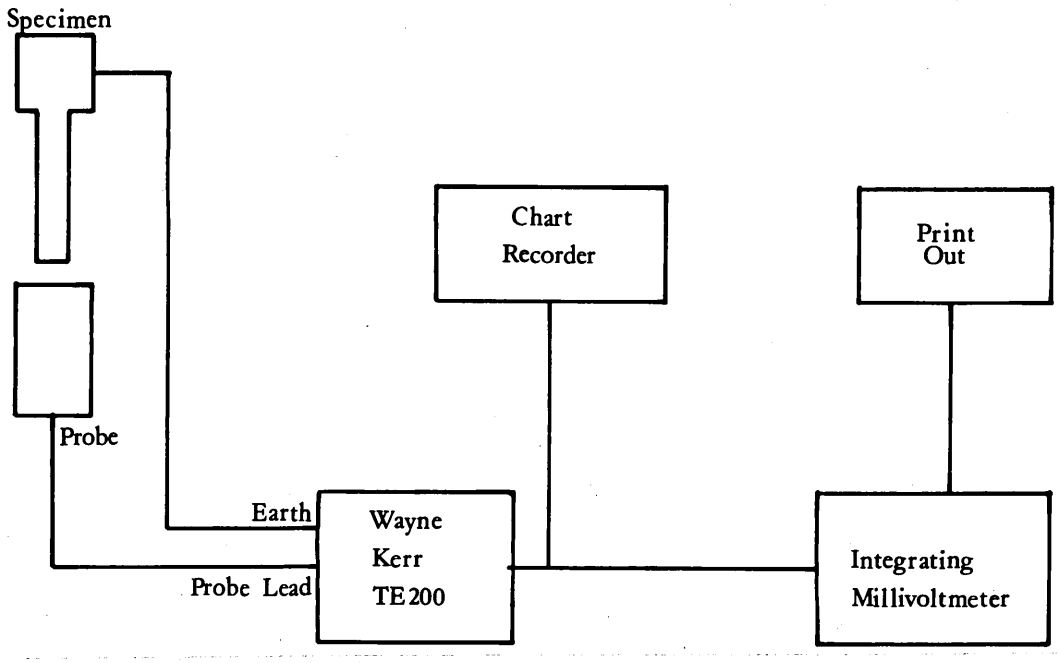


FIG. 9 Schematic diagram showing the monitoring system used to record specimen length changes with respect to time

It comprised three blocks, A, B and C, with A and C connected by two parallel spring strips 1 and 4, and C and B connected by two similar strips 2 and 3. If block A is fixed, any sideways movement of B will deflect C in a direction parallel to B and A.

The actual design used in this work is shown in Fig. 11 and varies from Fig. 10 in that the springs connecting the three blocks were rotated through an angle of $90^{o}$ so that blocks C and B were free to move only vertically. The transducer probe was located through a hole drilled in block C and blocks A and B had extension arms as shown in Fig. 12. This diagram shows the parallel movement device secured to the water-cooled table via block A, which as in Fig. 10 remained in a fixed position. Therefore if block B is caused to move up or down in the vertical mode, block C will move in the same direction parallel to B. Manual positioning of the transducer control was by movement of block B. To allow this the design incorporated extension arms to blocks A and B. By screwing R through a thread cut into A

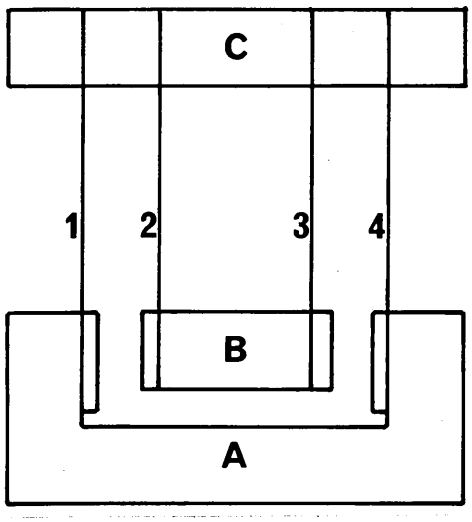


FIG. 10 Schematic diagram showing the elastically deforming parallel movement device used by E. M. Eden at N.P.L.

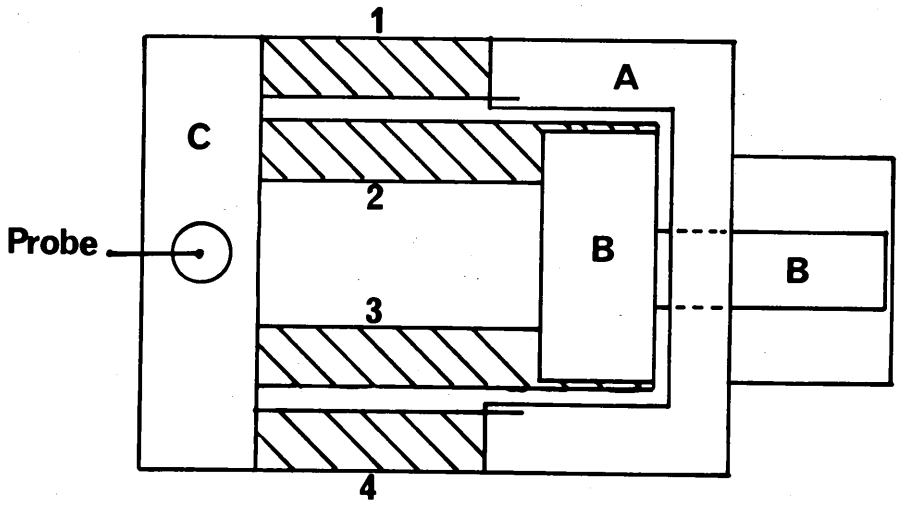


FIG. 11 Schematic diagram showing the parallel movement device developed during this study to ensure precise positioning of the transducer

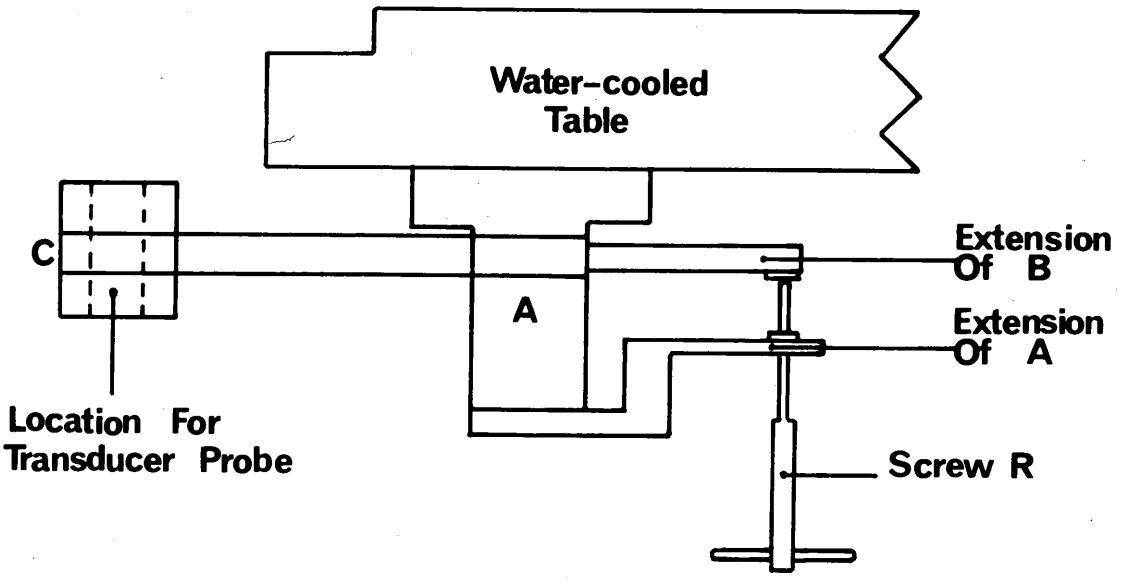


FIG. 12 Diagram showing the parallel movement device secured to the base of the water-cooled table

so as to press on B, B could be moved relative to the fixed position of A. By a clockwise movement of R onto the extension of B, B and C both were raised in a truly vertical motion An anti-clockwise movement had the opposite effect. By careful manipulation of the screw R the transducer probe could be positioned to within $\pm$ 1 $\mu$m at any required distance from the specimen face.

To manipulate the screw R from a position outside the vacuum system, which enclosed the entire apparatus, a rotary shaft vacuum seal was led through the base plate and attached to the linkage of R.

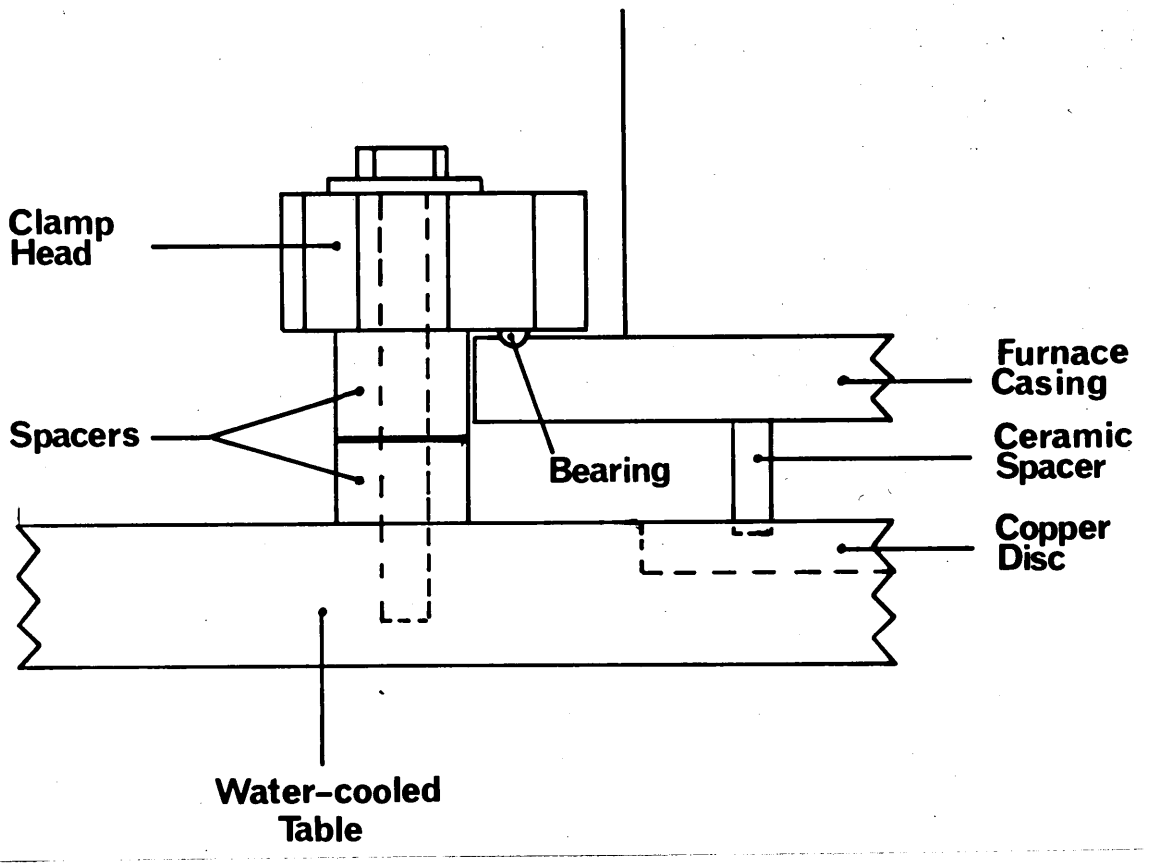


FIG. 13 Sectioned diagram showing one of the clamps developed to secure the furnace section to the water-cooled table

### 3.2.5 Securing the complete structure

The furnace and its heat shield were clamped to the triangular water-cooled table by means of three specially designed clamps. This clamping was performed by three spring-loaded ball bearings in contact with the flange spot-welded to the furnace heat shield. A schematic diagram of one of these clamping posts is shown in Fig. 13. Fig. 14 shows the furnace secured by the three clamps to the water-cooled table.

The spring loading was needed to accommodate any initial movement of the system which might occur due to thermal expansion. The 'dimples' in the flange housed the ball bearings and were equidistantly spaced around the circumference. The ceramic disc determined the spacing between the furnace and the copper disc, so governing the 'effective' length of each specimen.

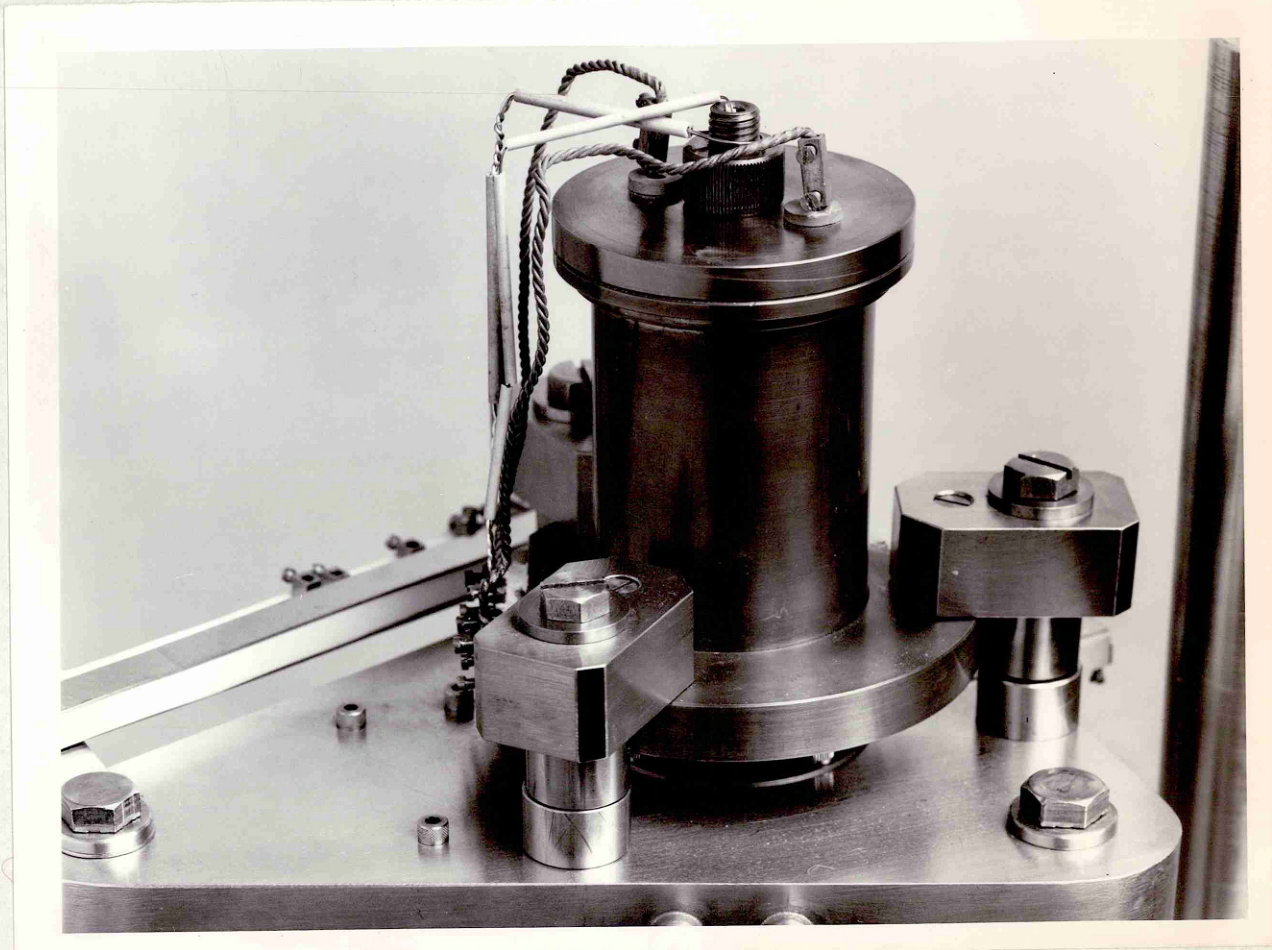

FIG. 14 Furnace assembly secured to water-cooled table by three clamps

### 3.2.6 Necessary precautions

#### 3.2.6.1 Centralising specimen

It was found difficult reliably to locate the specimens through the hole in the copper disc, and damage against the walls of the copper was frequent. To overcome this problem a jig was constructed to centralise the specimen as it passed through the copper onto the probe face. A diagram of this jig is shown in operation in Fig. 15. The jaws of the instrument clamp around the furnace casing while the hole at the far end is located over the stainless steel pipe used to cool the final heat shield. By lowering the jig down the length of this pipe, with the specimen and furnace securely clamped, it was possible to place the ceramic spacer and the specimen accurately through the copper cooling disc.

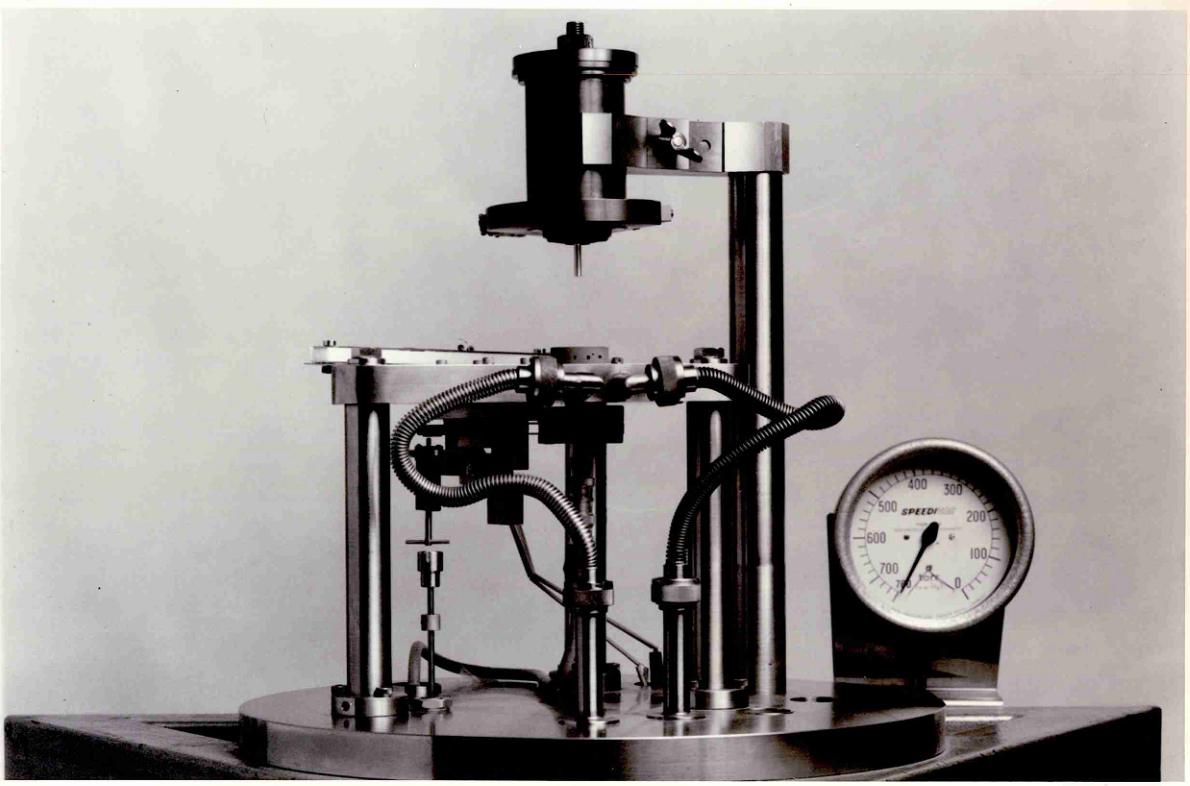

FIG. 15 Locating the furnace and specimen onto the ceramic spacer, using centralising jig. Also shows parallel movement device secured underneath water-cooled table

3.2.6.2 Mounting transducer and surface condition

It proved necessary to check the alignment of the transducer probe before each new specimen was mounted in the rig. This was done by first removing the probe from the parallel movement device and the copper disc from the water-cooled table. A stainless steel disc of the same dimension as the copper was positioned on the table. A hole in the disc, the same diameter as the probe, allowed insertion of a stainless steel rod through the disc and into position in the parallel movement device. If the hole in the disc and the movement device were not aligned, adjustment was made of the spring positions. It was found that this procedure was generally unnecessary, but it provided a satisfactory rapid check of this crucial alignment.

3.2.7 Vacuum system

To obtain an argon atmosphere, the complete system was enclosed in a bell jar. The air had first to be evacuated from this jar and the pumping system used is shown in Fig. 16. Sorption pumps were used to keep hydrocarbon contamination of the equipment to a minimum. The two used were capable of providing pressures to $10^{-3}$ torr.

3.3 Control and measurement

3.3.1 Furnace control

Control of the furnace was by an A.E.I. fully proportional temperature controller activated by a chromel/alumel thermocouple mounted inside the specimen close to its shoulder. The lower reference point was derived from a Sunvic cold-cell at a constant temperature of 318K. The control point could be set to within $\pm$ 0.5K, and after careful adjustment of the proportional bandwidth, would hold to within $\pm$ 0.1K over periods of days.

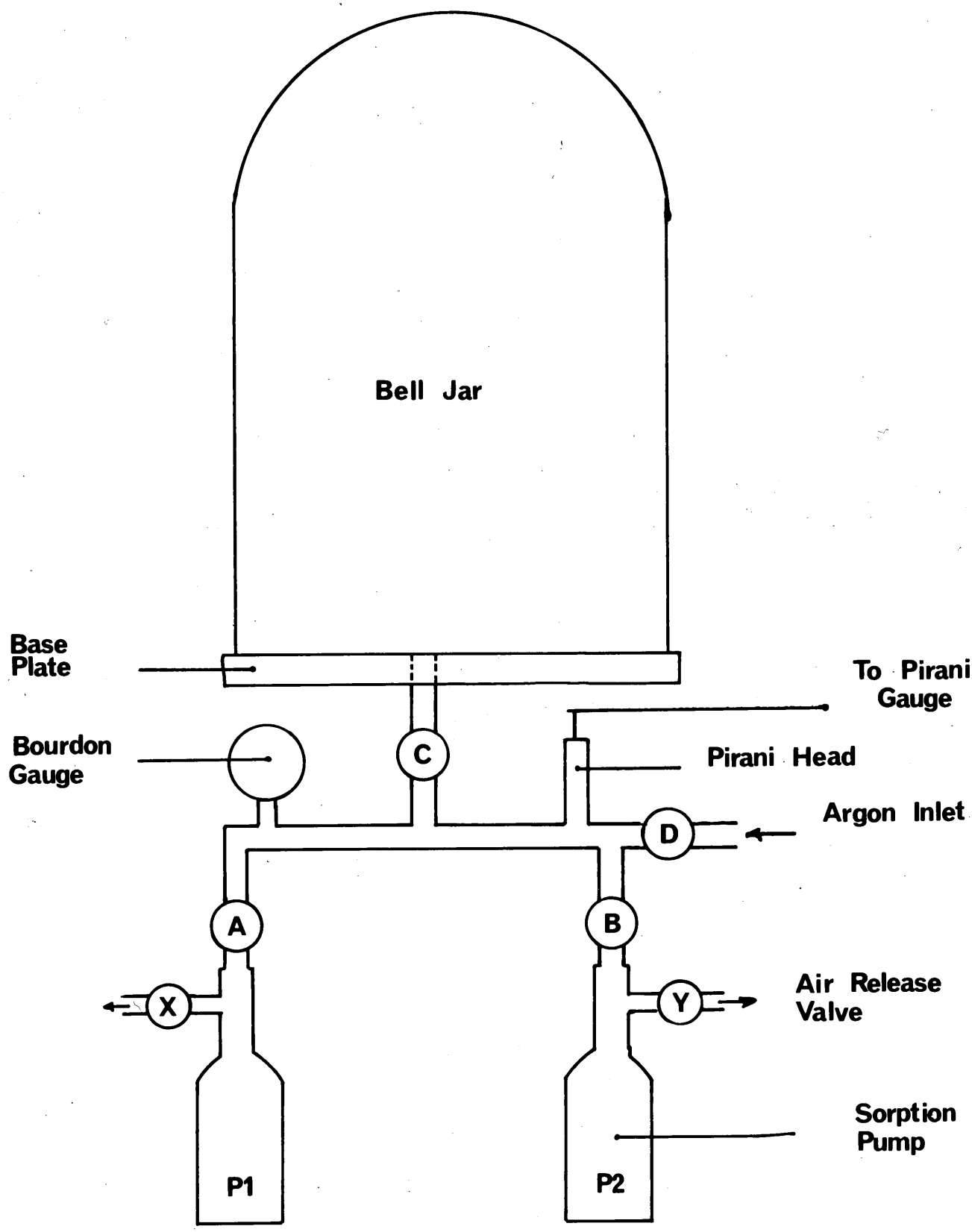


FIG. 16 Diagram showing the vacuum system

### 3.3.2 Measurement of the temperature

This type of experiment relies heavily on the precision with which specimen temperatures can be established.

In the previous section details of the furnace control system were discussed. A thermocouple positioned inside the shoulder of each specimen controlled the power supplied to the furnace windings. In this way a stable and measurable temperature could be maintained at one point in the specimen head.

For analysis of the data it was necessary to know the temperature distribution within the specimen stem. Ideally this would have been done by continuous measurement of temperatures at a series of points along the stem so for initial work three thermocouples were spot-welded at points along the specimen stems.

These three thermocouples were very fine platinum-platinum/rhodium wires spot-welded to the specimen surface at measured distances from the shoulder, whilst the separate wires of each couple were brought out through holes drilled into the ceramic spacer to be monitored continuously by digital voltmeters. Since the distance of each couple was known an extrapolation of the results could be achieved to obtain a value for the gradient between the shoulder and the mid-point of the gallium.

All the thermocouples, both the controlling couple and the gradient-measuring couples, were calibrated regularly between specimen studies and each couple was monitored via a cold-cell which compensated for any fluctuations which might occur in the room temperature.

## 3.4 Conclusion

This chapter has discussed in full the design and construction of equipment to allow measurement of dimensional changes in metal specimens created by biased atomic motion in a temperature gradient. Such changes may be related to the heat of transport of the metal.

The next chapter describes the specimen preparation and the early studies performed on lead specimens. Also in this chapter mention is made of the early teething problems with the technique and the ways in which they were overcome.

# CHAPTER 4

## Specimen preparation and early observations

# CHAPTER 4

## Specimen preparation and early observations

### 4.1 Introduction

Chapter 3 describes the apparatus designed and produced to make a detailed study of the effect of thermal diffusion on pure metals. This chapter deals with the results obtained from early studies and the initial preparations of each specimen necessary before subjection to a thermal gradient. These preparations include the machining of the specimens into the required shapes and sizes and the annealing of the polycrystalline structures.

The three metals studied in this work are lead, aluminium and cadmium; measurements were obtained for dimensional changes in both the single and the polycrystals. It may be noted that all these materials have a close-packed structure: lead and aluminium are face centred cubic metals whilst cadmium is hexagonal close-packed.

Cadmium, since it is a hexagonal structure, has two principal directions along which diffusion can occur: parallel to the C axis and perpendicular to the C axis. This study examines diffusion along the direction parallel to the C axis and results are compared with those obtained, for the diffusion coefficient D, by Wajda, Shirn and Huntington.

### 4.2 Specimen preparation

The length and major diameter of all the specimens were fixed mainly by the clamping procedure and the range of positions accessible to the transducer probe. Some small variations in specimen length were possible but there were limitations set by the machining operation. The main freedom in specimen geometry was therefore in the diameter of the thin specimen stem.

It was known from marker-motion experiments, that specimens with small diameters exhibit lateral dimension changes, as predicted by Penney in his elastic-plastic theory of deformation. To avoid the possibility of such changes in our work specimens with length to diameter ratios in the range 1 to 2 were chosen.

With these sizes some opportunity was given to check the predicted diameter variations of the Penney model and also through the length changes to take some account of creep should this emerge as of importance.

### 4.2.1 Machining of single and polycrystal specimens

The polycrystalline materials of 5N purity were obtained from Johnson Mathey in rods 150mm long by 7mm diameter. These rods were machined to the necessary dimensions in a precision lathe, great care being taken to ensure that the bottom face was flat enough to permit operation of the transducer.

Single crystals of lead, aluminium and cadmium were obtained from Metals Research Ltd. The metals were delivered in rod form, 7mm in diameter and 25mm long with a purity better than 5N. The orientation of these specimens varied depending on the metal, from random for lead and aluminium to an orientation parallel to the C axis for cadmium.

Since the specimens already had the correct length, the only machining necessary was in producing the narrow stem section. To do this, machining in the precision lathe used for producing the polycrystalline specimens would have proved unsuitable since the heat and strain produced on the crystal by the lathe tool would have caused recrystallisation at the temperatures of the experimental runs.

A Servomet spark cutter manufactured by Metals Research Ltd. was therefore used for all cutting and shaping of single crystals.

This Servomet removes metal from the area in the immediate vicinity of the tool, without mechanical contact with the crystal, by generating a series of controlled spark discharges between the tool and the specimen; each spark removes a small crater of metal by melting and vapourising, and by the use of suitably shaped tools metal can be removed to provide almost any finished shape. This spark erosion process has a cutting accuracy of about $\pm$ 0.005mm.

4.2.2 Annealing of polycrystal specimens

The grain structure of a polycrystal may be changed by annealing at high temperatures. Since such grain movements may produce small overall changes in the dimensions of a specimen they represent an effective noise source to the present experiments. It is therefore necessary to produce a very stable grain structure in the polycrystal specimens. The procedure for this was to anneal cut specimens at temperatures very close to their melting point.

This was done by vacuum sealing the specimens of each material in a number of quartz envelopes at a pressure of $10^{-1}$ torr, to prevent oxidation of the specimen surface at high temperature. These quartz envelopes were then mounted vertically in a furnace so that the specimens were annealed suspended under their own weight and supported within the envelopes by wire clamps securing each specimen at the larger diameter section, so preventing them from slipping from the vertical position. Annealing of the specimens in any other mode would have created 'sagging' due to the softness of the structure at such high temperatures.

The temperature field inside the silica tube of the furnace was plotted to ensure that the two specimens in each quartz envelope were subjected to a uniform temperature. This was done by insertion of two thermocouples at each end of the tube and measuring the temperatures at points along the tube.

The lead specimens were initially annealed at a temperature of 593K for two to three hours but later this annealing period was extended to six hours: reasons for this increase in the annealing time are discussed later.

The aluminium polycrystal specimens were annealed at 923K for six hours. Once the annealing was complete the specimens were allowed to cool slowly within the quartz envelopes.

## 4.3 Preparatory procedures

The first trial study was performed on a polycrystalline lead specimen which had been annealed at 593K for three hours and then had had its surface cleaned by a light etch. The overall length of this specimen was 25mm, the thin stem having a diameter of 3mm and an 'effective' length of 5mm. The head of this specimen, that is, the 6mm diameter end, was positioned inside the molybdenum collet and inserted in the furnace. As mentioned earlier it is the height of the ceramic spacer that governs the 'effective' length of each specimen and in these early experiments the height of the spacer was 6mm.

Once the specimen was positioned inside the furnace, three platinum-platinum/rhodium thermocouples were spot-welded to the surface at measured distances along the 5mm length. The controlling thermocouple was passed through the hollow collet and positioned in the head near the shoulder. This controlled, via the temperature controller, the furnace temperature, and,

therefore, the temperature at the top of the specimen. Having checked the calibration of the thermocouples, the furnace section and the ceramic spacer were located onto the copper disc as shown in Fig. 3 . The clamps retaining the furnace to the stainless steel table were then applied and the gallium inserted, via a hypodermic needle, to the well around the specimen. The 'effective' length was then the distance between the specimen

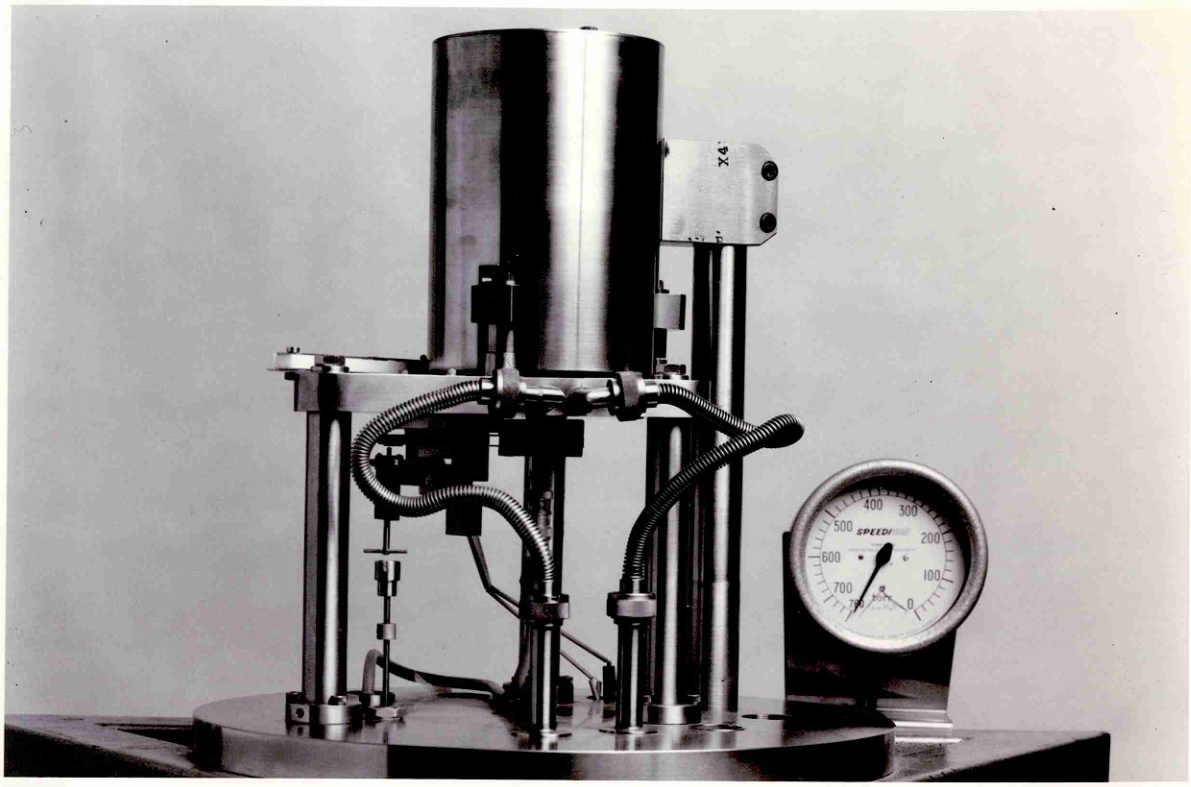


FIG. 17 Photograph showing the position of the final heat shield.

shoulder and the point of the specimen at half the gallium depth. The final heat shield shown in Fig. 17 was positioned and an argon atmosphere was then supplied to the bell jar.

4.3.1 Original studies on lead

Using the parallel movement device, the transducer face was traversed to a position 7 microns from the specimen face. The transducer had already had its calibration checked by using a unit supplied by Wayne Kerr.

Warm water, 304K, was circulating through the cooling table to ensure that the gallium remained in a liquid form, before any heat was applied to the specimen.

The furnace was switched on, and allowed to produce a modest temperature of 423K at the specimen head. The probe at this stage was switched on simply to observe the expansion which occurred, and to check on the operation of the equipment. This temperature was kept constant for a few hours to allow the furnace to settle, and then increased by 50K each hour. The transducer probe was switched off at this stage and only reactivated when the temperature of the specimen had reached 573K. The temperature at the gallium-lead interface at this point had reached 333K, this value being deduced by extrapolation from measurement of the three thermocouples.

An hour after the linear gradient had been achieved, the transducer equipment was reactivated. Data from the probe were observed via the print-out integrating millivoltmeter, operating on a fifteen minute print-out rate, and a chart recorder. The

output from the transducer was in the $\pm$ 1 volt range and the count rate on the millivoltmeter at a 300mV range of 3/sec.

The behaviour of the transducer over the next few hours was extremely erratic and no sensible results were recorded. The furnace temperature was reduced and the monitored output from the transducer displayed on a chart recorder, where it was seen that the erratic behaviour still persisted but to a lesser degree.

The three thermocouples attached to the specimen appeared to function correctly and a linear thermal gradient was recorded but unfortunately no measurements of specimen dimension changes were observed due to the behaviour of the transducer.

Because of doubts that the thermocouple wires might have been responsible for the undesired effects, this specimen was replaced by a similar sample this time without thermocouples so no recording of the thermal gradient could be made during this experimental study. A temperature of 553K was achieved at the specimen shoulder and the transducer was set into operation. The erratic behaviour had disappeared and a seemingly reasonable specimen length change with time was displayed on the chart recorder.

Since the probe did not function correctly with the thermocouple attachments it was assumed that the presence of these platinum-platinum/rhodium wires upset the earthing conditions which were necessary between the probe and the specimen. Replacing the thermocouples on the next specimen proved this point as the erratic behaviour returned. It became obvious, therefore, that we could not measure the thermal gradient and the length changes simultaneously and an alternative arrangement had to be found.

4.3.2 The need for dummy specimens

Instead of working on one specimen, two specimens were machined and annealed. One was used for the mass flow examination, the second to establish the gradient. These 'dummy' specimens had three thermocouples spot-welded along their lengths and were subjected to the same temperature fields as before. A metered quantity of gallium was inserted into the well through which the narrow stem of the specimen projected. Hot and cold end temperatures of the specimens were varied via the controller and water bath temperatures, and the temperature gradients were monitored by the three thermocouples. Repeated mounting of these specimens showed a consistency of thermal contact which preserved the relationships between the outputs of the thermocouples in the specimen head and coolant water and those of the thermocouples spot-welded to the stem to better than $\pm$ 0.5K.

By using such 'dummy' specimens before each examination, reproducible values for the temperature gradients were obtained in terms of the temperatures in the specimen head and the coolant water. The three platinum-platinum/rhodium thermocouples were calibrated each time using a triple point cell. In use the cold-cell mentioned in connection with the furnace controller compensated for room temperature fluctuations.

4.3.3 Further measurement on lead

A fourth lead specimen, having the same dimensions as the previous three, was loaded into the equipment, without the platinum-platinum/rhodium thermocouples attached. A temperature of 573K was obtained and the transducer was activated once sufficient time had elapsed to enable a linear thermal gradient to become established.

Results over the next six hours are shown graphically in Fig. 18. The results for this plot of length change versus time were obtained from the integrating millivoltmeter, where the count rates per fifteen minutes were converted to distance measurements.

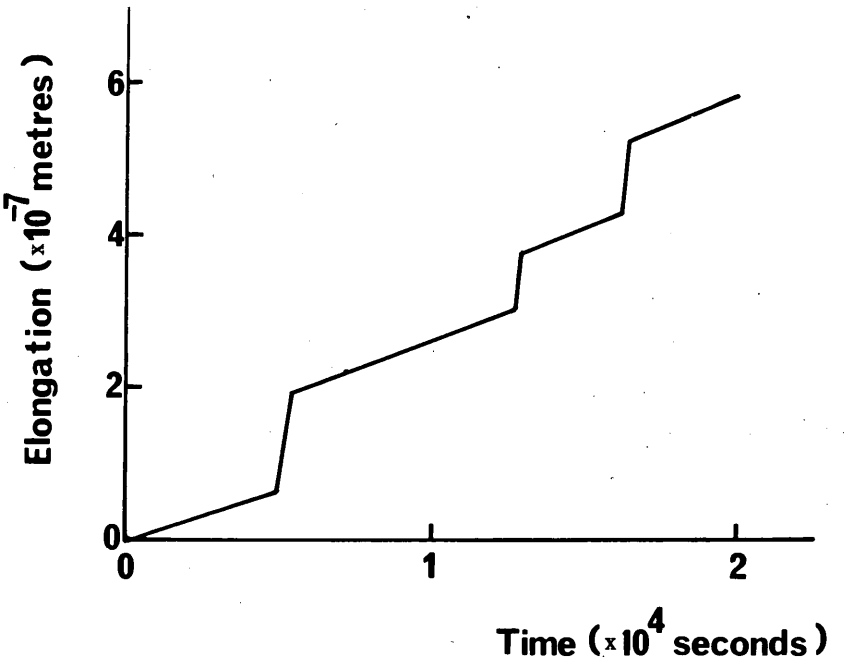


FIG. 18 Elongation of the lead specimen with time

One would expect a linear length change with time, but this is only true if the steps in the gradient are ignored. After these steps, which occur over several minutes, the plot returns to a steady gradient parallel to the previous gradient. Chang and Grant (40) observed very similar movements when studying metals at temperatures close to their melting point where grain boundaries become glissile so that individual grains slide over one another in a jerky fashion, so causing these sharp steps on the graph.

Mclean (41) describes two possible causes for these movements. One is that a certain amount of deformation energy is stored in the grains in the form of dislocations, and grain boundaries will tend to migrate into the grain having the larger stored energy. The other is that since grain boundaries hold up dislocations, dislocations will push grain boundaries.

In later experiments with polycrystals of lead, the drift velocity obtained from this specimen at 573K agreed well with later results at the same applied temperature and it was only these sharp steps which appeared as unknown phenomena.

## 4.4 The problems encountered

### 4.4.1 Grain movement and temperature stability

These gradient changes had two possible causes: temperature instability or grain movement. It was possible that the grains were moving through the material, eventually dissipating at the surface causing small, rapid changes in the specimen dimensions.

As a check on the temperature stability the output from the thermocouple in the specimen head was monitored using a Tinsley potentiometer. After balancing, the galvanometer output of the potentiometer was displayed on a chart recorder, thus giving a backed-off and sensitive record of temperature fluctuations. It was found that the temperature varied by $\pm$ 1K over a ten-minute period.

This fluctuation was completely unacceptable due to the thermal expansion which, on the transducer, was indistinguishable from a flow due to thermomigration. As the observed temperature change would result in a length change of 0.3 microns or $\pm$ 0.15 microns per ten minutes, this was potentially a very serious

problem and therefore the temperature controller was very carefully adjusted to a sensitivity just short of oscillatory control. In this condition a temperature stability of better than $\pm$ 0.125K over a range 473K to 583K was obtained. These minor fluctuations occurring frequently over one-to two-hour periods, gave possible expansion rates which resulted in changes in length by $\pm$ 0.02 microns. It will be shown later how these fluctuations affect the transducer output, and how these effects are negligible when compared with the drift rate values.

Observation of the drift rate after these adjustments showed a far more stable gradient, but jumps still occurred occasionally. It was then decided to try an increase in the annealing time for the specimens from two to six hours at 593K in the furnace. Two new lead polycrystalline specimens, of the same dimensions, were treated in this way.

One of these specimens, without the gradient measuring thermocouples attached, was subjected to a thermal gradient and the resulting drift rate, monitored by the transducer probe, was observed using a chart recorder and the integrating voltmeter. This time the distance-time plot was unaffected by sharp jumps and a well defined gradient was obtained, suggesting that the steps were due to sharp increases in the specimen length caused by grain movement.

### 4.4.2 Pitting

On withdrawing the first specimens from the apparatus it was noticed that severe pitting had occurred at the gallium-lead interface. Since such an effect could modify the specimen length this was another potential source of error.

There were two possible solutions to this problem: either the lower end temperature governed by the coolant water temperature could be reduced, or the region of the specimen in contact with the liquid gallium could be coated with a higher melting point metal, such as gold.

It was decided to reduce the coolant temperature and run experiments with the water flowing at a temperature of 283K. This reduction in temperature had to occur after the specimen stem had been raised to a temperature greater than 303K, so that the main body of the gallium did not solidify. By this adjustment the rate of chemical reaction at the cool end of the specimen was greatly reduced at high furnace temperatures. Observation of the specimen after this exposure to gallium showed no pitting over a four-day period.

A number of experiments were carried out under these conditions but in a later study a lead specimen was coated with gold at the gallium interface as a check on the reliability of this method.

With this modification of procedure the overall system was thought sufficiently reliable to perform detailed studies of thermal diffusion in lead specimens and results obtained from both single and polycrystals are detailed in Chapter 5.

## 4.5 Conclusion

In this chapter a detailed description of specimen preparation has been given. A discussion of various teething problems and the modifications necessary to minimise these problems have also been given.

Chapter 5 deals with the presentation of the results obtained from the three metals under observation and the further preparation given to the aluminium and cadmium specimens.

# CHAPTER 5

## Results obtained from studies of thermomigration in lead, aluminium and cadmium

# CHAPTER 5

# Results obtained from studies of thermomigration in lead, aluminium and cadmium

## 5.1 Introduction

Chapter 4 detailed the initial preparation of the specimens and the start-up problems that were discovered during early studies on a lead polycrystal specimen. Once these problems had been overcome a detailed study of thermomigration in the three metals was possible.

This chapter details the early experiments on lead polycrystals followed by the data obtained from single crystal specimens. Data from aluminium and cadmium specimens are detailed later in this chapter as well as an interpretation of grain boundary diffusion observed during the study on the lead specimens.

## 5.2 Thermomigration in lead

In the study of thermomigration in lead, four specimens were used of varying geometry and structure. The results from the first polycrystal specimen are discussed in detail and the remaining three specimens, two polycrystals and a single crystal, are discussed in a following section where the degree of internal consistency obtained during these studies is examined.

### 5.2.1 Lead polycrystal I

The initial polycrystal specimen had a mean grain diameter of $8.5 \times 10^{3} m^{-1}$, a minor diameter of 3mm and an overall length of 25mm. The 'effective' length, between the shoulder of the specimen and the cool region passing through the gallium pool, was 5mm. This specimen was examined under ten different annealing conditions with peak temperatures ranging from 530K to 583K, while

the temperature gradients ranged from $4.5 \times 10^{4} Km^{-1}$ to $5.4 \times 10^{4} Km^{-1}$.

Length changes and temperatures were monitored by the techniques detailed in Chapter 4. Observation of the resulting drift rates for each applied temperature occupied about ten hours, and a two- to three-hour change over period was necessary before results from the next applied annealing temperature could be monitored due to the thermal instability during this period.

5.2.1.1 Results

The results from the first lead specimen are given in full to indicate the types and variations of the values of the various drift rates obtained from ten different applied temperatures. The only exception to this is that the print-outs from the integrating millivoltmeter are quoted at hourly intervals and not every fifteen minutes as was actually recorded during the study. The results obtained from all further specimens will only be presented graphically or in a tabulated form.

Tables 1-10 show the results obtained from the millivoltmeter, in column 2, at hourly intervals whilst these results are converted to voltage readings and then actual distance measurements in columns 3 and 4 respectively.

Graphs 1-5 show the results obtained from these specimens in the form of length changes, $\Delta l$, against time, t: two runs are displayed on each of these graphs. These results are summarised in Table 11 and they show that the drift velocity varies from $1.917 \times 10^{-12} ms^{-1}$ at 538K to $1.146 \times 10^{-11} ms^{-1}$ at 583K.

| Time (Hours) | Integrated count | Voltage ($10^{-2}$V) | $\Delta l$ ($10^{-8}$m) |
|---|---|---|---|
| 0 | 2,487 | 9.211 | 0 |
| 1 | 2,471 | 9.152 | 1.20 |
| 2 | 2,413 | 8.937 | 5.50 |
| 3 | 2,358 | 8.733 | 9.55 |
| 4 | 2,303 | 8.530 | 13.60 |
| 5 | 2,248 | 8.326 | 17.70 |
| 6 | 2,189 | 8.107 | 22.00 |
| 7 | 2,137 | 7.915 | 26.00 |
| 8 | 2,079 | 7.700 | 30.20 |
| 9 | 2,024 | 7.496 | 34.30 |

TABLE 1 The increase in length with time when T = 583K and $\nabla T = 5.39 \times 10^{4} Km^{-1}$

| Time (Hours) | Integrated count | Voltage ($10^{-2}$V) | $\Delta l$ ($10^{-8}$m) |
|---|---|---|---|
| 0 | 2,363 | 8.752 | 0 |
| 1 | 2,320 | 8.593 | 3.20 |
| 2 | 2,270 | 8.407 | 6.90 |
| 3 | 2,228 | 8.252 | 10.00 |
| 4 | 2,183 | 8.085 | 13.30 |
| 5 | 2,133 | 7.900 | 17.00 |
| 6 | 2,088 | 7.733 | 20.40 |
| 7 | 2,041 | 7.559 | 23.90 |
| 8 | 1,995 | 7.389 | 27.30 |
| 9 | 1,948 | 7.215 | 30.70 |
| 10 | 1,900 | 7.037 | 34.30 |

TABLE 2 The increase in length with time when T = 578K and $\nabla T = 5.30 \times 10^{4} Km^{-1}$

| Time (Hours) | Integrated count | Voltage ($10^{-2}$V) | $\Delta l$ ($10^{-8}$m) |
|---|---|---|---|
| 0 | 2,342 | 8.674 | 0 |
| 1 | 2,327 | 8.618 | 1.10 |
| 2 | 2,308 | 8.548 | 2.50 |
| 3 | 2,268 | 8.400 | 5.50 |
| 4 | 2,231 | 8.263 | 8.20 |
| 5 | 2,190 | 8.111 | 11.30 |
| 6 | 2,151 | 7.967 | 14.10 |
| 7 | 2,113 | 7.826 | 17.00 |
| 8 | 2,078 | 7.696 | 19.55 |
| 9 | 2,037 | 7.544 | 22.60 |
| 10 | 1,998 | 7.400 | 25.50 |
| 11 | 1,960 | 7.259 | 28.30 |

TABLE 3 The increase in length with time when T = 573K and $\nabla T = 5.20 \times 10^{4} Km^{-1}$

| Time (Hours) | Integrated count | Voltage ($10^{-2}$V) | $\Delta l$ ($10^{-8}$m) |
|---|---|---|---|
| 0 | 2,500 | 9.259 | 0 |
| 1 | 2,472 | 9.156 | 2.05 |
| 2 | 2,444 | 9.052 | 4.15 |
| 3 | 2,415 | 8.944 | 6.30 |
| 4 | 2,384 | 8.830 | 8.60 |
| 5 | 2,352 | 8.711 | 10.95 |
| 6 | 2,323 | 8.604 | 13.10 |
| 7 | 2,293 | 8.493 | 15.30 |
| 8 | 2,262 | 8.378 | 17.60 |
| 9 | 2,229 | 8.256 | 20.10 |
| 10 | 2,201 | 8.148 | 22.20 |
| 11 | 2,168 | 8.030 | 24.60 |

TABLE 4 The increase in length with time when T = 567K and $\nabla T = 5.09 \times 10^{4} Km^{-1}$

| Time (Hours) | Integrated count | Voltage ($10^{-2}$V) | $\Delta l$ ($10^{-8}$m) |
|---|---|---|---|
| 0 | 2,263 | 8.381 | 0 |
| 1 | 2,237 | 8.285 | 1.90 |
| 2 | 2,209 | 8.181 | 4.00 |
| 3 | 2,183 | 8.085 | 5.90 |
| 4 | 2,159 | 7.996 | 7.70 |
| 5 | 2,132 | 7.896 | 9.70 |
| 6 | 2,104 | 7.793 | 11.80 |
| 7 | 2,079 | 7.700 | 13.60 |
| 8 | 2,053 | 7.604 | 15.50 |
| 9 | 2,030 | 7.518 | 17.30 |
| 10 | 2,000 | 7.407 | 19.50 |
| 11 | 1,978 | 7.326 | 21.10 |

TABLE 5 The increase in length with time when T = 563K and $\nabla T = 5.02 \times 10^{4} Km^{-1}$

| Time (Hours) | Integrated count | Voltage ($10^{-2}$V) | $\Delta l$ ($10^{-8}$m) |
|---|---|---|---|
| 0 | 2,565 | 9.500 | 0 |
| 1 | 2,547 | 9.433 | 1.35 |
| 2 | 2,527 | 9.359 | 2.80 |
| 3 | - | - | - |
| 4 | 2,479 | 9.181 | 6.40 |
| 5 | 2,459 | 9.107 | 7.90 |
| 6 | 2,438 | 9.030 | 9.40 |
| 7 | 2,416 | 8.948 | 11.05 |
| 8 | 2,395 | 8.870 | 12.60 |
| 9 | 2,373 | 8.789 | 14.20 |
| 10 | 2,354 | 8.719 | 15.60 |
| 11 | 2,331 | 8.633 | 17.35 |
| 12 | 2,308 | 8.548 | 19.05 |

TABLE 6 The increase in length with time when T = 558.5K and $\nabla T = 4.93 \times 10^{4} Km^{-1}$

| Time (Hours) | Integrated count | Voltage ($10^{-2}$V) | $\Delta l$ ($10^{-8}$m) |
|---|---|---|---|
| 0 | 2,067 | 7.655 | 0 |
| 1 | 2,052 | 7.600 | 1.10 |
| 2 | 2,031 | 7.522 | 2.70 |
| 3 | 2,011 | 7.448 | 4.15 |
| 4 | 1,993 | 7.381 | 5.50 |
| 5 | 1,977 | 7.321 | 6.70 |
| 6 | 1,956 | 7.245 | 8.20 |
| 7 | 1,941 | 7.189 | 9.30 |
| 8 | 1,921 | 7.115 | 10.80 |
| 9 | 1,904 | 7.052 | 12.10 |
| 10 | 1,884 | 6.978 | 13.55 |
| 11 | 1,875 | 6.944 | 14.20 |
| 12 | 1,849 | 6.847 | 16.15 |

TABLE 7 The increase in length with time when T = 553.5K and $\nabla T = 4.84 \times 10^{4} Km^{-1}$

| Time (Hours) | Integrated count | Voltage ($10^{-2}$V) | $\Delta l$ ($10^{-8}$m) |
|---|---|---|---|
| 0 | 2,530 | 9.371 | 0 |
| 1 | 2,512 | 9.304 | 1.35 |
| 2 | 2,499 | 9.255 | 2.30 |
| 3 | 2,486 | 9.207 | 3.30 |
| 4 | 2,470 | 9.148 | 4.45 |
| 5 | 2,456 | 9.096 | 5.50 |
| 6 | 2,441 | 9.041 | 6.60 |
| 7 | 2,429 | 8.996 | 7.50 |
| 8 | 2,413 | 8.937 | 8.70 |
| 9 | 2,399 | 8.885 | 9.70 |
| 10 | 2,384 | 8.830 | 10.80 |
| 11 | 2,368 | 8.770 | 12.00 |
| 12 | 2,356 | 8.726 | 12.90 |

TABLE 8 The increase in length with time when T = 549K and $\nabla T = 4.76 \times 10^{4} Km^{-1}$

| Time (Hours) | Integrated count | Voltage ($10^{-2}$V) | $\Delta l$ ($10^{-8}$m) |
|---|---|---|---|
| 0 | 2,112 | 7.822 | 0 |
| 1 | 2,098 | 7.770 | 1.05 |
| 2 | 2,085 | 7.722 | 2.00 |
| 3 | 2,072 | 7.674 | 2.95 |
| 4 | 2,058 | 7.622 | 4.00 |
| 5 | 2,047 | 7.581 | 4.80 |
| 6 | 2,035 | 7.537 | 5.70 |
| 7 | 2,023 | 7.493 | 6.60 |
| 8 | 2,014 | 7.459 | 7.25 |
| 9 | 1,998 | 7.400 | 8.45 |
| 10 | 1,981 | 7.337 | 9.70 |
| 11 | 1,973 | 7.307 | 10.30 |
| 12 | 1,962 | 7.267 | 11.10 |

TABLE 9 The increase in length with time when T = 543.5K and $\nabla T = 4.66 \times 10^{4} Km^{-1}$

| Time (Hours) | Integrated count | Voltage ($10^{-2}$V) | $\Delta l$ ($10^{-9}$m) |
|---|---|---|---|
| 0 | 2,486 | 9.207 | 0 |
| 1 | 2,476 | 9.170 | 7.40 |
| 2 | 2,467 | 9.137 | 14.00 |
| 3 | 2,461 | 9.115 | 18.50 |
| 4 | 2,445 | 9.056 | 30.00 |
| 5 | 2,439 | 9.033 | 35.00 |
| 6 | 2,432 | 9.007 | 40.00 |
| 7 | 2,421 | 8.967 | 48.00 |
| 8 | 2,416 | 8.948 | 52.00 |
| 9 | 2,403 | 8.900 | 61.50 |
| 10 | 2,385 | 8.833 | 75.00 |
| 11 | 2,386 | 8.837 | 74.00 |
| 12 | 2,376 | 8.800 | 81.40 |
| 13 | 2,363 | 8.752 | 91.00 |

TABLE 10 The increase in length with time when T = 538K and $\nabla T = 4.56 \times 10^{4} Km^{-1}$

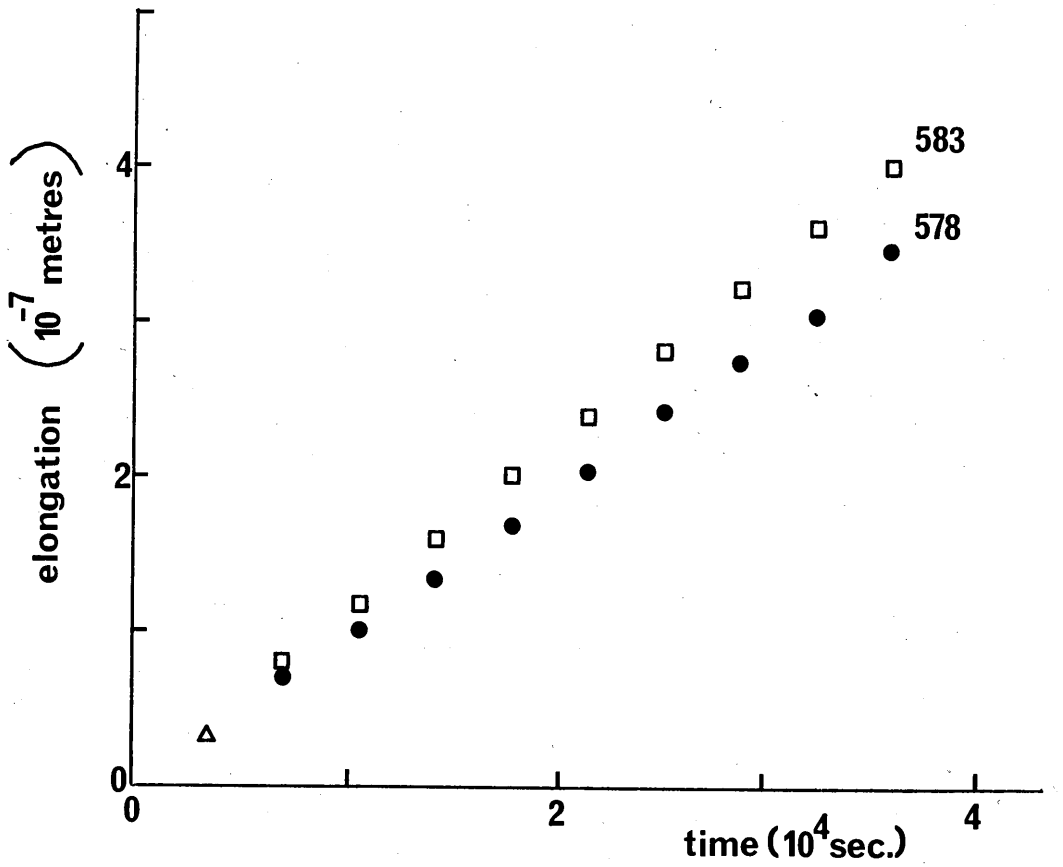


GRAPH 1 Elongation against time at annealing temperatures of 583K and 578K

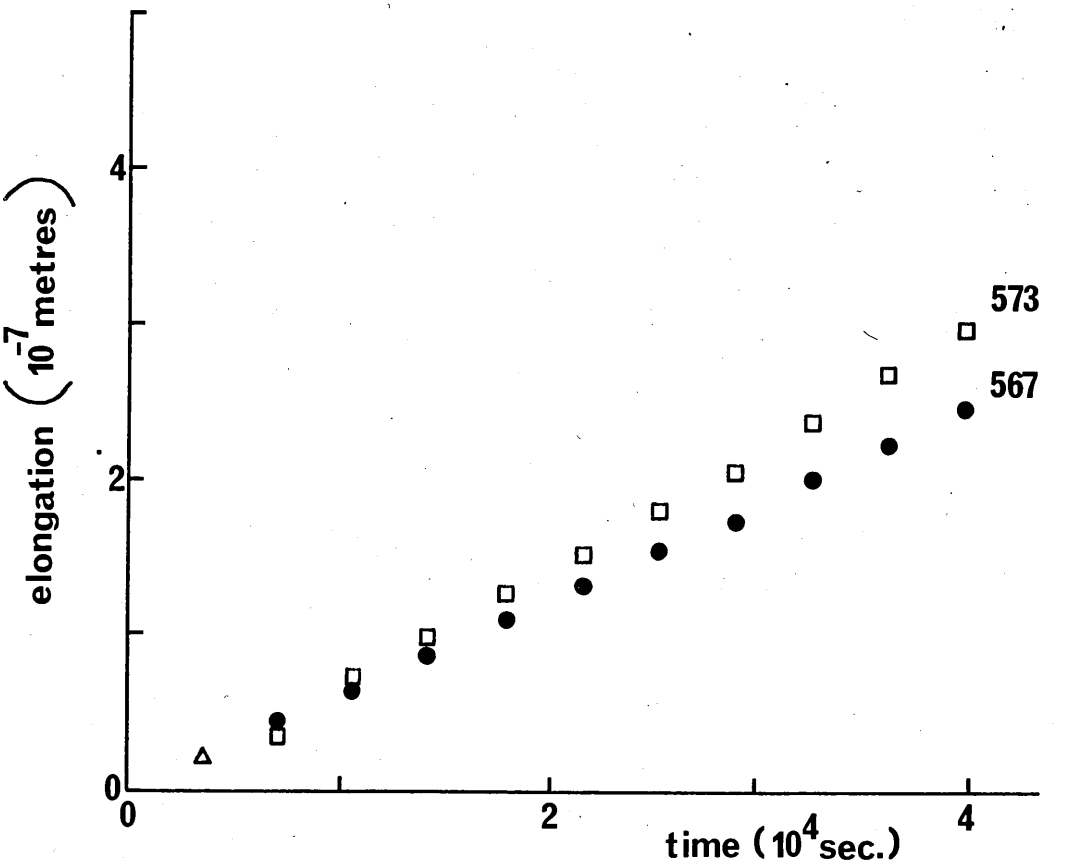


GRAPH 2 Elongation against time at annealing temperatures of 573K and 567K

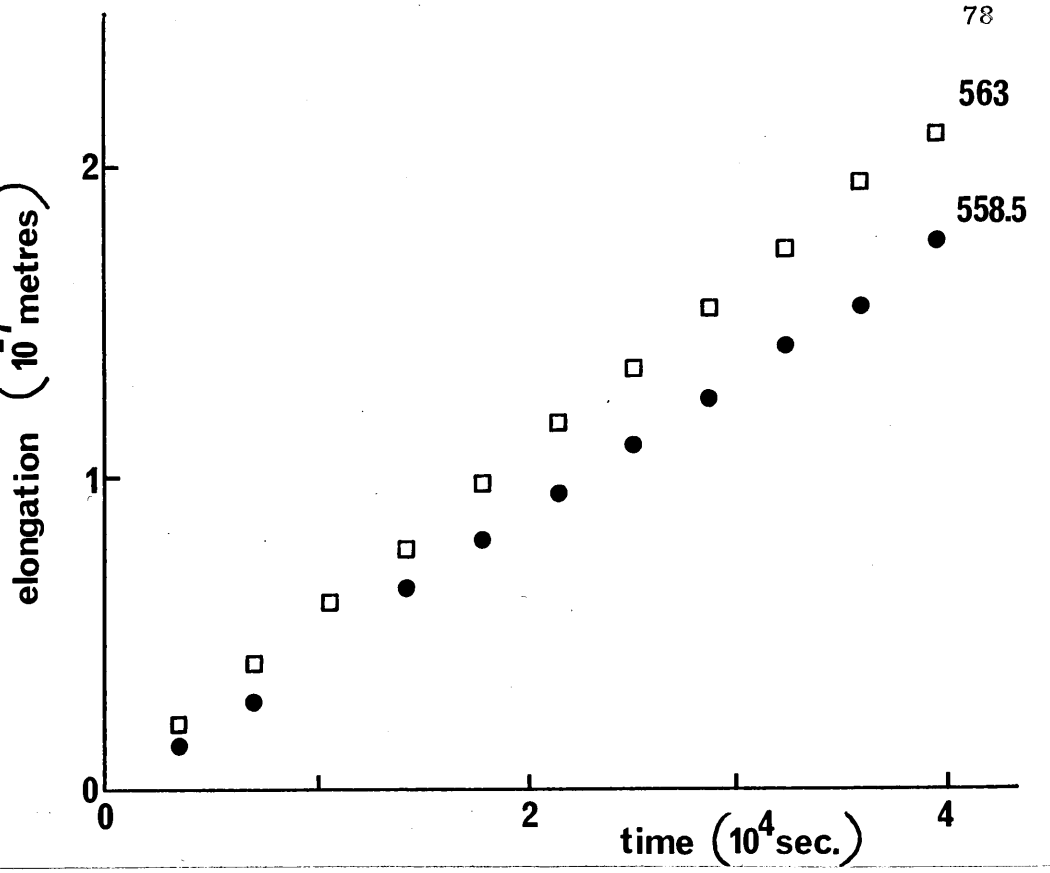


GRAPH 3 Elongation against time at annealing temperatures of 563K and 558.5K

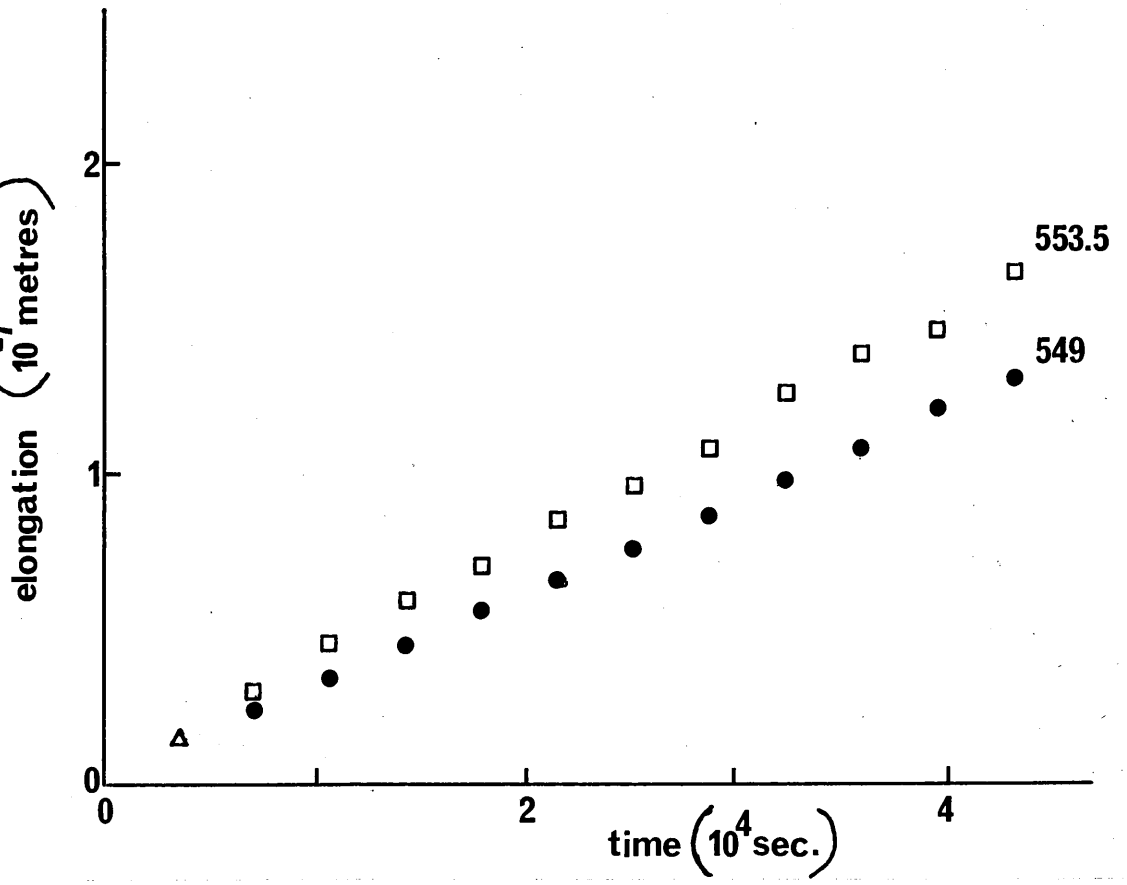


GRAPH 4 Elongation against time at annealing temperatures of 553.5K and 549K

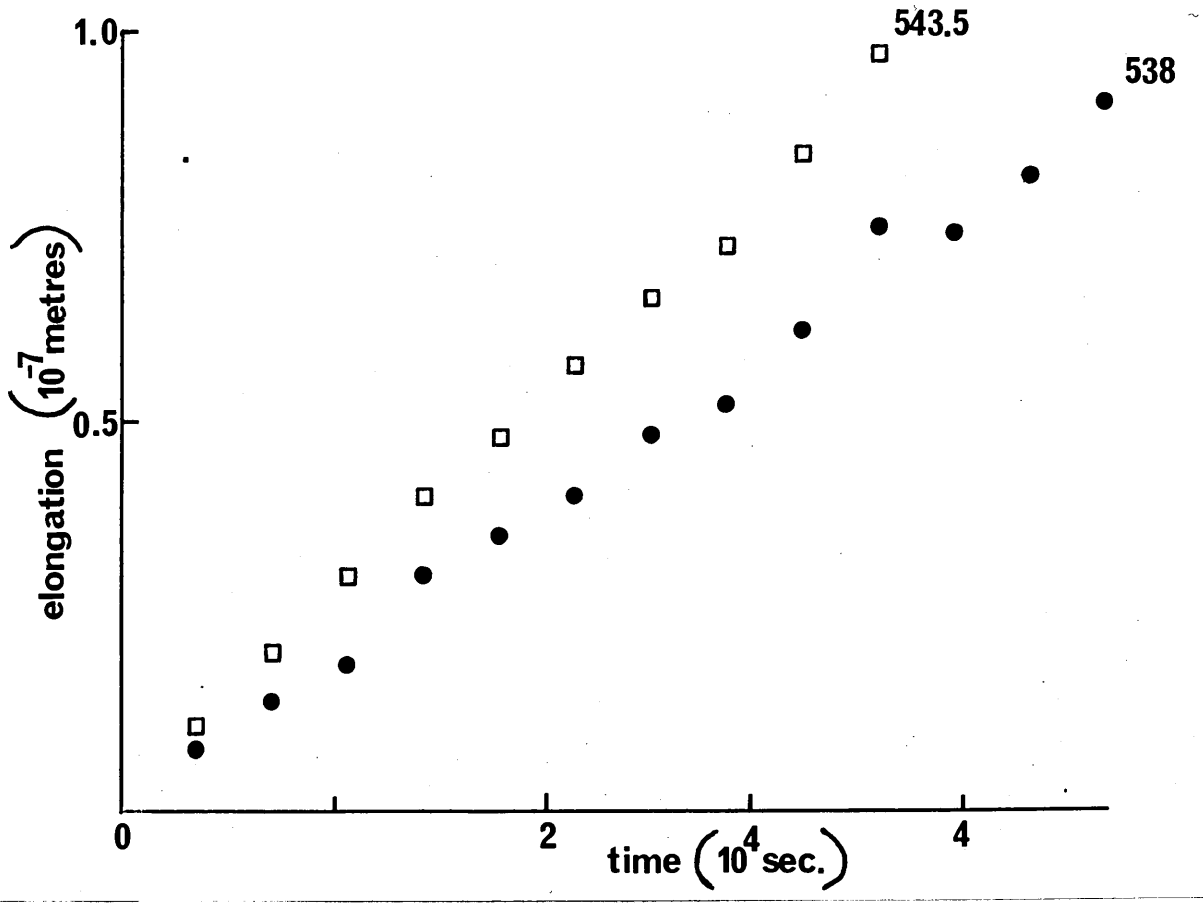


GRAPH 5 Elongation against time at annealing temperatures of 543.5K and 538K

From the equation which derives a relationship between the drift velocity and the heat of transport:

$$v_m = \frac{D}{fkT^2} (Q^* - \Delta H_f) \nabla T$$

values can now be obtained for $D (Q^* - \Delta H_f)$ as $v_m$, T and $\nabla T$ have been measured experimentally.

Using Hudson and Hoffman's (35) value for the self-diffusion coefficient of lead ($D = 0.69 \exp - (1.070/kT)$) the observed combinations of temperature distribution and drift velocity allow values of $(Q^* - \Delta H_f)$ to be computed for each run. The individual data are shown in Table 11, but taken together give an estimated value for the heat of transport in lead of

$$(Q^* - \Delta H_f) = 0.106 \pm 0.003 \text{ eV}$$

Using Feder and Nowick's (42) value for the enthalpy of formation for lead:

$$\Delta H_f = 0.52 \text{ eV}$$

defines a value for the reduced heat of transport in lead of

$$Q^* = + 0.626 \text{ eV}$$

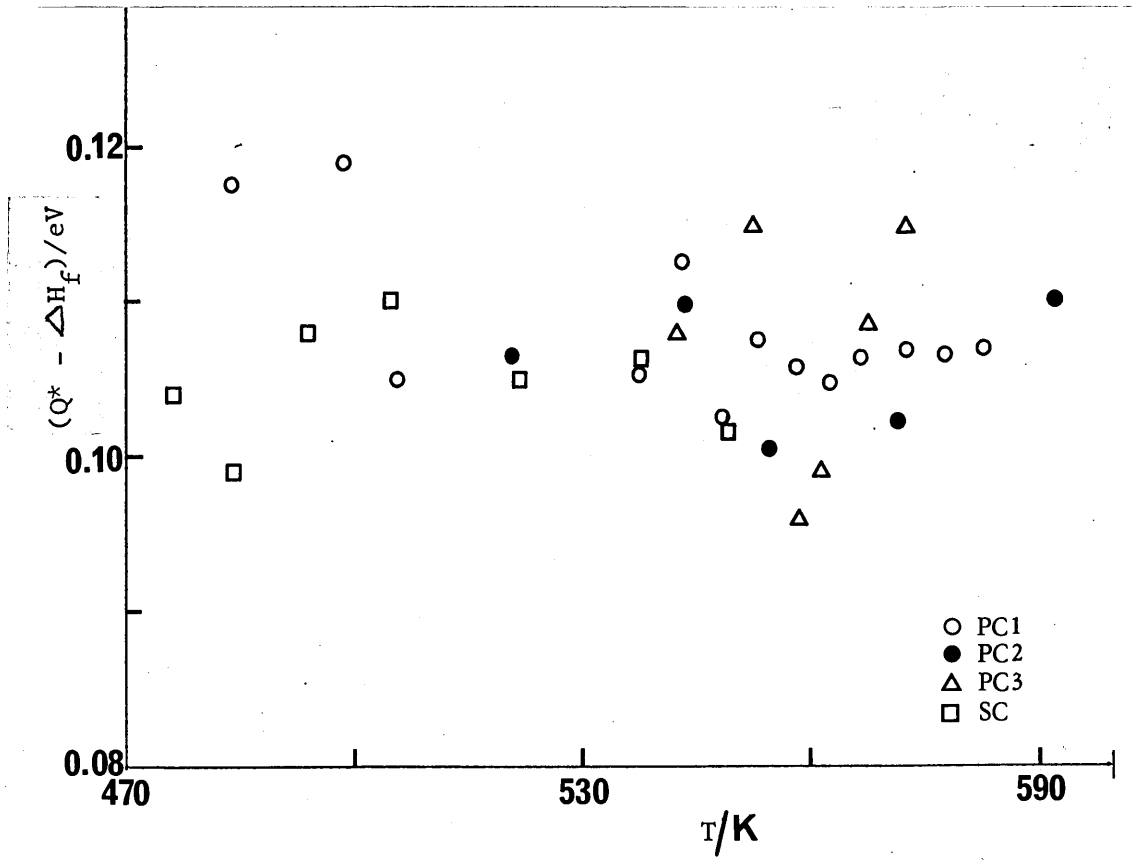


GRAPH 6 Plot of $(Q^* - \Delta H_f)$ against temperature with the results obtained from the four lead specimens

| $T/K$ | $10^4 \nabla T/Km^{-1}$ | $10^{-12} v_m/ms^{-1}$ | $\ln (v_m kT^2/\nabla T)$ | $10^3 K/T$ | $10^{-13} D/m^2 s^{-1}$ | $(Q^* - \Delta H_f)/eV$ |
|---|---|---|---|---|---|---|
| 583.0 | 5.39 | 11.460 | - 32.7098 | 1.7150 | 45.500 | 0.1069 |
| 578.0 | 5.30 | 9.520 | - 32.8957 | 1.7300 | 37.890 | 0.1066 |
| 573.0 | 5.20 | 7.917 | - 33.0784 | 1.7450 | 31.460 | 0.1069 |
| 567.0 | 5.09 | 6.278 | - 33.3101 | 1.7640 | 25.055 | 0.1065 |
| 563.0 | 5.02 | 5.300 | - 33.4797 | 1.7760 | 21.470 | 0.1048 |
| 558.5 | 4.93 | 4.470 | - 33.6480 | 1.7900 | 17.998 | 0.1057 |
| 553.5 | 4.84 | 3.717 | - 33.8320 | 1.8070 | 14.745 | 0.1074 |
| 549.0 | 4.76 | 2.964 | - 34.0581 | 1.8215 | 12.285 | 0.1028 |
| 543.5 | 4.66 | 2.580 | - 34.1957 | 1.8400 | 9.790 | 0.1126 |
| 538.0 | 4.56 | 1.917 | - 34.4491 | 1.8590 | 7.760 | 0.1055 |

TABLE 11 Results obtained from lead polycrystal I

As indicated by the direction of mass flow, that is an elongation of the specimen, $Q^*$ is a positive quantity, the magnitude of which confirms a theoretical calculation previously made by Lodding and Thernqvist (32).

Graph 6 shows the relationship between the values of $(Q^* - \Delta H_f)$ obtained over the applied temperature range and indicates that the heat of transport does not vary with temperature.

In section 2.5.3 it was shown that temperature variations of the product $DQ^*$ could be estimated from a plot of $\ln (vkT^2 / \nabla T)$ versus $1/T$, deviations of the gradient from the expected value of $E_d/k$ being preserved due to a temperature variation of $Q^*$. Using this calculation an estimate was made for $E_d$ and the result compared with that obtained by Hudson and Hoffman (35).

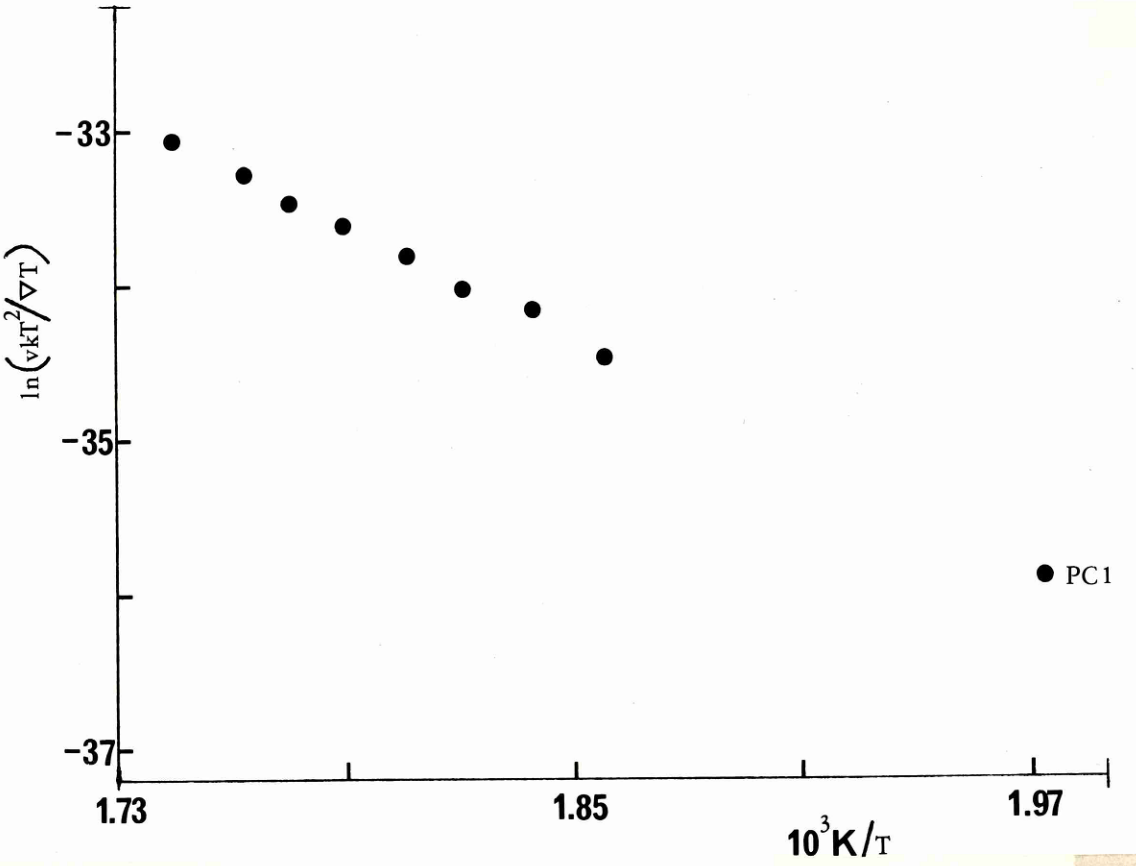


GRAPH 7 Plot of $\ln (vkT^2/\nabla T)$ against $1/T$ with the results obtained from the first polycrystal specimens of lead

Graph 7 shows such a plot with the values obtained from the polycrystal specimen, documented in Table 11, which yields a value for the activation energy of self-diffusion in lead such that

$$E_d = 1.062 \pm 0.005 \text{ eV}$$

This value agrees with the result obtained by Hudson and Hoffman (35) that

$$E_d = 1.070 \pm 0.025 \text{ eV}$$

and validates the use of their D value in calculation of $(Q^* - \Delta H_f)$.

5.2.2 Further lead studies

The reason for the examination of three further lead specimens subjected to temperatures ranging from 520K to 595K was to observe whether the results obtained were (i) dependent on specimen geometry, (ii) dependent on specimen structure, and (iii) internally consistent.

To achieve these objectives three specimens of varying diameter, length and structure were used. Two specimens were polycrystals with dimensions different to specimen I and the third specimen was a single crystal.

The second specimen studied was a polycrystal with a diameter of 3.5mm and an 'effective' length of 5mm. It was subjected to six different temperatures ranging from 520K to 595K with a respective gradient range from $4.25 \times 10^4 Km^{-1}$ to $5.6 \times 10^4 Km^{-1}$. The length change of each specimen with time was monitored by the same system as was described for specimen I, and the resulting drift rates varied from $9.55 \times 10^{-13} ms^{-1}$ to $2.75 \times 10^{-11} ms$. A full set of results for this specimen is shown

| $T/K$ | $10^4 \nabla T/Km^{-1}$ | $10^{-12} v_m/ms^{-1}$ | $\ln (v_m kT^2/\nabla T)$ | $10^3 K/T$ | $10^{-12} D/m^2 s^{-1}$ | $(Q^* - \Delta H_f)/eV$ |
|---|---|---|---|---|---|---|
| 595.0 | 5.58 | 27.610 | - 31.8244 | 1.6810 | 7.245 | 0.1627 |
| 592.5 | 5.55 | 17.190 | - 32.3013 | 1.6880 | 6.640 | 0.1102 |
| 572.0 | 5.16 | 7.560 | - 33.1203 | 1.7480 | 3.155 | 0.1023 |
| 555.0 | 4.84 | 3.835 | - 33.7954 | 1.8020 | 1.633 | 0.1006 |
| 544.0 | 4.66 | 2.680 | - 34.1559 | 1.8380 | 1.043 | 0.1099 |
| 521.0 | 4.26 | 0.950 | - 35.1896 | 1.9195 | 0.384 | 0.1066 |

TABLE 12 Results obtained from lead polycrystal II

in Table 12 and Graph 8 shows a plot of $\ln (vkT^2/\nabla T)$ versus $1/T$ which yields a value of the activation energy such that

$$E_d = 1.062 \pm 0.004 \text{ eV}$$

An overall value for the heat of transport of the atom was obtained from the results in Table 12 such that

$$(Q^* - \Delta H_f) = 0.106 \pm 0.005 \text{ eV}$$

Further results plotted in Graph 6 again indicate that $(Q^* - \Delta H_f)$ was independent of temperature.

The third specimen, another polycrystal, had the same structure and geometry as specimen I and was subjected to ten different temperatures ranging from 540K to 582K, with resulting gradients of $4.48 \times 10^4 Km^{-1}$ to $5.18 \times 10^4 Km^{-1}$.

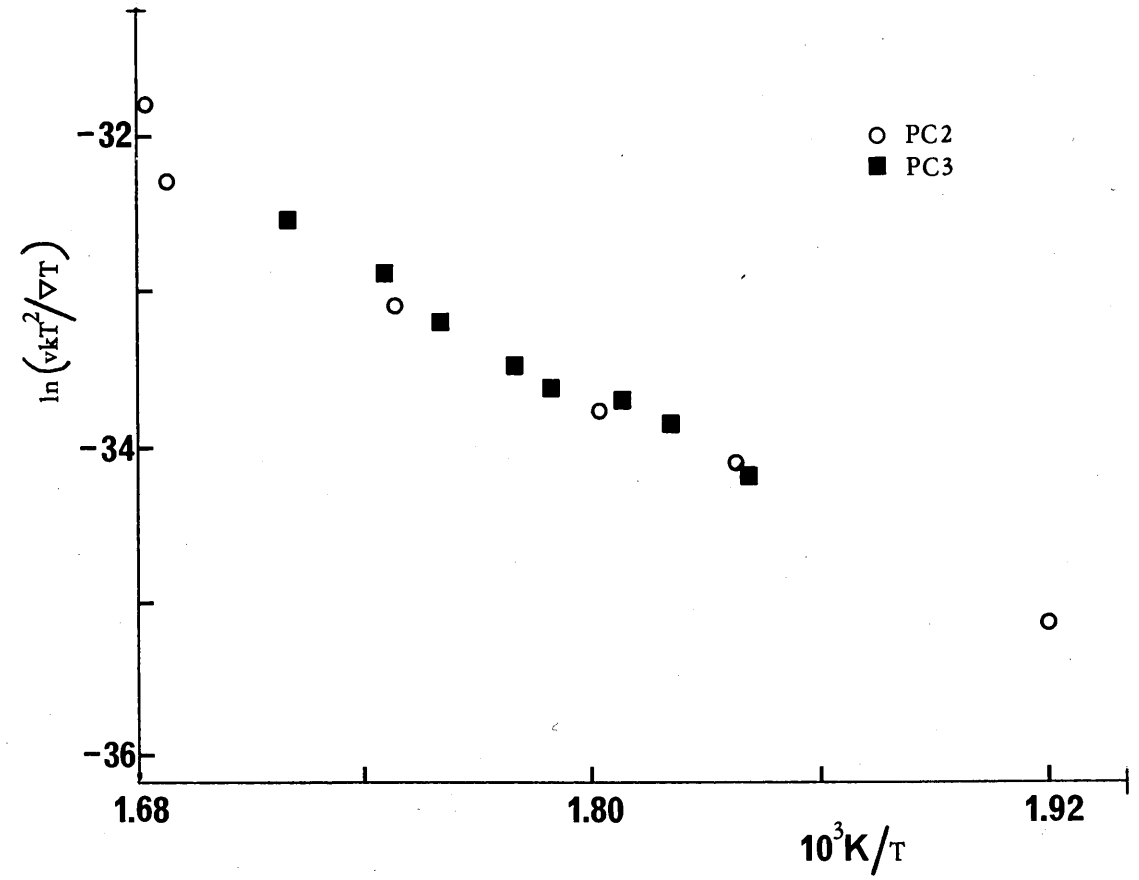


GRAPH 8 Plots of $\ln (vkT^2/\nabla T)$ against $1/T$ with the results obtained from the second and third polycrystal specimens of lead

| $T/K$ | $10^4 \nabla T/Km^{-1}$ | $10^{-12} v_m/ms^{-1}$ | $\ln (v_m kT^2/\nabla T)$ | $10^3 K/T$ | $10^{-12} D/m^2 s^{-1}$ | $(Q^* - \Delta H_f)/eV$ |
|---|---|---|---|---|---|---|
| 581.5 | 5.18 | 12.780 | - 32.5663 | 1.7200 | 4.4836 | 0.1252 |
| 573.0 | 5.02 | 8.930 | - 32.9228 | 1.7450 | 3.2760 | 0.1199 |
| 568.0 | 4.92 | 6.670 | - 33.2120 | 1.7605 | 2.7118 | 0.1085 |
| 562.0 | 4.84 | 4.850 | - 33.5355 | 1.7795 | 2.1520 | 0.0990 |
| 559.0 | 4.78 | 4.170 | - 33.6848 | 1.7890 | 1.9135 | 0.0958 |
| 553.0 | 4.68 | 3.940 | - 33.7419 | 1.8085 | 1.5071 | 0.1150 |
| 549.0 | 4.60 | 3.417 | - 33.8816 | 1.8215 | 1.2816 | 0.1175 |
| 543.0 | 4.48 | 2.442 | - 34.2131 | 1.8415 | 1.0005 | 0.1081 |

TABLE 13 Results obtained from lead polycrystal III

Over this range, drift rates varied between $2.45 \times 10^{-12} ms^{-1}$ and $1.28 \times 10^{-11} ms^{-1}$, and these values plus those for the diffusion coefficients and the heats of transport are shown in Table 13.

Graph 8 shows the plot of $\ln (vkT^2/\nabla T)$ versus $1/T$ for this specimen which yields an activation energy value such that

$$E_d = 1.060 \pm 0.009$$

An overall value for the heat of transport of the atom yields the result that

$$(Q^* - \Delta H_f) = 0.11 \pm 0.01 \text{ eV}$$

These results show in Graph 6 that the heat of transport is independent of temperature.

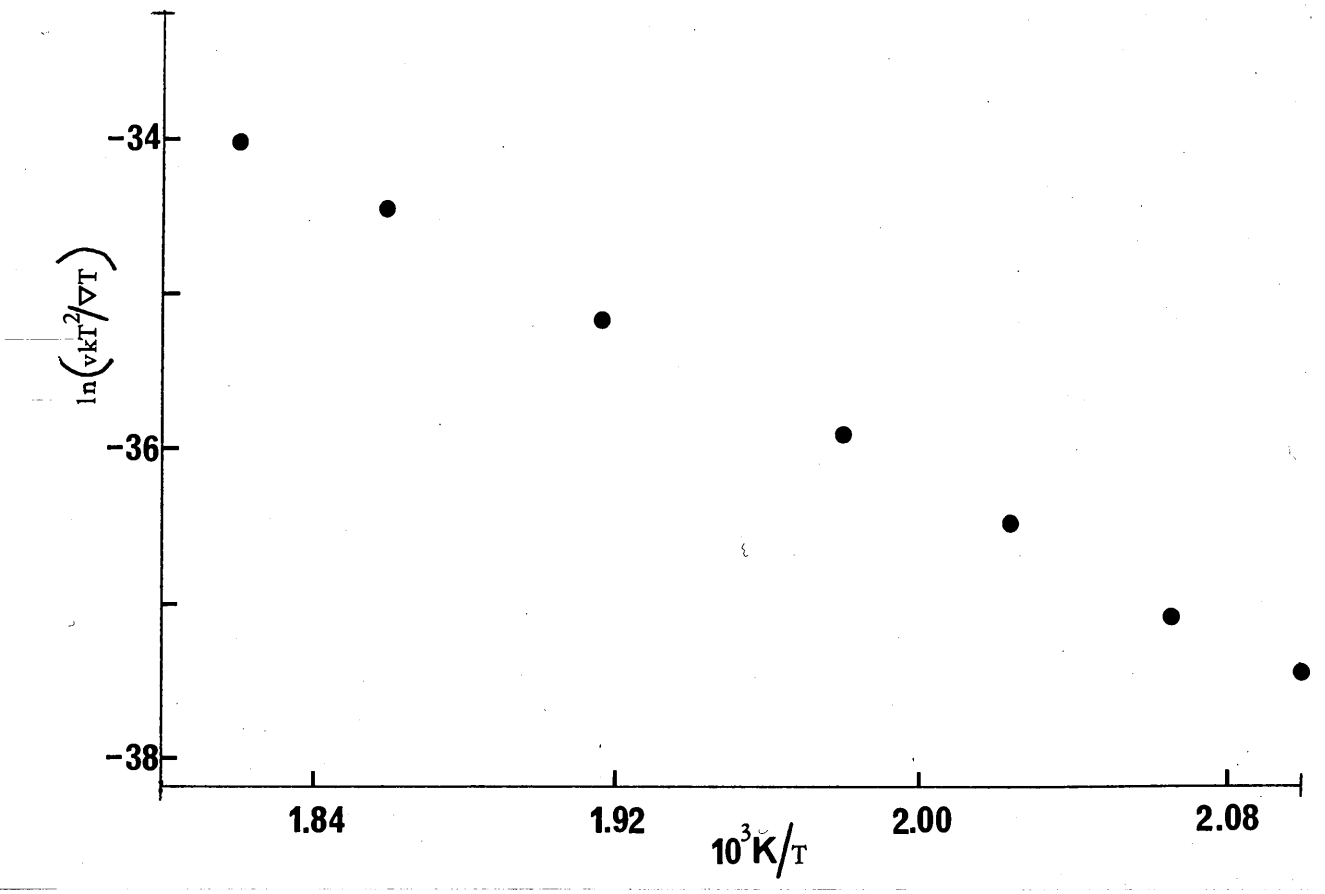


GRAPH 9 Plot of $\ln (vkT^2/\nabla T)$ against $1/T$ with the results obtained from the single crystal of lead

The fourth specimen, a single crystal, had the same dimensions as specimen I and was subjected to seven temperatures in turn, varying from 476K to 550K, with subsequent variations in the gradient ranging from $3.50 \times 10^4 Km^{-1}$ to $4.80 \times 10^4 Km^{-1}$. A complete set of results from this specimen is seen in Table 14, and Graph 9 provides a means of determining the activation energy of self-diffusion in lead with

$$E_d = 1.061 \pm 0.004 \text{ eV}$$

Further calculation leads to an overall value for the heat of transport of

$$(Q^* - \Delta H_f) = 0.105 \pm 0.004 \text{ eV}$$

### 5.2.3 Conclusion for thermomigration in lead

Measurements have been made of thermomigration in four lead specimens of varying geometry, three of which were poly-crystals, the fourth a single crystal.

It may be seen that the results obtained from these specimens agree well with each other although their geometry and structure vary. From least square fits to the results plotted on Graphs 7, 8 and 9, four values for the activation energy of self-diffusion in lead were obtained and are shown in Table 28.

| Specimen | $(Q^* - \Delta H_f)$/eV | Activation energy/eV |
|---|---|---|
| PC I | $0.106 \pm 0.003$ | $1.062 \pm 0.005$ |
| PC II | $0.106 \pm 0.005$ | $1.062 \pm 0.004$ |
| PC III | $0.110 \pm 0.010$ | $1.060 \pm 0.009$ |
| SC I | $0.105 \pm 0.004$ | $1.061 \pm 0.004$ |

TABLE 28 $(Q^* - \Delta H_f)$ and activation energy, $E_d$, values obtained from the four lead specimens.

| $T/K$ | $10^{4}\nabla T/Km^{-1}$ | $10^{-12}v_{m}/ms^{-1}$ | $\ln (v_{m}kT^{2}/\nabla T)$ | $10^{3}K/T$ | $10^{-13}D/m^{2}s^{-1}$ | $(Q^{*} - \Delta H_{f})/eV$ |
|---|---|---|---|---|---|---|
| 549.5 | 4.77 | 3.0000 | - 34.0463 | 1.8200 | 12.5390 | 0.1020 |
| 538.0 | 4.56 | 1.9250 | - 34.4872 | 1.8590 | 7.7630 | 0.1059 |
| 522.0 | 4.28 | 0.9444 | - 35.1964 | 1.9160 | 3.8500 | 0.1051 |
| 505.0 | 3.98 | 0.4494 | - 35.9325 | 1.9800 | 1.7375 | 0.1100 |
| 494.0 | 3.79 | 0.2514 | - 36.5085 | 2.0240 | 1.0090 | 0.1080 |
| 484.0 | 3.62 | 0.1361 | - 37.1172 | 2.0660 | 0.6027 | 0.0990 |
| 476.0 | 3.48 | 0.0933 | - 37.4887 | 2.1010 | 0.3928 | 0.1041 |

TABLE 14 Results obtained from lead single crystal IV

These values result in an overall value for the diffusion energy, $E_d$, of

$$E_d = 1.062 \pm 0.006 \text{ eV}$$

which agrees with previous results by Hudson and Hoffman (35) and Nachtrieb and Handler (43) which are quoted in the previous section.

It can be seen that the results from the four specimens are consistent and therefore their range of geometry and structure produce no systematic variation in drift rate above 523K beyond what would be expected from volume diffusion in lead.

By using the diffusion coefficients documented by Hudson and Hoffman (35) values for the heat of transport in lead were obtained for the four specimens and are shown in Table 28.

From these results it was possible to calculate a value for the heat of transport of the atom over a temperature range of 513K to 573K such that

$$(Q^* - \Delta H_f) = 0.107 \pm 0.002 \text{ eV}$$

It may be observed, however, that the results quoted for the single crystal specimen are over a larger range, that is, 473K to 573K and that the value of $(Q^* - \Delta H_f)$ is slightly smaller than those obtained from the polycrystalline specimens. All four results, however, statistically agree with each other, but it is possible that the values for the two structures are slightly different, and that this discrepancy is due to the presence of grain boundaries in the polycrystal specimens.

As shown in Graph 6, a plot of ($Q^* - \Delta H_f$) against temperature for the results obtained from the four specimens indicates that the heat of transport does not vary with temperature. A least square fit to these results verifies this assessment.

Statistically the results from the four lead specimens are internally consistent over the temperature range 513K to 573K. This justifies the assumption made that the heat flow through the specimen stem, from the shoulder to the heat sink, is uniaxial. It also justifies the assumption that the lattice accommodation factor $\alpha$ is constant, although according to Penney (30), using specimens of different length to radius ratios, should vary the value of $\alpha$, his assumptions being based on the fact that $\frac{\pi r}{L} < 0.1$ whereas in these experiments $\frac{\pi r}{L} > 1$, where r and L are the radius and length of the specimens respectively.

As postulated in Appendix 4, a more likely effective value for $\frac{\pi r}{L}$ in these experiments is 10, since the Penney calculation probably over-estimates the extent of plastic flow in specimens due to the very rapid fall off of flow rate with temperature.

In Penney's (30) theory the geometrical length L is too large an estimate of the region which accommodates to the material flow and, as shown in Appendix 4 a better estimate would be $\lambda = kT_o^2 / \nabla T \, E_d$. In the case of the specimens used in these experiments $\lambda = 0.5$mm, and so the ratio of $\pi r$ to L is $\simeq 10$. The specimens are very short and squat and suit the assumption that $\alpha = 1$.

It is noticeable that above 573K, as seen in the results from the second polycrystal, the influence of high temperature creep greatly modifies the observable drift rate, and, as is shown later, polycrystal specimens subjected to annealing temperatures less than 513K exhibit an enhanced drift velocity or mass flow due to the effects of grain boundary diffusion.

During these experiments on lead the temperature stability over the total range was better than $\pm$ 0.125K.

## 5.3 Thermomigration in aluminium

### 5.3.1 Further preparation of specimens

The second metal studied was aluminium. This again is a face centred cubic structure, but its melting point temperature at 934K is considerably higher. This higher temperature poses two problems: (i) that if the 'effective' length of the specimens is the same as that used for the lead specimens the gradient is much larger with a corresponding increase in the gallium-aluminium interface temperature, and (ii) a high temperature at the lower end of the specimen upsets the reliability of the transducer equipment.

To overcome the first problem the aluminium specimens were coated over the region in contact with the liquid gallium. This was done by anodising the specimens to produce a protective, oxide coating on this area of the aluminium surface. This work was done by Alcan International of Banbury, where anodised coatings are produced for commercial purposes.

As only the cooler ends of the specimens were to be coated, the remaining regions were masked off with adhesive aluminium tape. The electrolyte used was 3N sulphuric acid and the cathode was a

cylinder of aluminium. The specimen used as the anode, was suspended at the centre of the cylinder within the electrolyte solution and maintained at a temperature of 295K to 297K. A 12 volts d.c. voltage was applied over a twelve-minute period and this produced an oxide film on the surface, a few microns thick.

Five different specimens were anodised by Alcan, three polycrystals and two single crystals. The polycrystal specimens had varying geometry: one had a diameter of 3mm and overall length of 25mm, another with a diameter of 3.5mm and length 25mm, and a third specimen with a diameter of 3.5mm and length 27mm. Two of these specimens were used with 'effective' lengths of 5mm and the third with an 'effective' length of 7mm.

The two single crystals had 'effective' lengths of 5mm, their diameters being 3mm and 3.5mm.

Three specimens of each type and size were anodised and this enabled simple experiments to be performed on the possibility of gallium reacting with the anodised region. This coated layer was an oxide, therefore no reaction was expected, and in fact over a period of five days the specimens immersed in liquid gallium at temperatures exceeding 423K showed no tendency to react with the gallium. This successful technique allowed thermomigration studies to be performed on both single and polycrystal aluminium specimens.

### 5.3.2 Results from aluminium

The five aluminium specimens were subjected to annealing temperatures in the range 723K to 913K and the subsequent values for the thermal gradients were obtained by using the dummy specimen technique as described in the previous chapter.

The results from these specimens are detailed in Tables 15-19.

From the measured values of the drift velocity, temperature and thermal gradients obtained, it was possible to derive values for $D(Q^* - \Delta H_f)$ from the expression

$$v_m = \frac{D}{fkT^2} (Q^* - \Delta H_f) \nabla T$$

Using Lundy and Murdock's (36) value for the self-diffusion coefficient of aluminium ($D = 1.71 \exp - (1.478/kT)$) values were derived for $(Q^* - \Delta H_f)$. These individual values for $(Q^* - \Delta H_f)$ in each specimen are shown in Tables 15-19.

Table 29 shows the estimated values of $(Q^* - \Delta H_f)$ in aluminium obtained from the individual specimens. From these results a value for the heat of transport of the atom in aluminium was calculated where

$$(Q^* - \Delta H_f) = - (8.32 \pm 0.07)10^{-2} eV$$

Simmons and Ballufi (44) recorded a value for the enthalpy of formation of a vacancy in aluminium of

$$\Delta H_f = 0.825 \text{ eV}$$

Therefore, the reduced heat of transport can be derived such that

$$Q^* = + 0.742 \text{ eV}$$

Graph 10 shows individual values of $(Q^* - \Delta H_f)$ obtained from the five specimens plotted against temperature. A least square fit to these results indicates that $(Q^* - \Delta H_f)$ does not vary with temperature.

| $T/K$ | $10^4 \nabla T/Km^{-1}$ | $10^{-11} v_m/ms^{-1}$ | $\ln (v_m kT^2/\nabla T)$ | $10^3 K/T$ | $10^{-12} D/m^2 s^{-1}$ | $10^{-2}(Q^* - \Delta H_f)/eV$ |
|---|---|---|---|---|---|---|
| 874.5 | 9.69 | 7.9110 | - 30.5535 | 1.1435 | 51.689 | - 8.129 |
| 851.0 | 9.40 | 4.7417 | - 31.0894 | 1.1750 | 30.070 | - 8.176 |
| 825.0 | 8.97 | 2.5306 | - 31.7326 | 1.2120 | 15.930 | - 8.112 |
| 810.0 | 8.76 | 1.8000 | - 32.0863 | 1.2345 | 10.839 | - 8.370 |
| 797.5 | 8.55 | 1.2764 | - 32.4369 | 1.2540 | 7.780 | - 8.213 |
| 785.5 | 8.35 | 0.9583 | - 32.7301 | 1.2730 | 5.599 | - 8.512 |
| 770.0 | 8.12 | 0.5950 | - 38.2187 | 1.2990 | 3.607 | - 8.106 |
| 747.5 | 7.79 | 0.3056 | - 33.9028 | 1.3380 | 1.845 | - 8.023 |

TABLE 15 Results obtained from aluminium polycrystal I

| $T/K$ | $10^4 \nabla T/Km^{-1}$ | $10^{-11} v_m/ms^{-1}$ | $\ln (v_m kT^2/\nabla T)$ | $10^3 K/T$ | $10^{-12} D/m^2 s^{-1}$ | $10^{-2}(Q^* - \Delta H_f/eV$ |
|---|---|---|---|---|---|---|
| 888.5 | 9.94 | 10.5280 | - 30.2614 | 1.1255 | 70.4100 | - 7.9920 |
| 864.5 | 9.58 | 6.3890 | - 30.7787 | 1.1570 | 41.1950 | - 8.1420 |
| 858.5 | 9.51 | 5.5486 | - 30.9264 | 1.1650 | 35.8600 | - 8.0700 |
| 839.0 | 9.21 | 3.6667 | - 31.3545 | 1.1920 | 22.5380 | - 8.3680 |
| 799.0 | 8.56 | 1.3639 | - 32.3680 | 1.2515 | 8.0975 | - 8.5235 |
| 775.0 | 8.19 | 0.6722 | - 33.0923 | 1.2900 | 4.1650 | - 7.9660 |
| 736.0 | 7.59 | 0.2282 | - 34.1999 | 1.3590 | 1.2890 | - 8.5040 |
| 727.5 | 7.44 | 0.1903 | - 34.3848 | 1.3745 | 0.9815 | - 9.2800 |

TABLE 16 Results obtained from aluminium polycrystal II

| $T/K$ | $10^{4}\nabla T/Km^{-1}$ | $10^{-12}v_m/ms^{-1}$ | $\ln (v_m kT^2/\nabla T)$ | $10^{3}K/T$ | $10^{-12}D/m^2s^{-1}$ | $10^{-2}(Q^* - \Delta H_f)/eV$ |
|---|---|---|---|---|---|---|
| 815.0 | 6.414 | 14.444 | - 31.9824 | 1.2270 | 12.3430 | - 8.1560 |
| 760.0 | 5.780 | 3.414 | - 33.4604 | 1.3160 | 2.6905 | - 8.5330 |
| 714.0 | 5.315 | 0.838 | - 34.9060 | 1.4005 | 0.6285 | - 8.6050 |
| 708.5 | 5.257 | 0.664 | - 35.1433 | 1.4114 | 0.5215 | - 8.1800 |
| 700.0 | 5.157 | 0.502 | - 35.4279 | 1.4286 | 0.3887 | - 8.2625 |

TABLE 17 Results obtained from aluminium polycrystal III

| $T/K$ | $10^{4}\,\nabla T/Km^{-1}$ | $10^{-11}\,v_m/ms^{-1}$ | $\ln (v_m kT^2/\nabla T)$ | $10^{3}K/T$ | $10^{-11}\,D/m^2s^{-1}$ | $10^{-2}(Q^* - \Delta H_f)/eV$ |
|---|---|---|---|---|---|---|
| 895.5 | 10.04 | 12.3390 | - 30.0970 | 1.1167 | 8.1880 | - 8.297 |
| 889.5 | 9.95 | 11.2500 | - 30.1938 | 1.1242 | 7.1955 | - 8.367 |
| 874.5 | 9.71 | 8.0830 | - 30.5340 | 1.1435 | 5.1689 | - 8.289 |
| 862.5 | 9.54 | 6.2220 | - 30.8057 | 1.1594 | 3.9340 | - 8.300 |
| 847.5 | 9.30 | 4.4167 | - 31.1580 | 1.1800 | 2.7668 | - 8.297 |
| 830.0 | 9.04 | 2.9167 | - 31.5863 | 1.2050 | 1.8056 | - 8.280 |
| 816.0 | 8.85 | 2.1250 | - 31.9158 | 1.2255 | 1.2665 | - 8.495 |
| 786.5 | 8.37 | 0.9611 | - 32.7271 | 1.2715 | 0.5756 | - 8.290 |
| 733.5 | 7.53 | 0.2055 | - 34.3035 | 1.3630 | 0.1190 | - 8.305 |

TABLE 18 Results from aluminium single crystal IV

| $T/K$ | $10^{4}\,\nabla T/Km^{-1}$ | $10^{-11}\,v_m/ms^{-1}$ | $\ln (v_m kT^2/\nabla T)$ | $10^{3}\,K/T$ | $10^{-11}\,D/m^2s^{-1}$ | $10^{-2}(Q^* - \Delta H_f)/eV$ |
|---|---|---|---|---|---|---|
| 878.5 | 9.77 | 8.8330 | - 30.4423 | 1.1380 | 5.6520 | - 8.31 |
| 857.5 | 9.47 | 5.6110 | - 30.9133 | 1.1660 | 3.5030 | - 8.37 |
| 830.5 | 9.05 | 2.9583 | - 31.5721 | 1.2040 | 1.8280 | - 8.30 |
| 801.0 | 8.60 | 1.4097 | - 32.3346 | 1.2485 | 0.8540 | - 8.29 |
| 768.5 | 7.98 | 0.5778 | - 33.2345 | 1.3010 | 0.3454 | - 8.33 |

TABLE 19 Results obtained from aluminium single crystal V

| Specimen | $10^{-2}(Q^* - \Delta H_f)$/eV | Activation energy/eV |
|---|---|---|
| PC I | $-8.200 \pm 0.2$ | $1.483 \pm 0.015$ |
| PC II | $-8.250 \pm 0.4$ | $1.475 \pm 0.010$ |
| PC III | $-8.350 \pm 0.2$ | $1.480 \pm 0.010$ |
| SC I | $-8.325 \pm 0.07$ | $1.472 \pm 0.006$ |
| SC II | $-8.320 \pm 0.03$ | $1.479 \pm 0.008$ |

TABLE 29 $(Q^* - \Delta H_f)$ and activation energy, $E_d$, values obtained from the five aluminium specimens

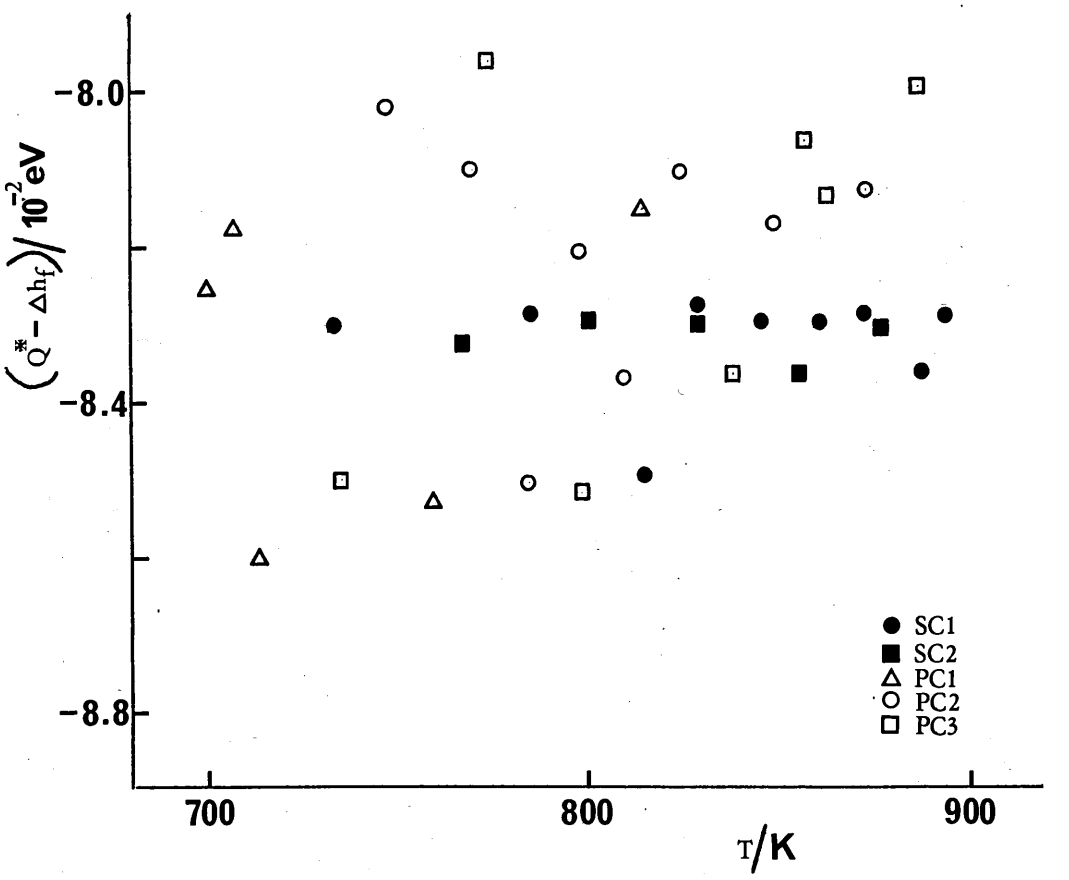


GRAPH 10 Plots of $(Q^* - \Delta H_f)$ against temperature with the results obtained from the five aluminium specimens

As a check on the validity of using the D values recorded by Lundy and Murdock, a value for the activation energy of self-diffusion $E_d$ was obtained for each specimen, and shown in Table 29.

The procedure for this calculation is the same as detailed in section 2.5.3, where a plot of $\ln (vkT^2/\nabla T)$ versus $1/T$ yields a slope which equals $E_d/k$.

An overall value for the activation energy of self-diffusion in aluminium was obtained from these five results such that

$$E_d = 1.48 \pm 0.01 \text{ eV}$$

which agrees with the results recorded by Lundy and Murdock (36) where

$$E_d = 1.48 \text{ eV}$$

and validates the using of the D values in deriving $(Q^* - \Delta H_f)$.

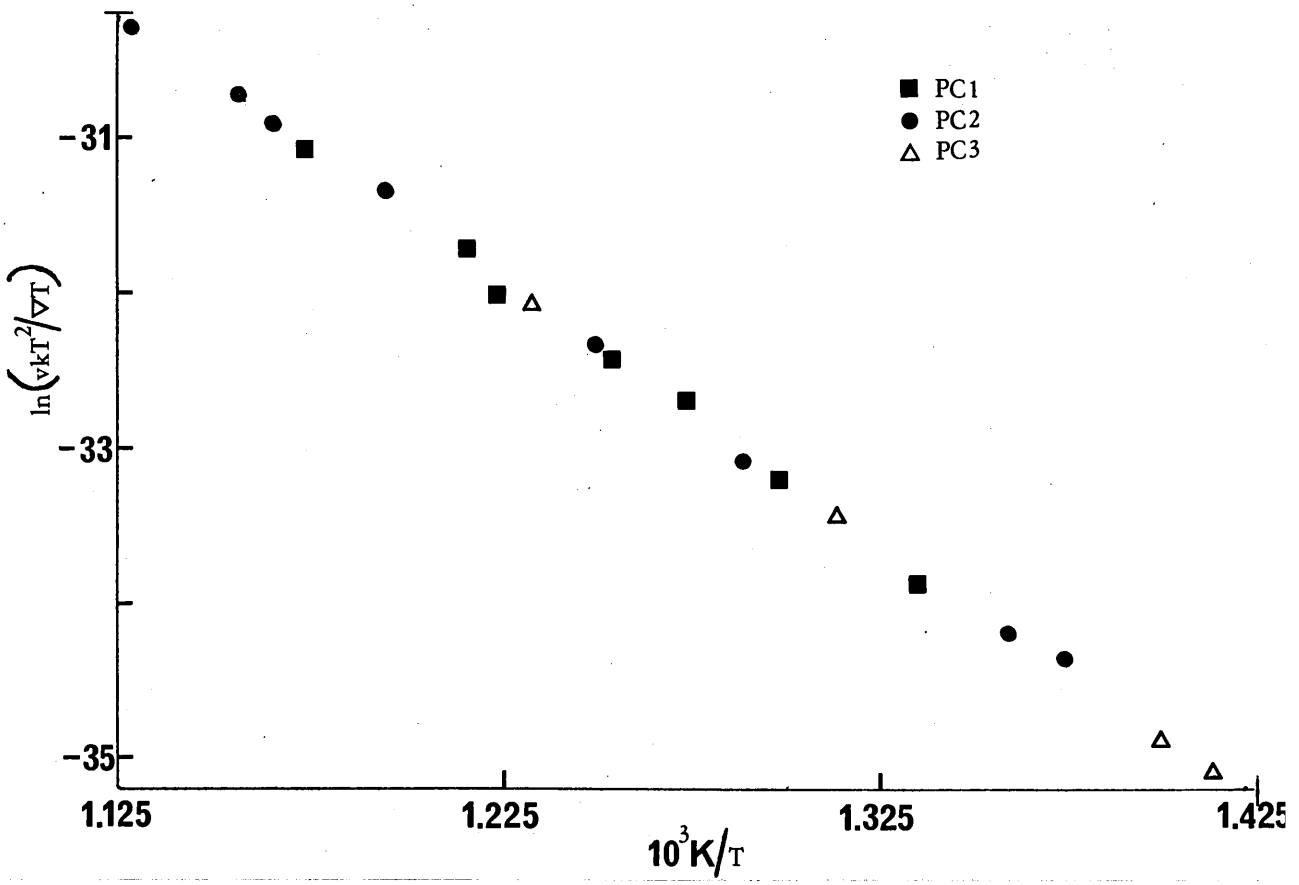


GRAPH 11 Plots of $\ln (vkT^2/\nabla T)$ against $1/T$ with the results obtained from the three polycrystal specimens of aluminium

Graph 11 shows the results from the three polycrystal specimens plotted as $\ln (vkT^2/\nabla T)$ versus 1/T. Graph 12 shows a similar plot for the two single crystal specimens.

5.3.3 Conclusion for thermomigration in aluminium

In this study of thermomigration in aluminium, five specimens were examined - three polycrystals and two single crystals.

The results obtained from these specimens establish a value for the activation energy of self-diffusion in aluminium which is in excellent agreement with Lundy and Murdock's (36) value of $E_d = 1.48$ eV.

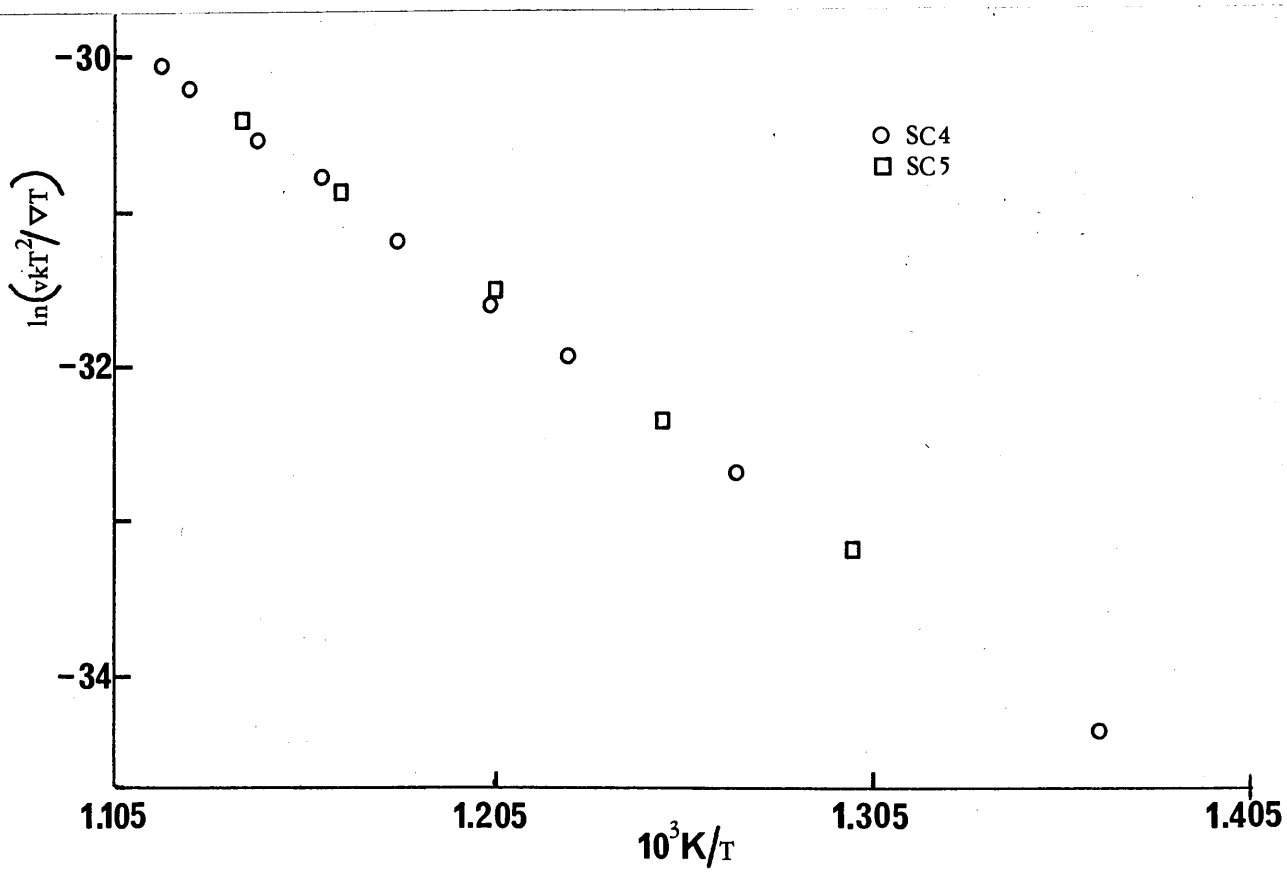


GRAPH 12 Plots of $\ln (vkT^2/\nabla T)$ against 1/T with the results obtained from the two single crystal specimens of aluminium

These values for the activation energy of aluminium are obtained from least square fits performed on results plotted in Graphs 11 and 12: Graph 11 shows the results from the three polycrystals and Graph 12 shows those obtained from the two single crystals.

Since the overall value for the activation energy was sufficiently close to the results obtained by Lundy and Murdock (36), it was assumed that their values for the diffusion coefficients over the temperature range 700K to 900K could be used for the calculation of the heat of transport in aluminium. From the five specimens a value for $(Q^* - \Delta H_f)$ was derived such that

$$(Q^* - \Delta H_f) = - (8.32 \pm 0.07)\ 10^{-2}\ \text{eV}$$

Here, unlike the results obtained from lead, $(Q^* - \Delta H_f)$ is a negative quantity confirming that specimens contracted when subjected to the annealing conditions described thus indicating an atomic flow in the opposite direction to the heat flow.

It may be seen in Table 29 that the results from the five specimens are in good agreement with each other, although the geometry and structure of the specimens is varied. This justifies further the assumptions made on the nature of the heat flow in the specimen stem and the value of the lattice accommodation factor $\alpha$.

The value derived for $(Q^* - \Delta H_f)$ agrees well with previous results recorded by Swalin and Yin (25) and Matlock and Stark (28) during studies of thermomigration in polycrystalline specimens of aluminium, where Swalin and Yin's value is

$$(Q^* - \Delta H_f) = - (6.52 \pm 1.3)\ 10^{-2}\ \text{eV}$$

and Matlock and Stark's value is

$$(Q^* - \Delta H_f) = - (8.70 \pm 6.09)\ 10^{-2}\ eV$$

When Matlock and Stark (28) studied thermomigration in single crystals of aluminium, however, they observed a specimen elongation when subjected to the annealing temperatures, as shown in Fig. 19. This indicates that $(Q^* - \Delta H_f)$ is a positive value and they obtained the result that

$$(Q^* - \Delta H_f) = + (47.83 \pm 2.61)\ 10^{-2}\ eV$$

Therefore, the results obtained by Matlock and Stark show a large discrepancy in the value of $(Q^* - \Delta H_f)$ for the two specimen structures. This is not in accordance, however, with the results obtained in this study where a consistent value for $(Q^* - \Delta H_f)$ was obtained from both single and polycrystal specimens of aluminium.

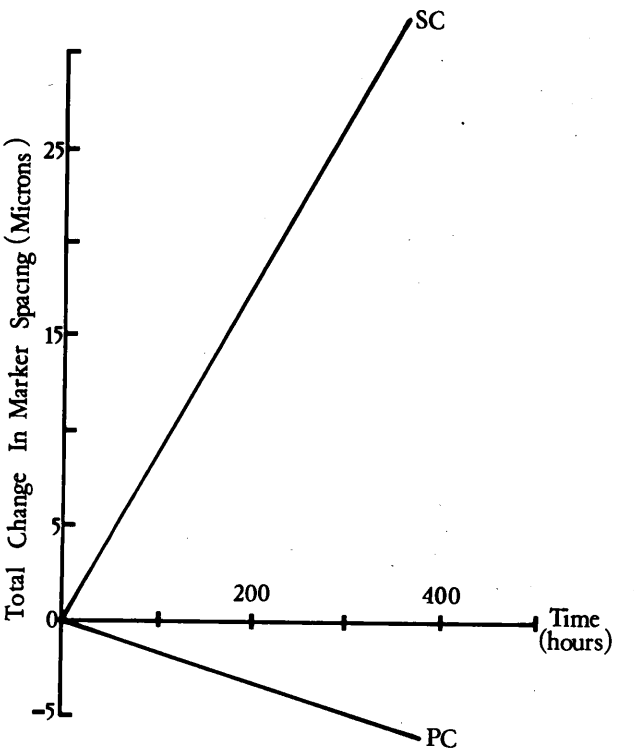


FIG. 19 Results obtained by Matlock and Stark (28) from thermomigration studies on single and polycrystal specimens of aluminium

Using Simmons and Bulluffi's (44) value for the enthalpy of vacancy formation, a value was obtained for the reduced heat of transport Q* in aluminium, such that

$$Q^* = + 0.742 \text{ eV}$$

In Graph 10 a plot of the $(Q^* - \Delta H_f)$ values obtained from the five specimens against temperature is shown. From a least square fit performed on these results it may be seen that $(Q^* - \Delta H_f)$ does not vary with temperature. It is noticeable that the scatter on the results from the single crystals is far less than that obtained from the polycrystal specimens, which may indicate that, as observed with the lead results, the grain structure of the polycrystal specimens slightly affects the thermomigration.

The temperature stability over the applied annealing range was better than $\pm$ 0.15K.

## 5.4 Thermomigration in cadmium

### 5.4.1 Further preparation

Cadmium has a hexagonal close packed structure and therefore there are two principal directions along which diffusion can occur: parallel to the C axis and perpendicular to the C axis. The three specimens used in this study were all single crystals with an orientation parallel to the C axis, two of them having identical geometry, the third having a larger stem diameter.

The basic preparation of these specimens was as described in Chapter 4. The cool end of the specimens was coated with a light gold layer, however, to minimise the possibility of a chemical reaction between cadmium and gallium. This was done using an Edwards vacuum coating unit. The specimens were rotated

about a horizontal axis while supported above the filament containing the gold evaporant. Under vacuum conditions, $10^{-3}$ torr, the gold wire was vapourised and a fine gold layer was coated onto what was to be the cool end of the specimens.

Tests were performed on the possible reaction between the gold coating and the gallium, using the procedure detailed in section 5.3.1. At temperatures exceeding 353K no surface pitting was observed over a four-day period.

5.4.2 Results obtained

The three single crystals of cadmium were subjected to annealing temperatures in the range 473K to 573K, the consequent thermal gradients being estimated using the dummy specimen technique described in section 4.3.2.

Using Wajda, Shirn and Huntington's (33) value for the self-diffusion coefficient of cadmium in this particular orientation ($D = 0.05 \exp - (0.79/kT)$), values were derived for $(Q^* - \Delta H_f)$ and are shown individually in Tables 20-22.

Table 30 shows the estimated values of $(Q^* - \Delta H_f)$ in cadmium derived from each specimen, and from these three results an overall value for $(Q^* - \Delta H_f)$ in cadmium may be derived such that

$$(Q^* - \Delta H_f) = - (3.68 \pm 0.05)\ 10^{-2}\ \text{eV}$$

To date, however, there is no documented information as to the value of the enthalpy of vacancy formation in cadmium.

Values for the activation energy of self-diffusion were obtained from the three specimens and the results are detailed in Table 30.

| $T/K$ | $10^{4}\nabla T/Km^{-1}$ | $10^{-11}v_m/ms^{-1}$ | $\ln (v_m kT^2/\nabla T)$ | $10^{3}K/T$ | $10^{-11}D/m^2s^{-1}$ | $10^{-2}(Q^* - \Delta H_f)/eV$ |
|---|---|---|---|---|---|---|
| 574.0 | 5.08 | 4.5000 | - 31.3139 | 1.7420 | 5.1670 | - 3.800 |
| 567.5 | 4.96 | 3.6110 | - 31.5329 | 1.7620 | 4.2980 | - 3.670 |
| 562.0 | 4.86 | 3.1390 | - 31.6721 | 1.7790 | 3.6650 | - 3.745 |
| 546.5 | 4.58 | 1.9440 | - 32.1478 | 1.8300 | 2.3000 | - 3.710 |
| 541.5 | 4.49 | 1.6390 | - 32.3170 | 1.8470 | 1.9680 | - 3.700 |
| 536.0 | 4.39 | 1.4030 | - 32.4704 | 1.8655 | 1.6520 | - 3.740 |
| 530.5 | 4.29 | 1.1805 | - 32.6407 | 1.8850 | 1.3820 | - 3.770 |
| 522.0 | 4.14 | 0.9170 | - 32.8900 | 1.9160 | 1.0400 | - 3.850 |
| 515.5 | 4.02 | 0.6940 | - 33.1642 | 1.9400 | 0.8330 | - 3.710 |
| 504.5 | 3.82 | 0.4580 | - 33.5720 | 1.9820 | 0.5635 | - 3.650 |
| 497.0 | 3.68 | 0.3500 | - 33.8335 | 2.0120 | 0.4275 | - 3.700 |

TABLE 20 Results obtained from cadmium single crystal I

| $T/K$ | $10^{4} \nabla T/Km^{-1}$ | $10^{-11} v_m / ms^{-1}$ | $\ln (v_m kT^2 / \nabla T)$ | $10^{3} K/T$ | $10^{-11} D/m^2 s^{-1}$ | $10^{-2} (Q^* - \Delta H_f)/eV$ |
|---|---|---|---|---|---|---|
| 572.5 | 4.98 | 4.139 | - 31.3829 | 1.7470 | 4.9540 | - 3.70 |
| 563.5 | 4.82 | 3.194 | - 31.6411 | 1.7745 | 3.8290 | - 3.70 |
| 557.0 | 4.70 | 2.622 | - 31.8365 | 1.7950 | 3.1625 | - 3.68 |
| 552.5 | 4.62 | 2.283 | - 31.9740 | 1.8100 | 2.7630 | - 3.67 |
| 543.0 | 4.45 | 1.697 | - 32.2278 | 1.8420 | 2.0627 | - 3.67 |
| 528.5 | 4.19 | 1.069 | - 32.7239 | 1.8920 | 1.2940 | - 3.71 |
| 517.0 | 3.98 | 0.689 | - 33.1557 | 1.9340 | 0.8770 | - 3.55 |
| 509.0 | 3.84 | 0.528 | - 33.4172 | 1.9645 | 0.6625 | - 3.62 |
| 492.0 | 3.53 | 0.278 | - 34.0424 | 2.0325 | 0.3540 | - 3.62 |
| 482.0 | 3.35 | 0.184 | - 34.4439 | 2.0750 | 0.2398 | - 3.59 |

TABLE 21 Results obtained from cadmium single crystal II

| $T/K$ | $10^{4}\nabla T/Km^{-1}$ | $10^{-11}v_m/ms^{-1}$ | $\ln (v_m kT^2/\nabla T)$ | $10^{3}K/T$ | $10^{-11}D/m^2s^{-1}$ | $10^{-2}(Q^* - \Delta H_f)/eV$ |
|---|---|---|---|---|---|---|
| 578.0 | 5.15 | 4.992 | - 31.2100 | 1.7300 | 5.77560 | - 3.77 |
| 554.5 | 4.73 | 2.467 | - 31.9127 | 1.8034 | 2.93500 | - 3.68 |
| 543.5 | 4.53 | 1.739 | - 32.2593 | 1.8400 | 2.09500 | - 3.64 |
| 533.0 | 4.34 | 1.228 | - 32.6034 | 1.8760 | 1.49930 | - 3.61 |
| 527.5 | 4.24 | 1.028 | - 32.7786 | 1.8960 | 1.25150 | - 3.63 |
| 519.5 | 4.10 | 0.783 | - 33.0478 | 1.9250 | 0.95585 | - 3.63 |
| 497.5 | 3.69 | 0.361 | - 33.8033 | 2.0100 | 0.43560 | - 3.74 |
| 489.0 | 3.54 | 0.243 | - 34.1921 | 2.0450 | 0.31550 | - 3.55 |
| 483.5 | 3.44 | 0.203 | - 34.3659 | 2.0680 | 0.25450 | - 3.64 |

TABLE 22 Results obtained from cadmium single crystal III

| Specimen | $10^{-2}$ $(Q^* - \Delta H_f)$/eV | Activation energy/eV |
|---|---|---|
| SC I | $-3.730 \pm 0.06$ | $0.795 \pm 0.01$ |
| SC II | $-3.650 \pm 0.05$ | $0.793 \pm 0.01$ |
| SC III | $-3.655 \pm 0.07$ | $0.804 \pm 0.015$ |

TABLE 30 $(Q^* - \Delta H_f)$ activation energy, $E_d$, values obtained from the cadmium specimens

These results give an overall value for the activation energy $E_d$ of

$$E_d = (0.797 \pm 0.006)\ eV$$

which compares favourably with the value derived by Wajda, Shirn and Huntington (33) of

$$E_d = (0.790 \pm 0.150)\ eV$$

and hence validates the use of the D values in the calculation of the value for $(Q^* - \Delta H_f)$.

Graph 13 shows a plot of $\ln (vkT^2/\nabla T)$ against $1/T$ for results obtained from the three single crystal specimens which yields the value for the activation energy of self-diffusion in cadmium.

5.4.3 Conclusion for thermomigration in cadmium

In this study of thermomigration in cadmium, three single crystal specimens having the same orientation were examined.

The value obtained for the activation energy of self-diffusion in cadmium agreed well with Wajda, Shirn and Huntington's (33) value of $E_d = 0.79 \pm 0.15$ eV and validated the use of the D values in the calculation of the value of $(Q^* - \Delta H_f)$, where it

was shown that

$$(Q^* - \Delta H_f) = - (3.68 \pm 0.05)\ 10^{-2}\ eV$$

Here, as observed in aluminium, $(Q^* - \Delta H_f)$ is a negative value and indicates that the atomic migration is in the opposite direction to the heat flow.

Graph 14 shows a plot of $(Q^* - \Delta H_f)$ values, obtained from the three specimens, against temperature and as with lead and aluminium it may be seen that $(Q^* - \Delta H_f)$ does not vary with temperature.

The temperature stability over the applied annealing range, 473K to 573K, was better than $\pm$ 0.1K.

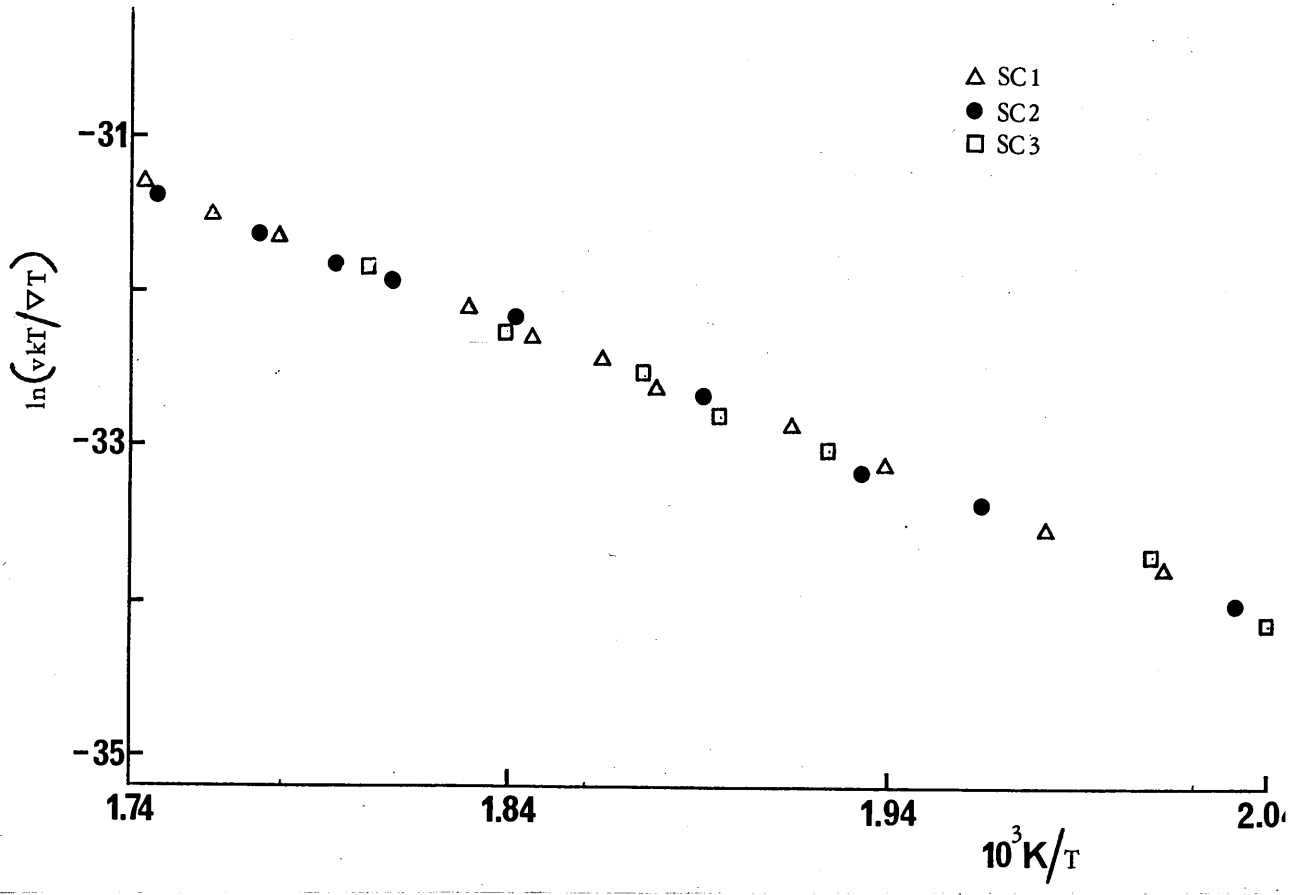


GRAPH 13 Plots of $\ln (vkT^2/\nabla T)$ against 1/T with the results obtained from the three single crystals of cadmium

## 5.5 Grain boundary diffusion observations in lead

### 5.5.1 Introduction

While studying thermomigration in lead it was observed that polycrystal specimens subjected to annealing temperatures below 513K exhibited a greater mass flow than might have been expected from extrapolation of the values at higher temperatures. Similar studies on single crystals of lead showed no such enhanced drift velocity over an applied temperature range 473K to 573K.

This discrepancy between high and low temperature values of the drift velocity in polycrystal specimens subjected to temperatures less than 513K was thought to be due to the influence of grain boundary diffusion.

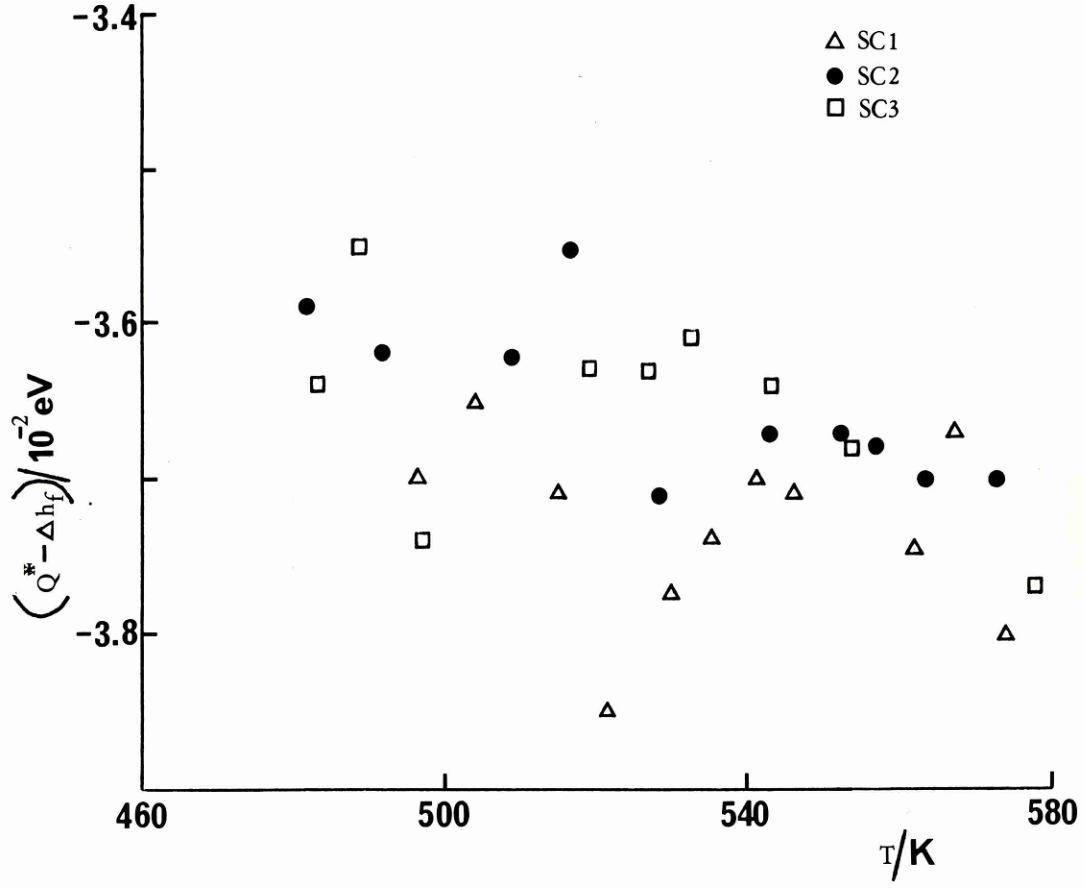


GRAPH 14 Plots of ($Q^*$ - $\Delta H_f$) against temperature with the results obtained from the three single crystal specimens of cadmium

It is well known that the diffusivity of a grain boundary greatly exceeds that of a crystal lattice adjoining it. Atoms in a boundary therefore have a higher jump frequency than those in grains. Therefore, the observed drift velocity in polycrystalline specimens is a combination of thermomigration in both the grains and the boundaries.

It is known also that the activation energy associated with thermomigration in grain boundaries is approximately a half that of the activation energy associated with thermomigration in the bulk, hence the contribution of such high diffusivity paths becomes more important at low temperatures. Results obtained by Turnbull (46), shown in Fig. 20, during a study of self-diffusion in both single and polycrystals of silver illustrates this effect.

It is therefore possible, if measurements can be made of the difference between the drift velocities in both single and polycrystal specimens at low annealing temperatures, to derive the parameters associated with thermal diffusion in grain boundaries.

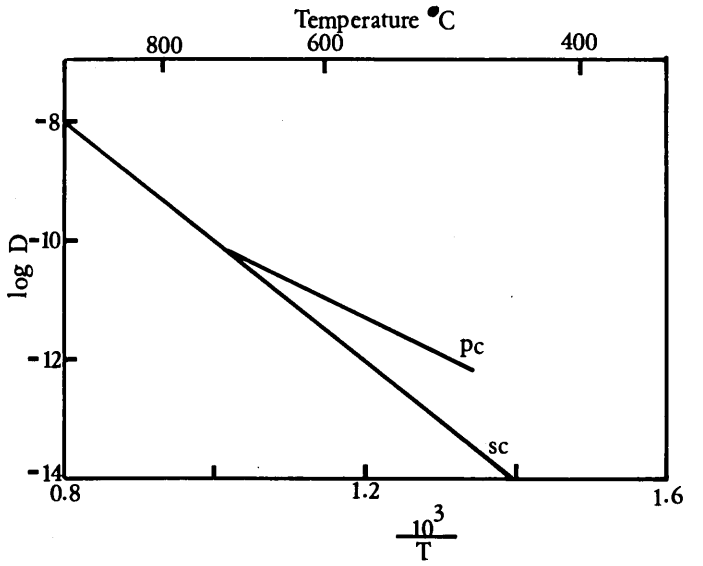


FIG. 20 Results recorded by Turnbull (46) from a study of self-diffusion in silver

A detailed examination of the theory of grain boundary thermomigration is shown in Appendix 3. It may be seen there that experimentally-derived drift velocities $\overline{V}$ arise from the summation of the drift velocities due to thermomigration both in the bulk and in grain boundaries, so that the interpretation of thermomigration at temperatures where the boundary process is significant will follow from

$$\overline{V} = v + v^1$$

where v is the drift velocity due to thermomigration in bulk and $v^1$ is the drift velocity due to thermomigration in the grain boundaries.

From the theory in Appendix 3

$$v + v^1 = \frac{\nabla T}{kT^2} \left( \frac{D}{f} (Q^* - \Delta H_f) \alpha + \frac{D^1}{f^1} \Delta E^1 \alpha^1 w \right)$$

where $D^1$ is the grain boundary diffusion coefficient, $f^1$ is another correlation factor, $\Delta E^1$ is the heat of transport associated with thermomigration in grain boundaries, $\alpha^1$ is another lattice accommodation factor and w is the effective width of the boundaries. It is this relationship which is used as the basis for interpretation of the experimental results obtained from this study.

5.5.2 Preparation of the polycrystal specimens

This study was performed with three different types of lead specimens: two polycrystalline samples having different grain diameters, 18.4 x $10^3 m^{-1}$ and 8.5 x $10^3 m^{-1}$, and a third single crystal specimen.

The larger grained polycrystal was machined to size with a diameter of 3.5mm and an 'effective' length of 7mm. The preparation of this sample before subjection to the annealing temperature was identical to that received by previous polycrystalline specimens in the thermomigration experiments.

The second polycrystal, having the smaller grain size, was produced by cold working the 5N purity lead rods manufactured by Johnson Mathey with the original grain size of $8.5 \times 10^{3} m^{-1}$. A 50mm length of 7mm diameter rod was 50 per cent cold worked by carefully clamping the material between parallel plates in a workshop vice. By locating this rod in various shaped cylinders to accommodate the increases in diameter, the plates were squeezed together inside the vice. These tubes prevented the rod from deforming and careful calculation of the change in diameter of the rod for varying degrees of cold working allowed the manufacture of tubes of various diameters. The specimens were then annealed to stabilise the grain structure and a mean grain diameter of $18.4 \times 10^{3} m^{-1}$ was obtained. The specimen was then machined to the correct size: a stem diameter of 3mm.

### 5.5.3 Results

#### 5.5.3.1 Single crystal specimen

The results obtained from this specimen are detailed in section 5.2.2 of this chapter and listed in Table 14. Over the applied annealing temperature range, 473K to 573K, measured values for the drift velocity were obtained and Graph 9 shows a plot of $\ln (vkT^{2}/\nabla T)$ against $1/T$.

#### 5.5.3.2 Large grained polycrystal specimen

The preparation and dimensions of this specimen have already been discussed in section 5.5.2. Eight different temperatures and temperature gradients were applied successively to this specimen, ranging from 478K to 543K and $2.53 \times 10^{4} Km^{-1}$ to $3.336 \times 10^{4} Km^{-1}$. Drift rates ranging from $9.4 \times 10^{-14} ms^{-1}$ to $1.7 \times 10^{-12} ms^{-1}$ were observed. These results are listed in Table 23 along with calculated values of $\ln (vkT^{2}/\nabla T)$ and $1/T$.

| $T/K$ | $10^4 \nabla T/Km^{-1}$ | $10^{-13} v_m/ms^{-1}$ | $\ln (v_m kT^2/\nabla T)$ | $10^3 K/T$ | $10^{-13} D/m^2 s^{-1}$ | $(Q^* - \Delta H_f)/eV$ |
|---|---|---|---|---|---|---|
| 543.0 | 3.336 | 16.8055 | - 34.2920 | 1.842 | 9.5866 | 0.1043 |
| 524.0 | 3.100 | 7.6944 | - 35.0711 | 1.908 | 4.2097 | 0.1090 |
| 511.5 | 2.936 | 4.6110 | - 35.5770 | 1.955 | 2.3690 | 0.1167 |
| 503.0 | 2.829 | 3.0889 | - 35.9741 | 1.988 | 1.5770 | 0.1179 |
| 496.0 | 2.750 | 2.2305 | - 36.2994 | 2.016 | 1.1160 | 0.1203 |
| 488.0 | 2.650 | 1.4528 | - 36.7236 | 2.049 | 0.7425 | 0.1183 |
| 484.5 | 2.607 | 1.3417 | - 36.8012 | 2.064 | 0.6190 | 0.1314 |
| 478.0 | 2.529 | 0.9417 | - 37.1518 | 2.092 | 0.4380 | 0.1308 |

TABLE 23 Results obtained from lead large grained polycrystal V

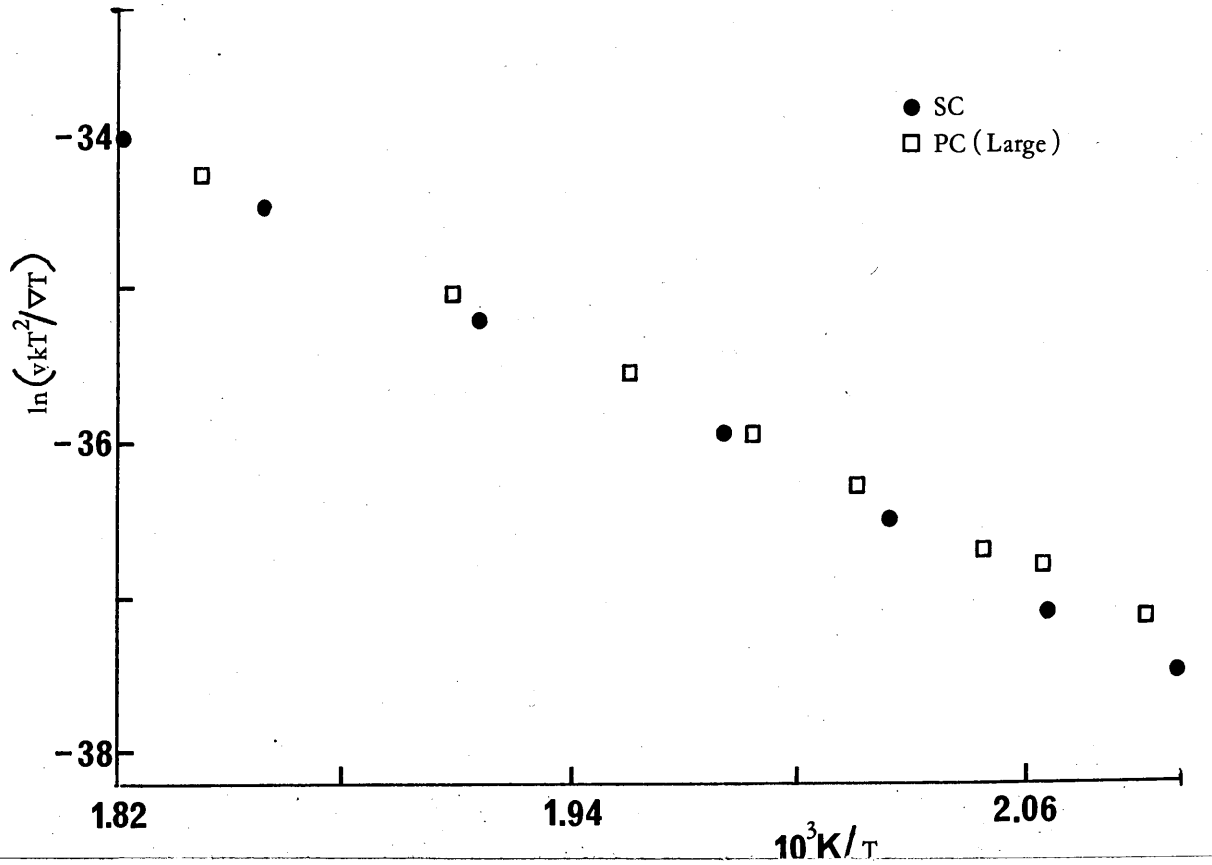


GRAPH 15 Plots of ln (vkT / ∇T) against 1/T with the results obtained from the large grained polycrystal and single crystal lead specimen

Graph 15 is a plot of $\ln (vkT^2/\nabla T)$ against 1/T with the results obtained from this polycrystal and the single crystal specimen. The lines drawn through the points obtained from these samples are as predicted from least square fits, and it may be seen that below 513K the results obtained from the polycrystal are consistently above those for the single crystal. It is this deviation of the polycrystal data that suggests that a low activation energy process begins to intervene at low temperatures, the association with crystal structure making grain boundary diffusion a likely candidate.

In the earlier study of thermomigration in lead a value for $(Q^* - \Delta H_f)$ was obtained by employing the use of the relationship

$$v_m = \frac{D}{fkT^2} (Q^* - \Delta H_f) \nabla T$$

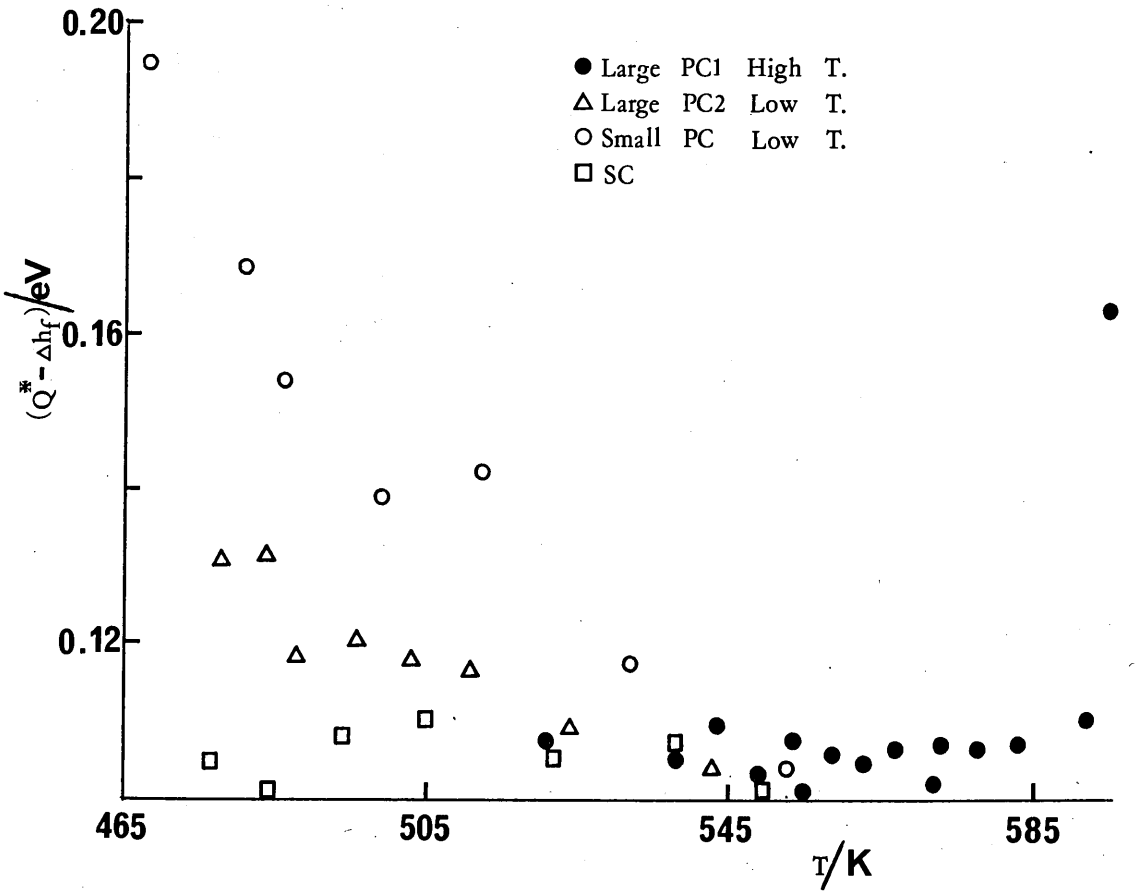


GRAPH 16 Plots of $(Q^* - \Delta H_f)$ against temperature with the results obtained from small and large grained polycrystals and single crystal lead specimens

Graph 16 shows the results from both specimens interpreted in this way, the single crystal and high temperature polycrystal runs giving a constant estimate of $(Q^* - \Delta H_f) = 0.106 \pm 0.01$ eV, while low temperature polycrystal runs give values ranging progressively to about 0.20 eV.

Interpretation of the polycrystal effect as grain boundary thermomigration was made in terms of equation A4 and A5 in Appendix 3. Taking the single crystal line as a base, differences were computed between individual polycrystal drift rates and interpolated single crystal drift rates appropriate to the same temperature. The difference was assumed to be grain boundary drift rate $v^1$. These results are shown in Table 26.

| Calculated for small grain polycrystal | | Calculated for single crystal | | Calculated for grain boundary | | |
|---|---|---|---|---|---|---|
| $10^{-13}\underline{v}/ms^{-1}$ | $\ln(v_m kT^2/\nabla T)$ | $\ln(v_m kT^2/\nabla T)$ | $10^{-13}\underline{v}/ms^{-1}$ | $10^{-13}\underline{v}/ms^{-1}$ | $\ln(v_m kT^2/\nabla T)$ | $10^3 K/\underline{T}$ |
| 7.6944 | - 35.0711 | - 35.1436 | 7.1556 | 5.3880 | - 37.7300 | 1.908 |
| 4.6110 | - 35.5770 | - 35.7123 | 4.0278 | 5.8320 | - 37.6447 | 1.955 |
| 3.0889 | - 35.9741 | - 36.1107 | 2.6944 | 3.9450 | - 38.0320 | 1.988 |
| 2.2305 | - 36.2994 | - 36.4597 | 1.9000 | 3.3050 | - 38.2087 | 2.016 |
| 1.4528 | - 36.7236 | - 36.8606 | 1.2667 | 1.8610 | - 38.7785 | 2.049 |
| 1.3417 | - 36.8012 | - 37.0596 | 1.0361 | 3.0555 | - 38.2807 | 2.064 |
| 0.9417 | - 37.1518 | - 37.3943 | 0.7389 | 2.0280 | - 38.6873 | 2.092 |

TABLE 26 Calculations for grain boundary drift velocity from large grained lead specimen ($8.5 \times 10^3 m^{-1}$)

5.5.3.3 Small grained specimen

Seven different thermal gradients were applied to this specimen, with temperatures ranging from 468K to 552K and respective thermal gradients of 3.34 x $10^4 Km^{-1}$ to 4.84 x $10^4 Km^{-1}$. Resulting drift rates and values calculated for ln ($vkT^2/\nabla T$) and 1/T are listed in Table 24.

Graph 17, a plot of ln ($vkT^2/\nabla T$) versus 1/T for results obtained from all three specimens in this study, shows the deviation of the polycrystal data at low temperatures for both grain size specimens from the data obtained from the single crystal. It is evident that the results from the small grained specimen lie consistently above those obtained from the larger grained specimen. This is to be expected since the small grained specimen has more paths of high diffusivity and hence the drift velocities due to grain boundary thermomigration from this specimen should be greater than those obtained from the larger grained specimen in the same thermal gradient.

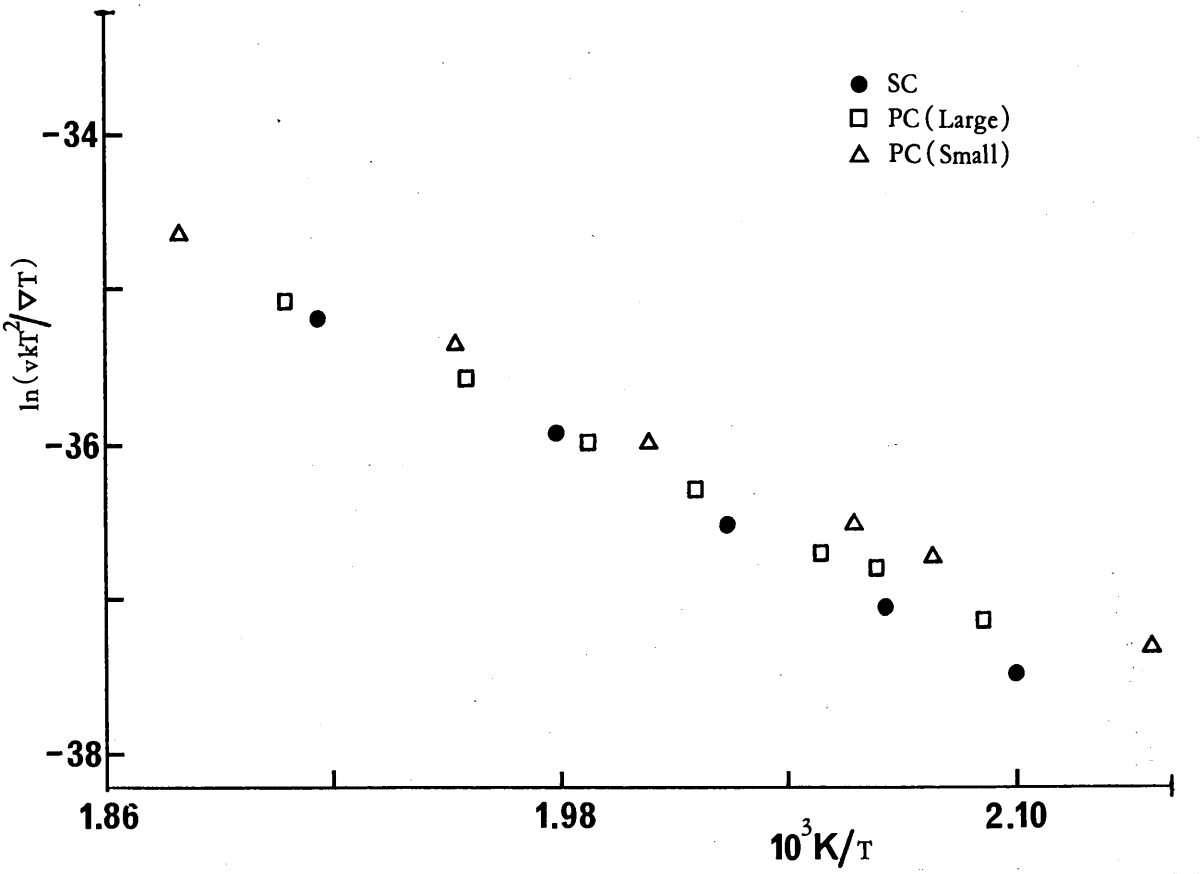


GRAPH 17

| $T/K$ | $10^4 \nabla T/Km^{-1}$ | $10^{-13} v_m /ms^{-1}$ | $\ln (v_m kT^2/\nabla T)$ | $10^3 K/T$ | $10^{-13} D/m^2 s^{-1}$ | $(Q^* - \Delta H_f)/eV$ |
|---|---|---|---|---|---|---|
| 553.0 | 4.84 | 35.2780 | - 33.8861 | 1.808 | 14.45150 | 0.1039 |
| 532.0 | 4.45 | 16.4720 | - 34.6411 | 1.880 | 5.99580 | 0.1176 |
| 512.0 | 4.09 | 8.0000 | - 35.3556 | 1.953 | 2.42570 | 0.1423 |
| 499.0 | 3.86 | 4.1528 | - 36.0048 | 2.004 | 1.29570 | 0.1391 |
| 486.5 | 3.63 | 2.4153 | - 36.5361 | 2.058 | 0.68690 | 0.1543 |
| 481.0 | 3.55 | 1.9750 | - 36.7367 | 2.079 | 0.51415 | 0.1685 |
| 468.0 | 3.32 | 1.1069 | - 37.3046 | 2.136 | 0.25230 | 0.1948 |

TABLE 24 Results obtained from lead small grained specimen VI

The grain boundary drift rate $v^1$ for this specimen was interpreted in a similar fashion to the previous polycrystal, that is, by taking the single crystal line as a base and computing the difference in drift rates at the positions of the individual polycrystal drift rates, as detailed in Table 25.

5.5.3.4 Calculation of the grain boundary activation energy

Graph 18 is a plot of $\ln (v^1 kT^2 / \nabla T)$ versus $1/T$ for both polycrystal specimens. By a least square fit it was found that the lines were parallel within experimental uncertainty. They give a common activation energy for what we presume to be grain boundary diffusion, such that

$$E_d^1 = 0.48 \pm 0.09 \text{ eV}$$

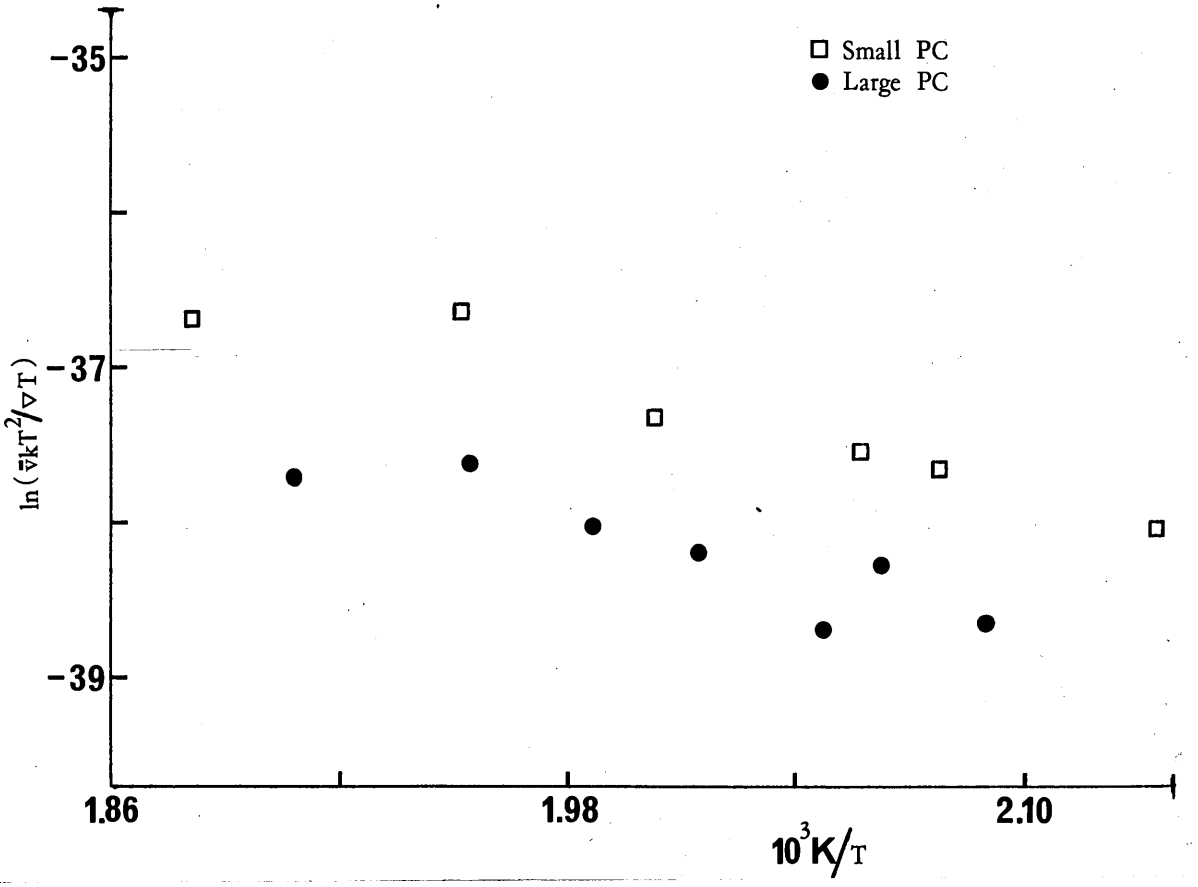


GRAPH 18 Plots of $\ln (v^1 kT^2 / \nabla T)$ against $1/T$ with the results obtained from the small and large grained polycrystal specimens of lead

At 45 per cent of the bulk diffusion activation energy this is what might be expected for grain boundary diffusion, although it is in accord with neither of the values previously recorded by Okkerse (47) - 0.68 eV in polycrystals and the band of values - 0.18-0.40 eV-reported by Stark and Upthegrove (48) in bicrystals.

The separation of the two lines on this graph corresponds to a factor of 2.46 in the polycrystalline drift rate attributable to the two specimens. This is to be compared with the grain length counts L of $(18.4 \pm 0.8) \times 10^3 m^{-1}$ and $(8.5 \pm 0.6) \times 10^3 m^{-1}$ which predicts a ratio of nearly 2.16. Graph 19 shows a plot of $\ln (v^1 kT^2 / \nabla T)$ against 1/T for both polycrystal specimens similar to Graph 18, except that the results from the smaller grained specimen have been corrected by the grain size actual and theoretical ratio factors, which are 2.16 and 2.46 respectively, as shown in Table 27. These results are compatible within experimental uncertainty.

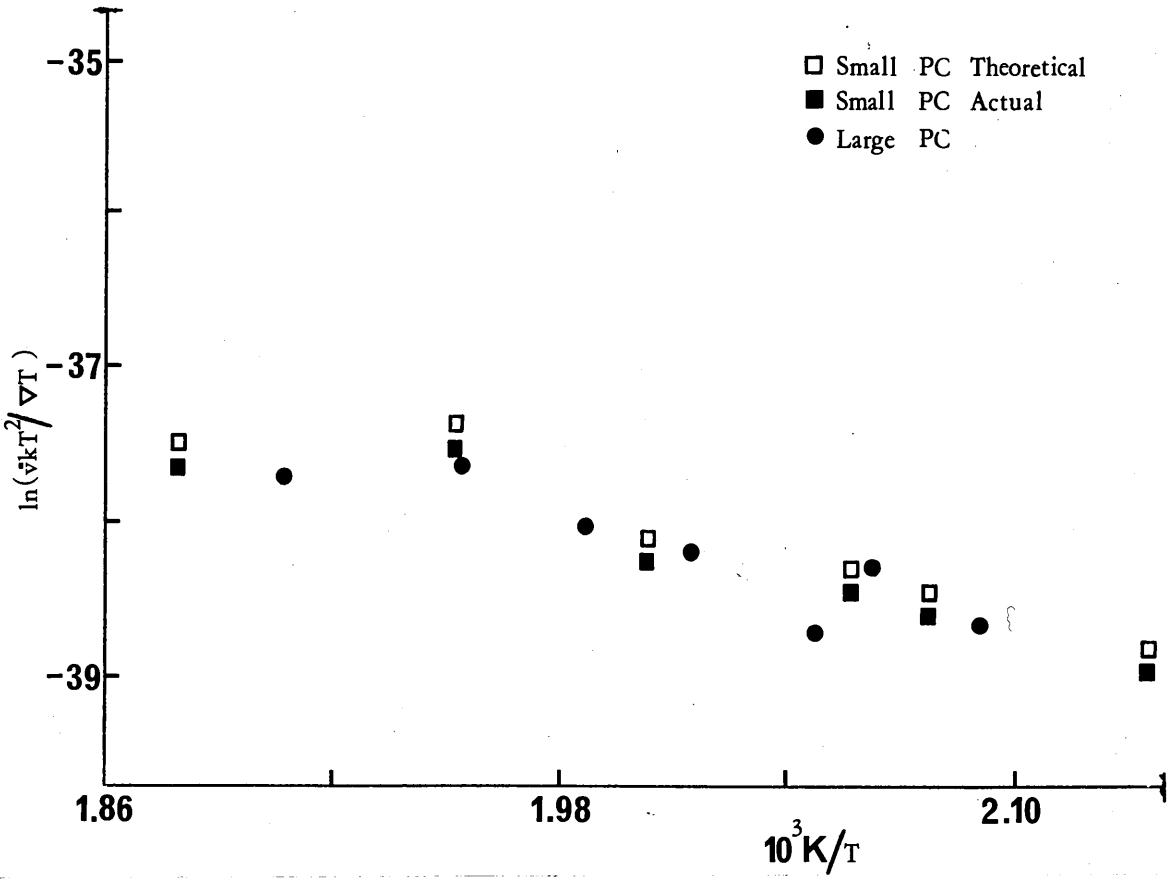


GRAPH 19 Plots of $\ln (v^1 kT^2 / \nabla T)$ against 1/T as in Graph 18 but with the small grained polycrystal results amended by the grain size ratio correction

| Calculated for small grain polycrystal | | Calculated for single crystal | | Calculated for grain boundary | | |
|---|---|---|---|---|---|---|
| $10^{-13}\underline{v}/ms^{-1}$ | $\ln(\underline{v}_m kT^2/\nabla T)$ | $\ln(\underline{v}_m kT^2/\nabla T)$ | $10^{-13}\underline{v}/ms^{-1}$ | $10^{-13}\underline{v}/ms^{-1}$ | $\ln(\underline{v}_m kT^2/\nabla T)$ | $10^3 K/\underline{T}$ |
| 35,2780 | - 33.8861 | - 33.8903 | 35.129 | 0.149 | - 39.3531 | 1.808 |
| 16.4720 | - 34.6411 | - 34.7747 | 14.411 | 2.061 | - 36.7196 | 1.880 |
| 8.0000 | - 35.3556 | - 35.6722 | 5.829 | 2.171 | - 36.6598 | 1.953 |
| 4.1528 | - 36.0048 | - 36.3108 | 3.058 | 1.095 | - 37.3378 | 2.004 |
| 2.4153 | - 36.5361 | - 36.9771 | 1.554 | 0.861 | - 37.5676 | 2.058 |
| 1.9750 | - 36.7367 | - 37.2269 | 1.211 | 0.764 | - 37.6875 | 2.079 |
| 1.1069 | - 37.3046 | - 37.9423 | 0.585 | 0.522 | - 38.0563 | 2.136 |

TABLE 25 Calculations for grain boundary drift velocity from small grained lead specimen ($18.4 \times 10^3 m^{-1}$)

| Grain boundary results from small grain specimen | | Theoretical grain size correction (x 2.16) | | Actual grain size correction (x 2.46) | | |
|---|---|---|---|---|---|---|
| $10^{-13}\underline{v}/ms^{-1}$ | $\ln(\underline{v}\, kT^2/\nabla T)$ | $10^{-14}\underline{v}/ms^{-1}$ | $\ln(\underline{v}_t kT^2/\nabla T)$ | $10^{-14}\underline{v}_a/ms^{-1}$ | $\ln(\underline{v}_a kT^2/\nabla T)$ | $10^3 K/\underline{T}$ |
| 2.061 | - 36.7196 | 9.5417 | - 37.4897 | 8.3780 | - 37.6197 | 1.880 |
| 2.171 | - 36.6598 | 10.0509 | - 37.4299 | 8.8252 | - 37.5600 | 1.953 |
| 1.095 | - 37.3378 | 5.0694 | - 38.1079 | 4.4512 | - 38.2380 | 2.004 |
| 0.861 | - 37.5676 | 3.9861 | - 38.3377 | 3.5000 | - 38.4677 | 2.058 |
| 0.764 | - 37.6875 | 3.5370 | - 38.4577 | 3.1057 | - 38.5877 | 2.079 |
| 0.522 | - 38.0563 | 2.4167 | - 38.8263 | 2.1220 | - 38.9564 | 2.136 |

TABLE 27 Theoretical and actual grain size correction to grain boundary drift velocities observed in the small grained polycrystal

5.5.3.5 Calculation of the grain boundary heat of transport

Because the activation energy for our polycrystalline drift rate lies between the two reported values for the activation energy of grain boundary diffusion in lead, yet differs significantly from both of them, it did not prove possible to evaluate a unique heat of transport for grain boundary thermomigration. Instead an evaluation was made at 493K, a temperature central to the experimental range and the one at which the best individual estimates of the grain boundary diffusion have been made.

For this calculation of the heat of transport values for the diffusion coefficient reported by Stark and Upthegrove (48) for bicrystals with $30^{o}$ of misfit in tilt boundaries were used. This seems to be the most reasonable assumption for the random misfits of a polycrystal, and leads to an estimate of the heat of transport in grain boundaries, such that

$$Q^{*1} = 0.25 \text{ eV}$$

The results and theory pertaining to this value are discussed more fully in a publication by Johns and Blackburn (49). Since this class of boundary has the highest diffusion coefficient so far reported, other assumptions about the boundary would necessarily reduce the coefficient giving, in our calculation, an increased estimate for $Q^{*1}$.

Due to the differences between reported activation energies for grain boundary diffusion and that derived from the polycrystalline drift rates, the estimate for this parameter varied with temperature. The variation from the value at 493K is described by a factor

$$\exp\left((Q^{1} - Q^{11})\,(1/T - 1/493)/k\right)$$

where $(Q^{1} - Q^{11})$ is the difference in activation energy between that for grain boundary drift rates and that for grain boundary diffusion.

Using the value $Q^{11} = 0.204$ eV reported by Stark and Upthegrove, gives a variation in $Q^{*1}$ from 0.31 eV to 0.19 eV over the effective experimental range of 473K to 513K. The value of $Q^{11} = 0.68$ eV reported by Okkerse, gives an opposite variation of from 0.20 eV to 0.30 eV over the same range.

## 5.6 Conclusion

This chapter has detailed the results obtained from studies of thermomigration in lead, aluminium and cadmium specimens of varying structure and geometry. Also discussed is the observed effect of grain boundary thermomigration in polycrystalline lead specimens at temperatures below 513K.

Chapter 6 interprets these results and discusses the reliability and reproducibility of the results obtained using this technique for measuring the atomic drift rate created by the subjection of the specimens to various annealing temperatures. The latter part of this chapter details ideas that could be implemented to allow further studies using this technique.

# CHAPTER 6

## Interpretation of the results and some ideas for further study using this technique

CHAPTER 6

## Interpretation of the results and some ideas for further study using this technique

### 6.1 Determination of Q*

Thermomigration was detected as a change in specimen length. The basis for this assessment was that diffusion rates towards the cold end of the specimen are effectively zero, while at the shoulder diffusion is rapid and is perturbed into a net flow by the applied thermal gradient. Material flow therefore takes place into or out of the stem at a rate appropriate to the temperature and gradient maintained at the shoulder, and this flow changes the overall length of the specimen projecting from the furnace assembly. By measuring the change in length, values are obtained for the drift velocity of the mass flow for various values of applied annealing temperatures.

Penney in his theory of elastic-plastic deformation states that if the ratio of length to radius of each specimen is small then the mass flow will be uniaxial, that is, the smaller the ratio the less lateral changes occur, and in the expression for the drift velocity

$$v_m = \frac{D \nabla T \, (Q^* - \Delta H_f)}{\alpha f k T^2}$$

the accommodating factor $\alpha$ will approach unity.

For these studies short, squat specimens were chosen so that the assumption that $\alpha = 1$ could be made. Hence:

$$v_m = \frac{D \nabla T}{f k T^2} (Q^* - \Delta H_f)$$

6.1.1 Measurement of Q*

In this work a unique method for observing these length changes was employed. In the past studies had been performed using a marker-motion technique, such that changes in length between surface markers were measured optically and a value for the drift velocity obtained. This method is tedious and very time-consuming, often taking days or weeks to obtain one value for the velocity at a particular thermal gradient. There was also some doubt as to the validity of such a technique since measurements were obtained at the surface and not in the bulk of the material.

Length changes in this study were monitored by a Wayne-Kerr capacitative type transducer. By use of an elastically deforming parallel movement device precise positioning of the probe at the specimen face was achieved. The specimen face and the probe face acted as parallel plates of a capacitor, and any changes in the separation varied the capacitance. This variation in capacitance was calibrated directly to produce recordings of actual distances moved.

Once measurements of $v_m$, T and $\nabla T$ had been obtained it was possible to derive a value for D ($Q^* - \Delta H_f$). Graphs 20 and 21 show the comparison between drift rates obtained from lead and cadmium over an applied temperature range of 475K to 550K where lead is seen to elongate with time and cadmium contract.

6.2 Thermomigration in lead, aluminium and cadmium

During the study of lead four specimens were examined with varying geometry and structure. From this study of thermo-

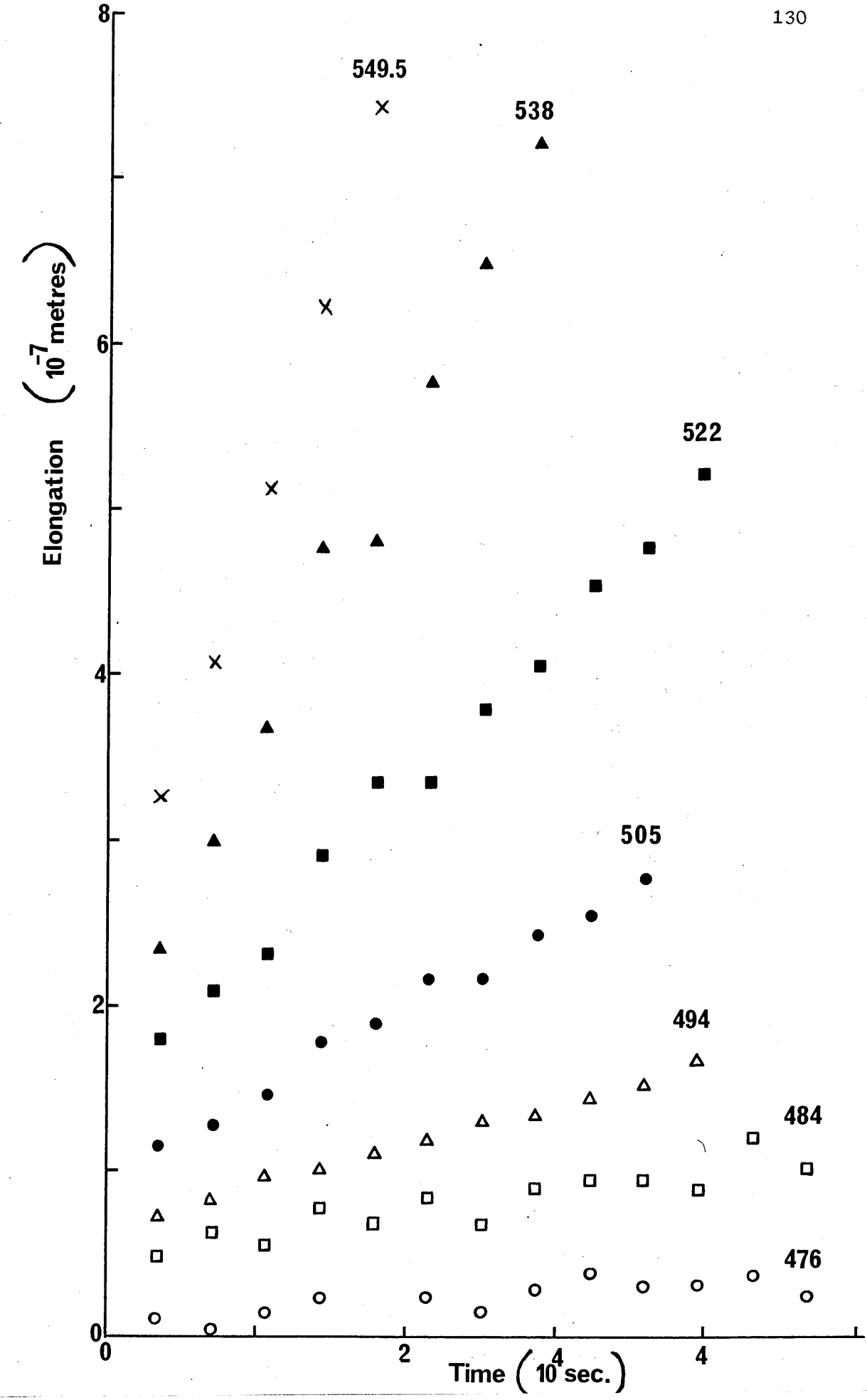


GRAPH 20 Elongation with time of a lead specimen subjected to seven annealing temperatures, ranging from 476K to 549.5K

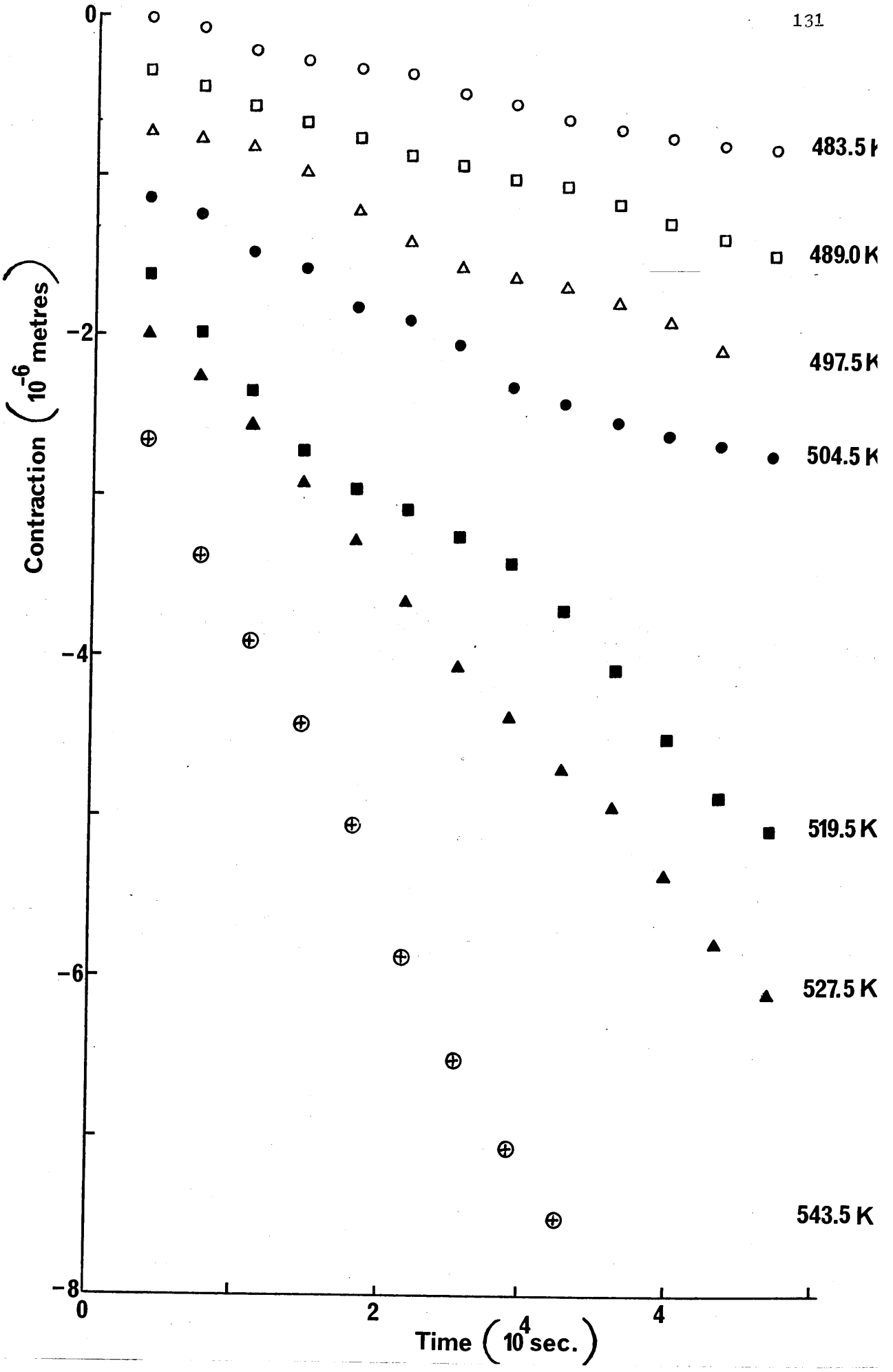


GRAPH 21 Contraction with time of a cadmium specimen subjected to seven annealing temperatures, ranging from 483.5K to 543.5K

migration in both single and polycrystal specimens an overall value for the heat of transport of the atom in lead was calculated such that

$$(Q^* - \Delta H_f) = + 0.107 \pm 0.002 \text{ eV}$$

In all, five specimens of aluminium were studied: three polycrystals and two single crystals, with variations in specimen geometry.

From the study of thermomigration in single and polycrystals of aluminium a value for the heat of transport of the atom in aluminium was obtained such that

$$(Q^* - \Delta H_f) = - (8.32 \pm 0.07)\ 10^{-2} \text{ eV}$$

Three single crystals of cadmium, having an orientation parallel to the C axis, were used in this study of thermomigration in cadmium. A value of the heat of transport of the atom in cadmium was obtained such that

$$(Q^* - \Delta H_f) = - (3.68 \pm 0.05)\ 10^{-2} \text{ eV}$$

### 6.2.1 Driving force and biased atomic motion

When a metal is subjected to a driving force, such as a thermal gradient a biased atomic motion is produced within the metal structure. In thermomigration studies this driving force can be expressed as

$$F_T = - Q^* \frac{\nabla T}{T}$$

as derived in Chapter 1.

The bias b can be expressed as:

$$b = \frac{F_T a}{2kT}$$

as derived in Appendix 2.

Table 31 shows the maximum and minimum values of the driving forces and the bias associated with the three metals studied.

| Metal | $F_T(max)eVm^{-1}$ | $F_T(min)eVm^{-1}$ | bias (max) | bias (min) |
|---|---|---|---|---|
| Lead | - 9.90 | - 8.75 | $3.450 \times 10^{-8}$ | $3.410 \times 10^{-8}$ |
| Aluminium | + 9.31 | + 6.12 | $1.726 \times 10^{-8}$ | $1.450 \times 10^{-8}$ |
| Cadmium | + 3.28 | + 2.56 | $9.775 \times 10^{-9}$ | $9.219 \times 10^{-9}$ |

TABLE 31

## 6.3 Summary

In this thesis a technique has been designed and produced that allows the determination of the mass flow which occurs when pure metal specimens are subjected to thermal gradients. This is achieved by recording the changes in specimen length and relating these changes to a drift velocity and subsequently to the heat of transport Q*. This technique is a unique method for performing such studies and proved reliable and accurate for the measurements made on the three metals studied. It is necessary when designing such a technique that the results obtained are not only accurate but that the process is internally consistent in producing consistent results for a particular metal. For this reason a number of specimens of each metal having variation in geometry and structure were examined, and the results obtained showed conclusively that atomic drift velocity associated with a

particular applied thermal gradient was independent of those geometrical and structural variations, and that they were internally consistent giving reliable values for the heat of transport in lead, aluminium and cadmium.

This consistency in the results obtained justified two assumptions that were made at the onset of these studies: (i) that the heat flow through the specimen stem between the shoulder and the heat sink could be treated as uniaxial and (ii) that the constant value assumed for the lattice accommodation factor $\alpha$ was correct. This assumption that $\alpha = 1$ was predicted by Penney for short, squat specimens and from Appendix 4 the length to radius ratio for the specimens used in these studies was approximately 1/3.

The value obtained for the heat of transport of the atom in lead agrees well with a theoretical calculation of this parameter made by Lodding and Thernqvist (32) while studying electrotransport in lead that $(Q^* - \Delta H_f) = + (0.09 \pm 0.18)$ eV.

For aluminium the $(Q^* - \Delta H_f)$ value calculated agrees well with two previous studies performed by Swalin and Yin (25) and Matlock and Stark (28) in thermomigration in polycrystalline specimens. However, during the study of thermomigration in single crystals of aluminium Matlock and Stark (28) derived a $(Q^* - \Delta H_f)$ value which was of different sign and magnitude to that value derived during their studies on polycrystal specimens. This discrepancy in the values of $(Q^* - \Delta H_f)$ derived in the single and polycrystal specimens by Matlock and Stark (28) is not in accordance with the results obtained during these studies, where a constant value of $(Q^* - \Delta H_f)$ was obtained for both types of specimen such that

$$(Q^* - \Delta H_f) = - (8.32 \pm 0.07)\ 10^{-2}\ \text{eV}$$

The value of $(Q^* - \Delta H_f)$ derived from the thermomigration study in cadmium is an original observation because to date there is no documentation of such a similar study being performed. Similarly there is no evidence as to the value of the enthalpy of vacancy formation in cadmium, $\Delta H_f$. Therefore, it is not possible to derive a value for the reduced heat of transport $Q^*$.

It was found during these experiments on thermomigration in lead, aluminium and cadmium that $(Q^* - \Delta H_f)$ does not vary with temperature. This agrees with a previous observation made by Lodding and Thernqvist (34), during a study of thermomigration in lithium, shown in Fig. 22. This observation is reasonable since $Q^*$ is defined as the constant of proportionality between a flow of heat and a flow of material:

$$Q_v^* = J_q / J_v$$

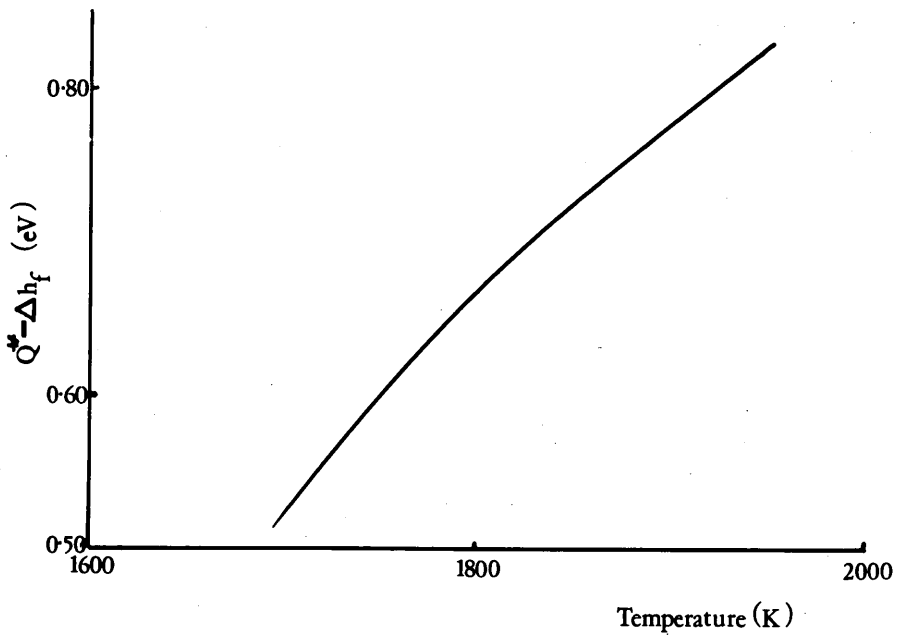


FIG. 21 Results obtained by Ho, Hehenkemp and Huntington (27) during a study of thermomigration in platinum

However, in a study of thermomigration in platinum, Ho, Hehenkemp and Huntington (27) observed that ($Q^* - \Delta H_f$) did vary with temperature, as may be seen in Fig. 21.

Ho, Hehenkemp and Huntington (27) did suggest, however, that this variation was due to a 15 per cent error in the values of the diffusion coefficient used to derive the ($Q^* - \Delta H_f$) values previously documented by Kidson (50).

This technique compares favourably with the marker-motion technique since it is far less time-consuming and allows a continuous monitoring of the dimension changes as well as an increased sensitivity in the measuring technique. Similarly it is far less time-consuming than the tracer technique and does not necessitate the destruction of the specimens, although the tracer technique is unquestionably superior in the directness of the relationship between the measured quantity and the parameter derived. It is also better in that it provides a value for the diffusion rate linked to the specimen itself.

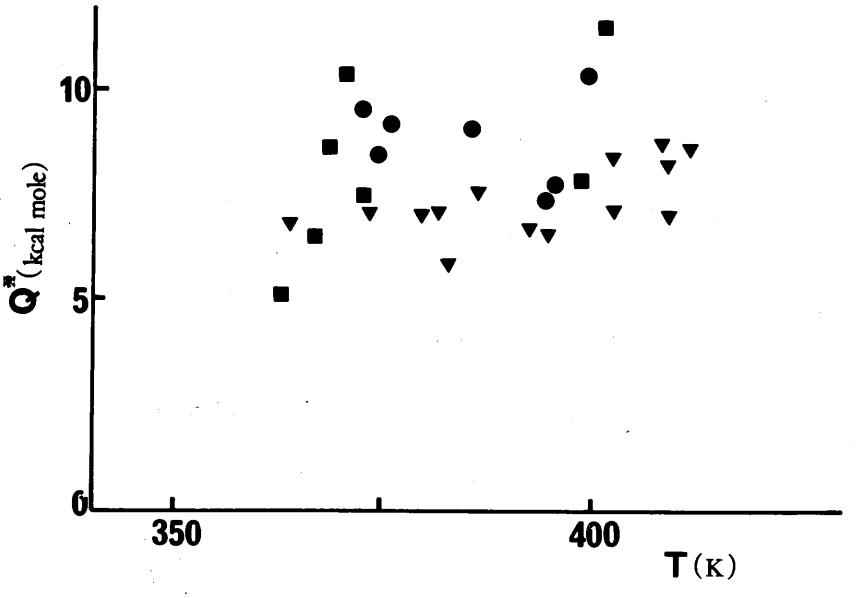


FIG. 22 Results obtained by Lodding and Thernqvist (34) during a study of thermomigration in lithium

It is unfortunate that the methods of this study depend on previous results for the diffusion coefficients obtained from radio-active tracer studies. An internal compensation, however, is that results obtained for the activation energies of each metal agree well with those measurements reported previously using the tracer technique. There is at least some confirmation therefore that diffusion enters the measured process in the manner predicted and required for the derivation of the ($Q^* - \Delta H_f$) values.

The main disappointment throughout this study was the impracticability of measuring drift rates and temperature gradients simultaneously, which necessitated the preparation of more specimens than was originally planned.

## 6.4 Relationship between $Q^*$ and $\Delta H_m$

The activation energy of self-diffusion $E_d$ is defined as the summation of two energy terms:

$$E_d = \Delta H_m + \Delta H_f$$

where $\Delta H_m$ and $\Delta H_f$ are the enthalpies of vacancy motion and formation respectively.

For lead and aluminium, documented values for the activation energy and the enthalpy of formation allow $\Delta H_m$ to be defined, such that for lead $\Delta H_m = 0.550$ eV and for aluminium $\Delta H_m = 0.653$ eV. Therefore, the ratio of the reduced heat of transport $Q^*$ to the enthalpy of vacancy migration for the two face centred cubic metals, lead and aluminium are 0.627 : 0.55 and 0.742 : 0.653, where for lead

$$\frac{Q^*}{\Delta H_m} = 1.138$$

and for aluminium

$$\frac{Q^*}{\Delta H_m} = 1.136$$

It may be seen that $\frac{Q^*}{\Delta H_m}$ is nearly equal for these two metals and $Q^* > \Delta H_m$.

This disagrees with the Wirtz-Brinkman theory which postulates that $Q^* \leq \Delta H_m$.

Haga (21) states, however, that although $\Delta H_m$ is the minimum energy required by an atom to move to a vacant lattice site, atoms will have energies exceeding $\Delta H_m$. A possible value for the reduced heat of transport $Q^*$ therefore is the mean value of the energy carried by atoms making a diffusion jump.

This mean value $\bar{E}$ may be defined:

$$\bar{E} \quad (E > \Delta H_m) = \frac{\int_{\Delta H_m}^{\infty} E \exp - (E/kT)\, dE}{\int_{\Delta H_m}^{\infty} \exp - (E/kT)\, dE}$$

where the limit $\Delta H_m$ excludes atoms making an approach to a jump while having an energy less than $\Delta H_m$. It follows therefore that

$$\bar{E} = \Delta H_m + kT = Q^*$$

Therefore for lead

$$\frac{Q^*}{\bar{E}} = \frac{0.627}{\Delta H_m + kT} = \frac{0.627}{0.55 + kT}$$

If we assume that T = 583K then

$$\frac{Q^*}{\bar{E}} = 1.02$$

For aluminium, if we assume that T = 900K, then

$$\frac{Q^*}{\bar{E}} = \frac{0.742}{0.725} = 1.02$$

Therefore it may be seen for lead and aluminium that $Q^* \simeq \bar{E}$ although the discrepancy exceeds experimental error.

This simple theory also indicates that $Q^*$ varies with temperature since

$$Q^* = \Delta H_m + kT$$

and

$$\frac{dQ^*}{dT} = k$$

Therefore

$$\Delta Q^* = \Delta T.k$$

where $\Delta Q^*$ and $\Delta T$ are the changes in $Q^*$ and temperature respectively.

Therefore

$$\frac{dQ^*}{dT} = 8.6 \times 10^{-5} \text{ ev } K^{-1}$$

From the experimental studies on lead and aluminium, it was seen that $Q^*$ did not noticeably vary with temperature since least square fits to the results yielded slopes with values in the region of $(5 \pm 5)\ 10^{-5}$ eV $K^{-1}$.

It was possible, therefore, that $Q^*$ did vary with temperature as described yielding a slope with the value of $8.6 \times 10^{-5}$ eV $K^{-1}$, but it was impossible to distinguish.

It is unfortunate that no value for the enthalpy of vacancy formation in cadmium has been documented so that a similar survey of the cadmium results could be made.

It is possible, however, to perform a rough calculation of the ratio of $Q^*$ to $\Delta H_m$ by using a relationship postulated by Shewmon (45) that

$$\frac{\Delta H_f}{E_d} \simeq 0.57$$

Therefore

$$\Delta H_f = 0.44 \text{ eV}$$

and hence

$$\Delta H_m = E_d - \Delta H_f$$

which leads to

$$\Delta H_m = 0.35 \text{ eV}$$

The reduced heat of transport Q* in cadmium is therefore approximately equal to 0.403 eV.

Therefore

$$\frac{Q^*}{\Delta H_m} = \frac{0.403}{0.350} = 1.14$$

This value is in good agreement with those obtained from lead and aluminium, although it is only a rough approximation, and again it may be seen that $Q^* > \Delta H_m$.

The ratio of the reduced heat of transport Q* to the mean value of the energy in excess of $\Delta H_m$ is:

$$\frac{Q^*}{\bar{E}} = \frac{0.403}{\Delta H_m + kT}$$

and if we assume that T = 573, then

$$\frac{Q^*}{\bar{E}} = \frac{0.403}{0.393} = 1.02$$

Therefore

$$Q^* \simeq \bar{E}$$

again in agreement with those results obtained from lead and cadmium.

The plot of $(Q^* - \Delta H_f)$ against temperature for cadmium yields a slope of the value $(6.5 \pm 6)\ 10^{-5}$ by a least square fit to the results obtained. So any variation of Q* with temperature due to the temperature term in $\bar{E}$ is unobservable.

### 6.4.1 Conclusion

The ratio of Q* to the enthalpy of vacancy formation is roughly constant for all three metals studied, although it must be noted that the value obtained from cadmium is quite approximate. From these results it can be seen that $Q^* > \Delta H_m$.

By assuming that the atoms have more energy than is required to jump from site to site, that is, $\Delta H_m$, a value for the mean of the energy in excess of $\Delta H_m$ is calculated, such that

$$\bar{E} = \Delta H_m + kT$$

For all three metals the ratio of the reduced heat of transport $Q^*$ to $\bar{E}$ is a constant, and within experimental uncertainty equal to 1.

Therefore

$$Q^* \simeq \bar{E}$$

## 6.5 Further studies

### 6.5.1 Other metals

With a better furnace design it would be possible to examine metals of much higher melting point temperatures, such as gold, silver, copper, etc. The limitations on the present design are such that temperatures no greater than 973K could be obtained and metals with melting points greater than this could not be studied. Since the apparatus can already be adapted to study specimens of various lengths, problems with temperature gradients at high furnace temperatures are non-existent.

### 6.5.2 Transducer

The capacitative transducer used in this study only allows the study of conducting materials since the specimens must be grounded with respect to the probe. This can be overcome to allow the study of non-metals simply by coating the bottom end of each specimen with a conducting layer, such as gold, and attaching an earthing connection to this coating.

Recently, however, an inductive transducer has been manufactured which does not require such a connection to the specimen, hence non-metallic materials such as glass, ceramics, etc., can be studied with very little modification to the existing equipment.

Thermomigration studies on ceramic material would then pose an interesting experiment for further work with this technique.

Similarly, using either type of transducer, a study of alloys and the effects of thermal diffusion on the order-disorder of crystal lattices would prove an equally valid follow-up to this work.

### 6.5.3 Electrotransport

Finally, by employing the existing equipment and by supplying the specimens with a direct electric current, effects of electrotransport could be monitored. Comparisons between atom drift rates from thermal and electrotransport experiments would be extremely useful, and could be achieved fairly readily for the same specimen. That is, apply a thermal gradient to the specimen and monitor the resulting atomic drift rate, then subject the specimen to a D.C. current and monitor the modification of the drift rates due to the added mass flow from electrotransport.

# APPENDIX 1

## Anisotropy

### A1.1 Theory of Penney

In this elastic plastic theory of deformation Penney describes how specimen geometry variations modify the direction of the mass flow in metal specimens subjected to electric fields.

He states that for specimens with large length to radius ratios the flow is anistropic whereas for specimens with small length to radius ratios the flow is totally uniaxial.

From consideration of simple elasticity and plasticity concepts Penney arrived at the following expression for m, the ratio of longitudinal to lateral strain:

$$m = 1 + \frac{(15b - 3)\ (\pi r/L)^2}{16 - (3b - 5)\ (\pi r/L)^2} \qquad A.1$$

where r and L are the radius and length of a cylindrical specimen respectively and

$$b = \frac{2 - 2v^1}{1 - 2v^1} \qquad A.2$$

where $0.5 > v^1 \geq v$ and v is the poisson ratio.

In Huntington's (51) notation this ratio m can be related to the lattice accommodation factor $\alpha$, such that

$$\alpha = \frac{m}{m + 2} \qquad A.3$$

### A1.2 Effects of anisotropic dimensional changes on the thermomigration experiments

By calculation of m for the three metals studied in these experiments a value for $\alpha$ is derived where it approximately equals unity.

The specimens used in these experiments had varying geometry and by calculation $\alpha$ varies by 8 per cent between the largest and smallest length to radius ratios. This variation should be observable in the results obtained, but since Penney's theory is based on the fact that $\frac{\lambda r}{L} < 0.1$ and in these experiments $\frac{\lambda r}{L} \sim$ little credibility can be given to these calculations.

As the specimens used have a very squat geometry $\alpha$ was assumed to equal unity as Penney suggests, and the consistency of the results obtained indicates that $\alpha$ is constant for all the specimens studied.

APPENDIX 2

Biased atomic motion

A2.1 Calculation of the bias b

Consider the case of a vacancy moving along the barrier axis which sees six potential barriers. There is a probability that: four of these barriers will require an energy $E_m$ for the vacancy to jump; one of the barriers requiring an energy $(E_m + \delta)$; and the sixth an energy of $(E_m - \delta)$.

Normally, with $\delta = 0$ the vacancy jump rate is $\partial$, where $D = 1/6\ a^2 \partial$. With the barriers as shown we have a $\partial_+$, a $\partial_-$ and 4 $\partial_o$ jump rates over the individual barriers. Therefore

$$\partial = \partial_+ + \partial_- + \partial 4_o$$

where

$$\partial_o = 1/6\ \partial$$

The flow of vacancies in the barrier axis is given by:

$$F_v = nC_v (\partial_+ - \partial_-) \qquad \text{A2.1}$$

where $n = N_a$ and is the number of atoms per unit area;
where N is the number of atoms per unit volume and a is the lattice width spacing.

Therefore

$$F_v = N_a C_v (\partial_+ - \partial_-)$$

Since $\frac{F_v}{NC_v} = v$, the drift rate, then

$$v = a (\partial_+ - \partial_-)$$

Now

$$\partial_o = 1/6\ \partial = 1/6\ \Theta \exp - (E_m/kT)$$

where $\Theta$ is the frequency of oscillation of an atom in the potential well.

$$\Gamma_+ - \Gamma_- = 1/6\,\Theta \exp - (E_m/kT)\,(\exp(\delta/kT) - \exp(\frac{-\delta}{kT}))$$

$$= 1/6\,\Theta\,(\exp - E_m/kT))\,(\frac{2\delta}{kT}) \qquad \text{A2.2}$$

$$\Gamma_+ - \Gamma_- = 1/6\,\Gamma\frac{2\delta}{kT}$$

Therefore

$$\frac{F_v}{NC_v} = v = a\,1/6\,\Gamma\frac{2\delta}{kT}$$

$$= a\,\frac{D_v}{a^2}\frac{2\delta}{kT}$$

Therefore

$$\frac{v}{D_v} = \frac{(2\delta/a)}{kT} \qquad \text{A2.3}$$

If we consider $(2\delta/a)$ is an 'effective steady force' acting on the vacancies, then equation A2.3 becomes Einstein equation.

In thermodiffusion this equivalent force F is given by

$$F_T = -\,Q^*\frac{\nabla T}{T} = \frac{2\delta}{a}$$

Therefore

$$\frac{v}{D_v} = -\,\frac{Q^*\nabla T/T}{kT} = -\,\frac{Q^*\nabla T}{kT^2}$$

The bias b is given by $\Gamma_+ - \Gamma_o = \frac{\delta}{kT}$

so $$b = \frac{\delta}{kT} = -\,\frac{1}{kT}\cdot\tfrac{1}{2}\,a\,\frac{\nabla T}{T}\,Q^*$$

$$= -\,\frac{a\nabla T}{2kT^2}\,Q^*$$

or, more generally, using a force $F_T$ where

$$F_T = \frac{2}{a} = \frac{2bkT}{a}$$

the bias b becomes

$$b = \frac{F_T a}{2kT}$$

Therefore, we can consider that a metal subjected to a thermal gradient will produce a biased atomic motion, and the value of the bias is given by

$$b = \frac{F_T a}{2kT}$$

APPENDIX 3

## Grain boundary diffusion

### A3.1 Drift rate due to grain boundary diffusion

The material flow, J, produced by a temperature gradient may be described by an energy $\Delta E$ where

$$J = D_s \Delta E \nabla T / fkT^2$$

In a material where vacancy concentration is described by a single formation enthalpy, $\Delta H_f$, this may be put into a reduced form with

$$J = D_s (Q^* - \Delta H_f) \nabla T / fkT^2 \qquad \text{A3.1}$$

where $Q^*$ is the reduced heat of transport, $D_s$ the self-diffusion coefficient and T the temperature.

An experimental measure of $Q^*$ may be made by following the movement of inert markers in a material, and from the Nernst-Einstein relation

$$v_m = D (Q^* - \Delta H_f) \nabla T / f\, kT^2 \alpha \qquad \text{A3.2}$$

where f is the correlation factor and $\alpha$ is the lattice accommodation factor describing the anisotropy with which the specimen takes up the material flow.

A polycrystalline material experiences an additional flow through grain boundaries. Within individual boundaries this may be defined as in the bulk by a flow $J^1$, where

$$J^1 = D^1 \Delta E^1 \nabla T / f^1 kT^2 \qquad \text{A3.3}$$

the primed quantities being grain boundary equivalents to those used previously in the bulk.

With this flow must be associated a contribution $v^1$ to the net specimen drift velocity, this contribution being functionally related to the number, arrangement and structure of the grain boundaries in the material.

To relate the boundary flow rate to the drift velocity, a model of the boundary structure and the flow pattern is required. For present purposes it will be assumed that a sufficient approximation is to treat all flow carrying surfaces as containing the flow axis, taking as an estimate of the active surface the length L of boundary exposed per unit area in a section of material cut normal to the flow axis. Accumulations of material due to changing flow rates will be taken to contribute to changes in specimen dimensions with an anisotropy identical with that for bulk flow. With these assumptions we can write the boundary contribution to the drift velocity as:

$$v^1 = wLD^1\Delta E^1\nabla T/f^1kT^2\alpha^1 \qquad \text{A3.4}$$

$\alpha^1$ being another accommodation factor and w an effective width for the boundaries.

Experimentally derived drift velocities, $\overline{V}$, can be seen as arising from a summation of the bulk and boundary drift processes to that interpretation of thermomigration at temperatures where the boundary processes are significant will follow from:

$$\overline{V} = v_m + v^1$$

$$= \frac{\nabla T}{kT^2}\left(\frac{D}{f\alpha}(Q^* - \Delta H_f) + \frac{D^1}{f\alpha^1}\Delta E^1 wL\right) \qquad \text{A3.5}$$

This equation will be used as the basis for interpretation of the experimental work of this paper.

## A3.2 Calculation of the heat of transport $E^1$

From a ratio of the drift velocity $v_m$ and $v^1$ derived in equations A3.2 and A3.4, an evaluation of the grain boundary heat of transport can be made:

$$\Delta E^1 = \frac{v^1 \alpha^1 f^1 D\,(Q^* - \Delta H_f)}{vwLD^1 f\alpha} \qquad \text{A3.6}$$

Assuming $\alpha = \alpha^1 = f^1 = 1$, then

$$\Delta E^1 = \frac{v^1 D\,(Q^* - \Delta H_f)}{vwLD^1 f} \qquad \text{A3.7}$$

Since the results from a single crystal of lead are available, values for D, $(Q^* - \Delta H_f)$, v and f, are known, and by obtaining values of $v^1$ from the experiment, values for $D^1\Delta E^1$ can be derived.

Using values of $D^1$ previously recorded by Okkerse (47) or Stark and Upthegrove (48), $\Delta E^1$ can be defined.

APPENDIX 4

The deformability of a material under stress

If a metal rod is subjected to a thermal gradient, plastic flow will occur, mainly at the hot region.

The deformability of a material under stress can be described:

$$c = a \exp - (E_d/kT) \qquad \text{A4.1}$$

where $a$ is a constant and $E_d$ is the activation energy.

The temperature T will obviously vary with position x and can be described as:

$$T(x) = T(o) + \alpha x \qquad \text{A4.2}$$

where $\alpha$ is dT/dx.

By substitution for T into equation A4.1, we obtain

$$c(x) = a \exp - (E_d/k\,(T(o) + \alpha x)) \qquad \text{A4.3}$$

which can be rewritten

$$c(x) = a \exp - \left(\frac{E_d}{k} \frac{1}{T(o)\,(1 + \alpha x/T(o))}\right) \qquad \text{A4.4}$$

Assuming $\frac{\alpha}{T(o)} \ll 1$, then

$$c(x) = a \exp - \left(\frac{E_d}{kT(o)}\,(1 - \frac{\alpha}{T(o)}\, x)\right)$$

$$= a \exp - \left(\frac{E_d}{kT(o)}\right) . \exp \left(\frac{E_d \alpha x}{kT(o)^2}\right) \qquad \text{A4.5}$$

Therefore

$$c(x) = c(o) \exp \left(\frac{E_d \alpha x}{kT(o)^2}\right) \qquad \text{A4.6}$$

$$c(x) = c(o) \exp x/\lambda \qquad \text{A4.7}$$

where $\lambda = \frac{kT(o)^2}{\alpha E_d}$ and is the length of the specimen over which the bulk of the plastic flow occurs, and in the case of the specimens used in these studies

$$\lambda = 0.5\text{mm}$$

REFERENCES


1. F. Reif : 'Fundamentals of Statistical and Thermal Physics, McGraw-Hill-Kogakusha (1965)

2. K. Compaan, Y. Haven : Trans. Faraday Soc. 52, 786 (1956)

3. K. Compaan, Y. Haven : Trans. Faraday Soc. 54, 1,498 (1958)

4. P. Mazur, S. R. DeGroot : 'Non-equilibrium Thermodynamics' North Holland, Amsterdam (1962)

5. C. Ludwig : Stizber, Akad, Wiss, Wien, Math. Natur. Kl, 20, 539 (1956)

6. Ch. Soret : Arch. de. Geneve 3, 48 (1879)

7. W. Shockley : Phys. Rev. 91, 1,563 (1953)

8. W. Shockley : Phys. Rev. 93, 345 (1954)

9. F. A. Nichols : Acta Met. Vol. 20, 207 (1972)

10. K. G. Denbigh : 'The Thermodynamics of the Steady State', Methuen, London (1951)

11. A. D. Leclaire : Phys. Rev. 93, 344 (1954)

12. J. A. Brinkman : Phys. Rev. 93, 345 (1954)

13. A. R. Allnatt, S. A. Rice : J. Chem. Phys. 33, 573 (1960)

14. W. G. Brammar : Acta Met. 8, 630 (1960)

15. K. Wirtz : Physik. Z, 44, 221 (1943)

16. R. A. Oriani : Trans. A.I.M.E. 233, 1,878 (1965)

17. R. A. Oriani : J. Phys. Chem. Solids 30, 339 (1969)

18. H.B. Huntington: J. Phys. Chem. Solids 29, 1,641 (1968)

19. H.B. Huntington: Rensselaer Polytechnic Report to be published (1974)

20. P. G. Shewmon : J. Chem. Phys. 29, 1,032 (1958)

21. E. Haga : J. Phys. Soc. Japan 15, 1,949 (1960)

22. C. Wert : Phys. Rev. 79, 601 (1950)

23. A. B. Lidiard : I.A.E.A. Symposium on Thermodynamics of Nuclear Materials, Vienna (1965)

24. P. G. Shewmon D. Jaffe : Acta Met. 12, 515 (1964)

25. R. A. Swalin, C. A. Yin : Acta Met. 15, 245 (1967)

26. P. S. Ho : J. Phys. Chem. Solids 27, 1,331 (1966)

27. P. S. Ho, Th. Hehenkemp, H.B. Huntington : J. Phys. Chem. Solids 26, 251 (1965)

28. J. H. Matlock, J. P. Stark : Acta Met. 19, 923 (1971)

29. N. V. Doan : J. Phys. Chem. Solids 31, 2,079 (1970

30. R. V. Penney : J. Phys. Chem. Solids 25, 335 (1964)

31. W. Mock : Phys. Rev. 179, 663 (1969)

32. A. Lodding, P. Thernqvist : Z. Naturforsch. 21a, 1,310, (1966)

33. E. S. Wajda, G. A. Shirn, H.B. Huntington : Acta Met. 3, 39 (1955)

34. A. Lodding, P. Thernqvist : Z. Naturforsch 21a, 857 (1966)

35. J. B. Hudson, R. E. Hoffman : Trans. Met. Soc. A.I.M.E. 221, 761 (1961)

36. T. S. Lundy, J. F. Murdock : J. Appl. Phys. 33, 1,671 (1962)

37. H.B. Huntington: P. S. Ho : J. Phys. Soc. Japan 18, Suppl. 2, 202 (1963)

38. M. Hanson : 'Constituion of Binary Alloys' McGraw-Hill, New York (1958)

39. R. V. Jones : J. Sci. Instrum. 39, 193 (1962)

40. H. C. Chang, N. J. Grant : T.A.I.M.E. 197, 1,175 (1953)

41. D. Mclean : 'Mechanical properties of metals', John Wiley and Sons Inc., New York

42. A. B. Feder, A. S. Nowick : Phys. Rev. 109, 1,959 (1958)

43. N. H. Nachrieb, G. S. Handler : J. Chem. Phys. 23, 1,569 (1955)

44. R. Simmons, R. Balluffi : Phys. Rev. 125, 862 (1962)

45. P. G. Shewmon : 'Diffusion in Solids', McGraw-Hill (1963)

46. D. Turnbull : 'Atom Movements' A.S.M., Ohio 129 (1951)

47. B. Okkerse : Acta Met. 2, 551 (1954)

48. J. P. Stark, W.R. Upthegrove : A.S.M. 59, 479 (1956)

49 R. Johns, D.A. Blackburn : Conference on Thermomigration in Pure Metals at low diffusion temperature, to be published

50. G. V. Kidson : Pro. Inter. Conf. Radioisotopes in Sci. Res., Paris, 185 (1957)

51. H.B. Huntington: A. R. Grone J. Phys. Chem. Solids 20, 76 (1961)

52. M. Gerardin : Compt. Rend. 53, 727 (1861)

53. L. S. Darken, R. A. Oriani : Acta. Met. 2, 841 (1954)

ACKNOWLEDGEMENTS

1. Dr. D. A. Blackburn, for his constant help, advice and encouragement throughout this research.

2. Processor C. W. A. Newey, for the use of the laboratory facilities at the Oxford Research Unit.

3. Colin Woods, Senior Technician in the workshop, for his excellent standard of work and without whose help I am sure this research would still be unfinished.

4. Clive Ward of Alcan International Ltd., for his help in specimen preparation.

5. Photographic and reprographic departments of the Open University for their help in the presentation of this thesis.

6. To my wife, for typing this thesis and her constant encouragement throughout the three years.